MODELLING THE SPATIAL CHARACTERISTICS OF HYDROMETEOROLOGY IN THE UPPER OLDMAN RIVER BASIN, ALBERTA

DENNIS LESLIE SHEPPARD
B.Sc. Memorial University of Newfoundland, 1990

A Thesis
Submitted to the Council on Graduate Studies
of The University of Lethbridge
in Partial Fulfilment of the
Requirements for the Degree

MASTER OF SCIENCE

LETHBRIDGE, ALBERTA
August, 1996

ABSTRACT

A characteristic of alpine drainage basins is the very sparse distribution of meteorological recording stations. This study models a contiguous distribution of microclimate and snowpack accumulation in the upper Oldman River basin. To accomplish this goal, gaps between weather recording stations are first filled using a modified MTCLIM climate simulation model in conjunction with the spatial analysis capabilities of the PAMAP geographic information system (GIS). The GIS provides terrain information such as elevation, slope, and aspect on a 100 metre grid as input into the microclimate simulator which, in turn, outputs daily meteorological conditions for a user-defined period of time.

The estimation of snowpack accumulation is achieved with another component of the model which makes use of the modelled microclimate to calculate daily accumulation and ablation on a grid point basis. Simulation results are returned to the GIS for display and spatial analysis. Discussion includes such things as the grouping of terrain variables and the derivation of an altitudinal precipitation profile, both of which are required for computational efficiency.

While regression analysis indicates a very close relationship between observed and simulated temperature, precipitation is less successfully modelled at the daily time scale. Comparisons of simulated temperature with observed data resulted in an $r^2 = 0.94$ and are therefore considered very reliable. Daily precipitation comparisons initially indicated a low correlation

between observed and simulated data. However, when monthly totals are considered instead, r^2 rises to 0.66. When snowpack conditions are simulated for several snow pillows in the region, regression analysis with observed data produces r^2 values as high as 0.896.

ACKNOWLEDGEMENTS

This research has been made possible with the support of a number of individuals to whom I am eternally grateful. My committee members, Dr. James Byrne, Dr. Robert Rogerson, and Dr. Rene Barendregt, have provided both encouragement and guidance throughout my program. Dr. Rogerson has been particularly helpful in the final stages of thesis preparation. I would also like to thank Dr. Nigel Waters (The University of Calgary) for acting as external examiner at my defence.

In addition to providing computer hardware and software, Dr. Byrne and the Water Resource Institute has generously donated funds to help finance my graduate education as well as to purchase a number of digital datasets which greatly expedited database compilation.

Ian Saunders has been a great friend without whom, I may not have survived such an arduous endeavour. He was instrumental in the search for both data and relevant literature. On a personal level, he provided a most unique perspective of the Alpine regions of Southern Alberta during several winter treks.

The single most important person in my life is my wife Shelley. She has been by my side to offer support, encouragement, and the occasional push when I needed it most. This one's for you!

Love and support from my family has been a major ingredient in my life and it is to them that I attribute much of my success. Their confidence in my abilities has been an inspiration whenever I have felt doubt. A special thanks to Mom, Dad, Peggy, Diane, and Snowden.

I will forever be indebted to Sun and Kathy Lim (Mom and Dad), whose kindness and generosity has made my experience so much less complicated by providing me with a home away from home.

I hope that I have not omitted anyone, but should that be the case please accept my apologies and know that your omission in no way diminishes the gratitude I extend.

TABLE OF CONTENTS

LIST OF FIGURES

LIST OF TABLES

Chapter 1

OVERVIEW

1.1 Introduction

The availability of water resources in southern Alberta is of paramount importance. As a result of the semi-arid climate experienced by much of the area, it is necessary to rely not only on inputs from precipitation to meet the many water demands of modern society. Common contenders for water include municipal water supplies, hydroelectric power producers, industry, and recreational activities. The region is characterized by an economy based heavily on the agrifood industry which means an additional demand on water for use in irrigation practices and for livestock production. The 1951-1980 mean annual total precipitation for much of southern Alberta is less than 500 mm which is insufficient to support all these needs thus a great deal of reliance is placed on runoff from water rich, snow fed, mountainous drainage basins. Streamflow rates reflect the condition of alpine snowpacks and the rate at which they melt. Therefore, attempts to improve estimation accuracy have obvious benefits to those living downstream. Another advantage of having accurate snow estimates is improved techniques for monitoring flood potential and therefore improved response contingencies. Both result in a reduced risk to human life and damage to property.

The research undertaken reflects the author's interest in the application of geographic information systems (GIS) to the analysis and management of our natural resources. The study explores the spatial distribution of water resources with a particular emphasis on modelling the hydrometeorologic conditions in the topographically diverse terrain found along the eastern slopes of the Canadian Rockies. The methods described illustrate the integration of GIS, Fortran programing, and database management.

The project can be divided into three broad stages; database creation, microclimate simulation, and snowpack simulation. The first of these involves the compilation and integration of datasets from several sources. This is done primarily within the PAMAP GIS through manual digitizing and database management. Data layers collected include basin boundary, rivers, lakes, forest cover, point features, elevation, slope, and aspect. While the first 5 are collected manually from paper maps and tabular data, the latter 3 are derived from raw elevation data purchased for this project.

The second stage, daily microclimate simulation, is accomplished with a modification of the MTCLIM microclimate simulation model (Hungerford *et al.*, 1989) used in conjunction with the spatially continous data contained within the GIS. The modified program, currently known as SIMGRID, is capable of accepting gridded terrain information from the GIS and using it to generate a complete microclimate coverage from the sparse distribution of weather recording stations. In essence, the Fortran program simulates grid point microclimate from observed station data by making adjustments for differences in elevation, slope, aspect, forest

cover, and obstructions to incoming solar radiation between the station and each individual grid point. In this investigation, a 100 metre grid spacing is used.

Snowpack simulation, the third stage, involves the utilization of previously simulated microclimate data to determine daily snow accumulation and melt on a grid point basis. The techniques used are based on the empirically-based accumulation model discussed by Wyman (1995) and the snow melt routines described by Pipes and Quick (1977). Within the model, daily maximum and minimum temperature is first used to ascertain whether falling precipitation takes the form of rain, snow, or some proportion thereof. Next, the temperature extremes are used to calculate daily melt expressed in millimetres of snow water equivalent (SWE). These two crucial pieces of information are finally applied in a balance equation which reflects daily fluctuations in total snowpack water equivalent.

To summarize, the major accomplishment of this research is the development of an alpine hydrometeorological simulation model (AHSM). The model includes detailed hydrometeorological Fortran code with database management linkages to a digital elevation model created within the PAMAP GIS. The AHSM has been calibrated with the best available data for the study area of interest, the Upper Oldman River basin. The model has been used to estimate the snow cover accumulation and ablation for the study basin over a period of 10 years (1970-1980) from which a number of interesting points arise. For example, the model indicates a sensitivity to the effects of aspect and elevation on certain simulated variables while apparently having no influence at all over others.

This analysis is part of a much larger project whose goal is to study the impacts of potential future climate change on agricultural viability in the Canadian Prairies. The larger project, funded by the Nat Christie Foundation, is a joint venture between the Economics and Geography Departments at the University of Lethbridge and the Agriculture and Agrifood Canada Lethbridge Research station. The project is divided into a number of components including historic and future climate analysis, insect infestation, economic impact analysis, and a hydrology component. The latter of these is the context in which this study is carried out.

1.2 Objectives:

In the design stages of the project, consideration was given to a number of possible avenues to proceed. The following is a brief overview of objectives established at that time.

1. To develop a spatially distributed hydrometeorological model for simulating daily microclimate, snow accumulation, and snow ablation in an alpine environment.

2. To simulate the microclimatic and snowpack conditions in the Upper Oldman River basin for a period of 10 years (1970 - 1980).

To accomplish these objectives a number of critical stages were identified;

(i) Create a comprehensive digital database covering the region under investigation. Data collected includes hydrographic features (rivers, lakes, and drainage basin boundaries), point features (settlements, hydrometric stations, and climate stations), land cover information (forested verses non-forested), historical environmental conditions (streamflow, temperature, precipitation, and snowpack), and complete digital elevation model (elevation, slope, and aspect).

(ii) Simulate the microclimate for a series of regularly spaced grid points using a modified version of the Fortran program, MTCLIM (Hungerford, *et al*, 1989), and historic climate data from nearby weather stations maintained by Atmospheric Environment Service (AES).

(iii) Develop Fortran code to model snowpack accumulation from the simulated

climate.

(iv) Generate a series of maps depicting snowpack conditions at several temporal scales using the GIS.

(v) Correlate modelled snowpack accumulation to sparse historic snow course data.

(vi) Estimate runoff based on volume of modelled snowpack.

Chapter 2

LITERATURE REVIEW

2.1 Alpine Hydrology/Hydrologic Cycle

Pertinent to the discussion of temperature and, more directly, precipitation is an overview of the process known as the hydrologic cycle. The hydrologic cycle involves the exchange of water molecules between the Earth and its surrounding atmosphere (Christopherson, 1992; Wilson, 1990; Maidment, 1993; and Environment Canada, 1994). Figure 2.1 is a representation of adaptations taken from a number of the referenced authors. Identified in the figure are the four principal processes of concern to hydrology: (i) evaporation/transpiration, (ii) precipitation, (iii) surface runoff, and (iv) groundwater flow. The relative percentages of total global water in each of ocean, atmosphere, lakes and rivers, and snow and ice are shown. The general distribution and interaction of water is depicted.

Distinction of the four processes is based upon their respective roles in the transformation and/or transportation of water throughout the cycle. Evaporation primarily from oceans, but also from lakes, rivers, and land surfaces and transpiration from vegetation are the means by which water molecules pass from liquid to vapor state. Once airborne, water vapor is carried

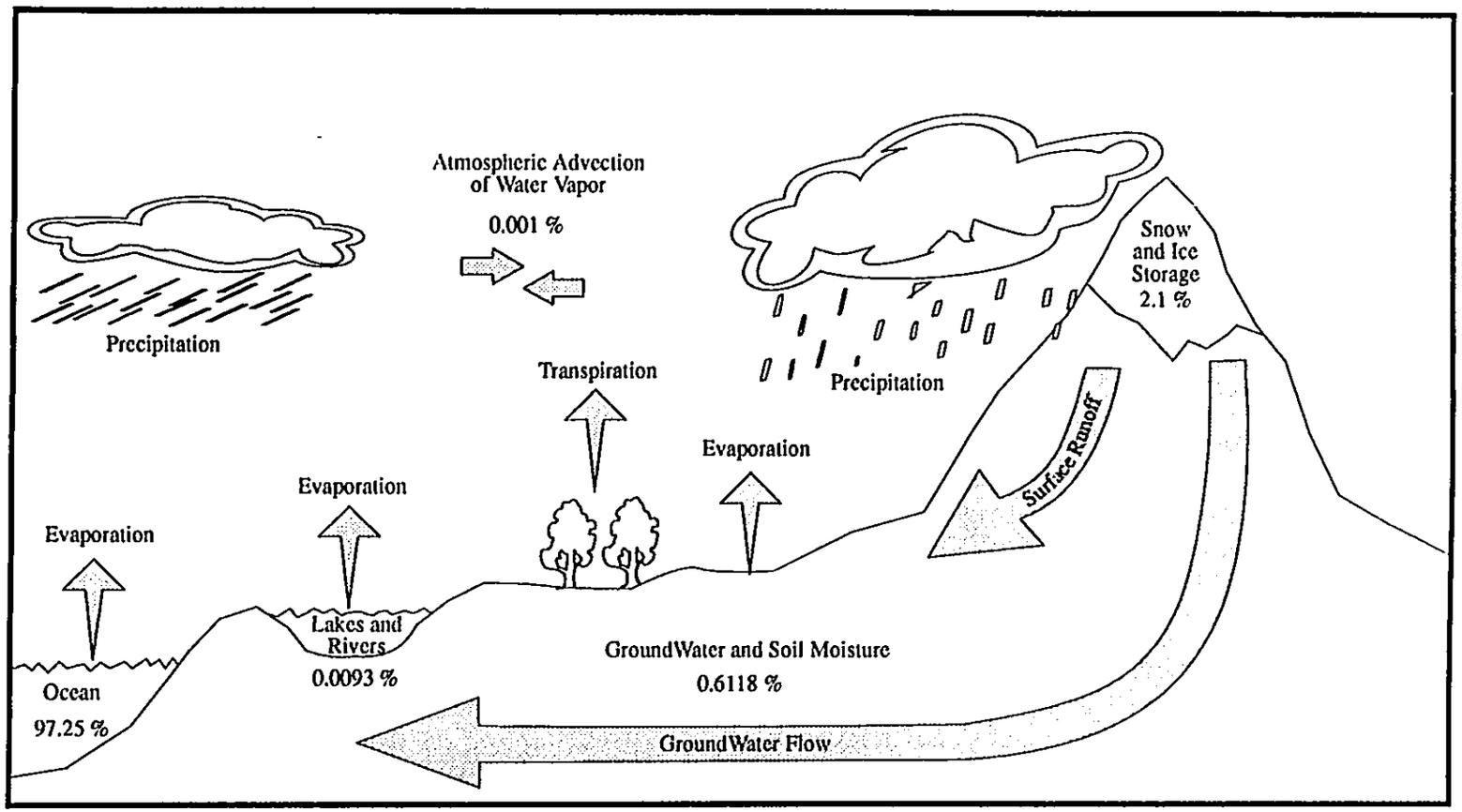

Figure 2.1 The hydrologic cycle. The four principal processes identified are: (i) evaporation/transpiration, (ii) precipitation, (iii) surface runoff, and (iv) groundwater flow. Numerical values represent the percentage of total global water found in each stage of the cycle. The total = 100.0 % (97.25 % + 0.0093 % + 0.001 % + 0.6118 % + 2.1 %).

by air masses until such time they are no longer capable of being supported. The amount of water vapor that an air mass may support is related to the temperature of the air and represented by the dewpoint. Dewpoint is the temperature to which air at a constant pressure and water vapor content must be cooled in order for saturation to occur. Precipitation occurs when an air mass cools to the dewpoint, condensation results, clouds form, and eventually water droplets coalesce and fall back to Earth as either rain, snow, or hail. Surface runoff by way of lakes and rivers or groundwater flow beneath the surface are both processes by which water is returned to the principal water storage source and sink, the oceans.

Oceans, which occupy roughly 70% of the total Earth's surface, make up the single largest source of water on the planet, approximately 97.25% of global water. The second largest store of water, at about 2.1%, is found in the form of ice and snow storage which includes polar ice caps, glaciers, and snow. Next, around 0.0093% of all water is held up in freshwater lakes and rivers. Fourth, 0.6118% of global water resources are maintained in ground water and soil moisture. Finally, a miniscule amount (0.001%) is found in the atmosphere.

The interactions taking place are important controls on the exchange of heat energy between the atmosphere and the Earth. As evaporation occurs at the surface of oceans, rivers, and lakes, energy is absorbed by the water vapor. This absorption of energy, known as latent heat of evaporation, is key to cooling in the Earth's energy budget. The reverse occurs when water vapor held up in the atmosphere cools and condenses. The energy previously absorbed is released as latent heat of condensation and thereby offsets some of the cooling which occurs

due to increases in altitude.

The mountainous areas under investigation in this thesis represent only a small portion of the Earth's hydrologic cycle as described above. As such, it is worth noting that many of the processes mentioned occur according to the general principles but deviate under the influence of alpine topography and land cover features. Distance from the primary sink of global water, the oceans, is another reason for this deviation from the global scheme of water interaction. Much of the precipitation in mountains is orographically driven by the westerly flow which picks up moisture from the Pacific Ocean and carries it eastward.

2.2 Temperature Variation in an Alpine Environment

Variations in local air temperature are driven primarily by the amount of solar radiation received at a given site. Solar radiation, in turn, is dependent upon such climatic controls as latitude, season, slope, and aspect. Proximity of the air mass to a heat source that may provide heating is also important to temperature. Shortwave incoming solar radiation is converted by the Earth into longwave radiation which, when emitted by the surface, warms the surrounding atmosphere. As a result, elevation or distance from the surface influences the amount of atmospheric heating.

Latitude and seasonality factor heavily in the receipt of solar radiation at a site. Latitude is very important because angular distance north or south of the Equator determines the angle

at which incoming solar radiation is incident upon the Earth's surface. As well, latitude in association with seasonality determines daylength or period of exposure.

Generally, the subsolar point which is the only point receiving insolation perpendicular to the surface, occurs in the lower latitudes. At the subsolar point, incoming solar radiation illuminates a small surface area and is therefore more intense. Areas other than the suspolar point receive insolation at an angle resulting in the energy being less concentrated. This diffusion of energy due to non-perpendicular incidence angles is more pronounced in the high latitudes where not only is the radiation spread over a larger surface area, but it must also travel through a greater depth of atmosphere before reaching the surface. The latter results in more scattering, absorption, and reflection by atmospheric materials. On an annual basis, the outer atmosphere above equatorial regions receives approximately 2.5 times more radiation than at the poles primarily as a result of variations in the angle of insidence alone (Christopherson, 1992).

The period of exposure to incoming radiation, daylight hours, is a product of both latitude and season. It is highly variable with the Equator being the only region on Earth that receives a constant 12-hour mix of daylight and darkness. The higher the latitude, the greater the deviation from the Equatorial situation. During their respective summer seasons, the North and South Poles each receive 24 hours of daylight. Conversely, during the winter they experience 24 hours of darkness. Obviously, this will greatly influence the amount of solar radiation received. In June, the North Pole actually receives slightly more solar radiation than

does the Equator as a result of the constant exposure. In December, radiation receipt at the South Pole is again more than at the Equator, but with a slight increase even over the North Pole.

According to Price (1981), mountains in the middle latitudes may experience an even greater intensity of solar radiation than surrounding lowland regions. This results from a combination of thinner atmosphere and solar rays striking slopes oriented directly toward the sun. Price states that a surface inclined 20° toward the sun in the mid-latitudes receives about twice as much radiation during the winter as a level surface. This certainly implies that slope and aspect are significant controls. Using Trier, West Germany and Tucson, Arizona (50°N and 32°N respectively) Barry (1992) illustrates that on south facing slopes there is a shift in the maximum intensity of direct radiation from steeper slopes in the winter to gentler ones in the summer. North facing slopes receive a maximum intensity on gentler slopes in both summer and winter, but summer does show slightly increased intensity at low to mid range slopes.

The last significant control acting upon air temperature is elevation. Much work has been done to determine the change in temperature with respect to increasing altitude. Although the Sun is the initial source of terrestrial energy, closeness to it does not imply an increase in temperature. On the contrary, shortwave radiation from the Sun is absorbed by the Earth's surface where it is converted into longwave energy. The Earth itself then becomes the radiating body so increasing distance from its surface means a decrease in heating. It is for this reason that highest temperatures usually occur at lower elevations (Price, 1981). In

addition, the atmosphere tends to be less dense and contains less water vapor and carbon dioxide, greenhouse gases, with increased altitude. Increased distance from a heat source and fewer greenhouse gases to absorb radiating energy result in an overall decrease in temperature.

Actual changes in temperature due to increasing or decreasing altitude have been quantified in terms of air mass characteristics. An unsaturated air mass is defined as one that has a relative humidity less than 100%. In other words, it does not contain the maximum number of water molecules it is capable of holding. Such an air mass is cooled or heated according to the dry adiabatic lapse rate (DALR) of approximately 10°C per 1000 metres of elevation. An unsaturated air mass may go through the cooling and then heating process such that it attains the same temperature at the same elevation on either the windward or leeward side of a mountain. If a similar air mass is cooled to its dew point, its relative humidity reaches 100% and it is said to be saturated. A saturated air mass is cooled or heated according to the wet adiabatic lapse rate (WALR) which is approximately 6°C per 1000 metres of elevation. The WALR is lower than the DALR because the process of saturation and then condensation results in a release of latent heat into the air mass. This release of heat offsets some of the cooling due to expansion related to the DALR. The average decrease in temperature with respect to elevation is approximately 6.5°C per 1000 metres in the troposhere (Ahrens, 1985).

2.3 Precipitation Variation in an Alpine Environment

Due to the lack of sufficient spatially diverse data, modelling of mountain precipitation is at best an inexact science. It has been discovered that the amount and spatial distribution of precipitation depends on a number of characteristics including wind direction, temperature, humidity, depth of the air mass and its relative stability at different elevations, and surface orientation and configuration of the landforms (Price, 1981). Three of the more important surface factors are (i) elevation, (ii) slope, and (iii) aspect. Studies on the degree to which each influences precipitation are discussed below. It is important to remember that relationships derived between precipitation and these factors are highly variable in different geographic locations around the globe.

The first, and certainly most important, control on precipitation is altitude. In looking at variation of precipitation with respect to elevation, it is important to consider temperature lapse rates according to relatively standard lapse rates. As mentioned in the previous section, an ascending air mass is cooled while descending air is heated. Lapse rates determine the temperature of an air mass and, in turn, determine its relative capacity to hold moisture. As rising air cools, relative humidity increases and the capacity to hold water vapor is reduced. Given that condensation occurs at or below the dewpoint temperature, when sufficient cooling takes place, the result will be the formation of clouds and eventually precipitation. It can be concluded then that as elevation increases, the greater the likelihood an air mass will have reached its dewpoint temperature, and therefore precipitate out more of its moisture.

When an air mass is forced to rise up and over an obstruction such as a mountain range, the resulting precipitation is known as orographic in nature. This is the case for air masses driven by the prevailing westerlies across the Rocky Mountains which run in a general northwest to southeast direction. This explains why orographic precipitation is common along the western (windward) slopes.

In addition to elevation, slope and aspect appear to be significant contributors to the amount of precipitation received in an area. The relevance of aspect lays in the fact that it designates a surface as either windward or leeward, important in terms of orographic precipitation and the rainshadow effect. Prevailling winds generally have a westerly component but may come from a variety of directions. Further complicating this generalization are individual storm circulation characteristics. As a result, storm approach direction is highly variable in nature. A surface which is windward for one storm may very well be a lee slope for the next. However, the direction from which storms "usually" approach may direct annual precipitation totals. In other words, it may be possible to define general synoptic patterns and their associated precipitation characteristics in relation to a given aspect (Yarnal, 1984; Saunders and Byrne, 1996).

Several examples below examine the variations resulting from differences in aspect. One in particular shows the marked difference between annual precipitation on windward and leeward slopes in the Austrian Alps (Barry, 1992). Often there exists a rainshadow effect on the leeward slopes of large mountain barriers produced by the descent of air. Not only does

the air mass lose much of its moisture as rain, snow, and clouds on the windward side, but also the descending air is also heated through compression, thus increasing its capacity to hold moisture. In other words, there tends to be less moisture on the lee slope due to a net drying by the descending airflow.

Slope, although apparently less significant, does appear to play a small role in precipitation. Storr and Ferguson (1972) suggest that the regression coefficient relating precipitation and elevation is improved only slightly with the inclusion of slope. Perhaps the best explanation of variation with slope is due to the rate at which an air mass is forced to rise. When it is forced to rise quickly, moisture is precipitated more quickly and over a shorter distance than if it were to ascend gradually over a greater distance. Therefore the depth per unit area, where the area is a projection onto a horizontal surface, is greater on steeper slopes.

Attempts at extrapolating moisture inputs for high altitude areas around the world are numerous. Since little exists in the way of recorded data for these sometimes inaccessible regions, it is necessary to devise methods by which to estimate such information. Barry (1992) summarizes a number of studies dating as far back as the late nineteenth century in the Himalayas and the Alps. One of the more significant surveys he mentions was one done by F. Lauscher in 1976. Lauscher succeeded in generating five generalized precipitation profiles using 1300 long term recording stations having an extensive horizontal and vertical coverage. He looked at 1029 stations below 1 km, 222 between 1-2 km, and 43 between 2-3 km for 10° latitude X 20° longitude sectors between 35°S-55°N and 130°E-110°W. He came up with

generalized precipitation profiles for tropical, equatorial, polar, transitional, and middle latitude climates. Figure 2.2 shows only those profiles for middle latitudes (M), tropical climates (T), and equatorial climates (E). The first two profiles (M and T) both imply an increase in precipitation with elevation at least until about 1.5 km at which time (T) reaches a maximum and then drops off higher up. The slope of (M) increases, indicating an even greater affect from 1.5km and higher. In contrast, (E) shows a general decline in precipitation with altitude. Once again there is a change in slope at about the 1.5 km mark.

Another important example which Barry describes takes into account the affect of aspect in combination with elevation on annual precipitation. The investigation was carried out again by Lauscher (1976), but this time for the eastern Alps in Austria. He illustrated that there is indeed a difference between the amount and vertical distribution of precipitation depending whether the site was windward or leeward. Figure 2.3 shows the profiles he devised for Austria as a whole, Bregenz (windward situation), and Ötz (leeward situation). It is apparent from the graph that windward slopes at the Bregenz district receive more precipitation and that there is a steep increase at lower elevations with a gradual levelling off higher up. The pattern differs for leeward slopes at Ötz which receive less overall precipitation and a small increase per unit in elevation at low altitudes, but increases more rapidly at higher elevations. A significant observation exhibited by this work is that the elevation-precipitation relationship tends to be quite complex regardless of whether or not other factors are included.

Storr and Ferguson (1972) investigate the distribution of precipitation in several mountainous

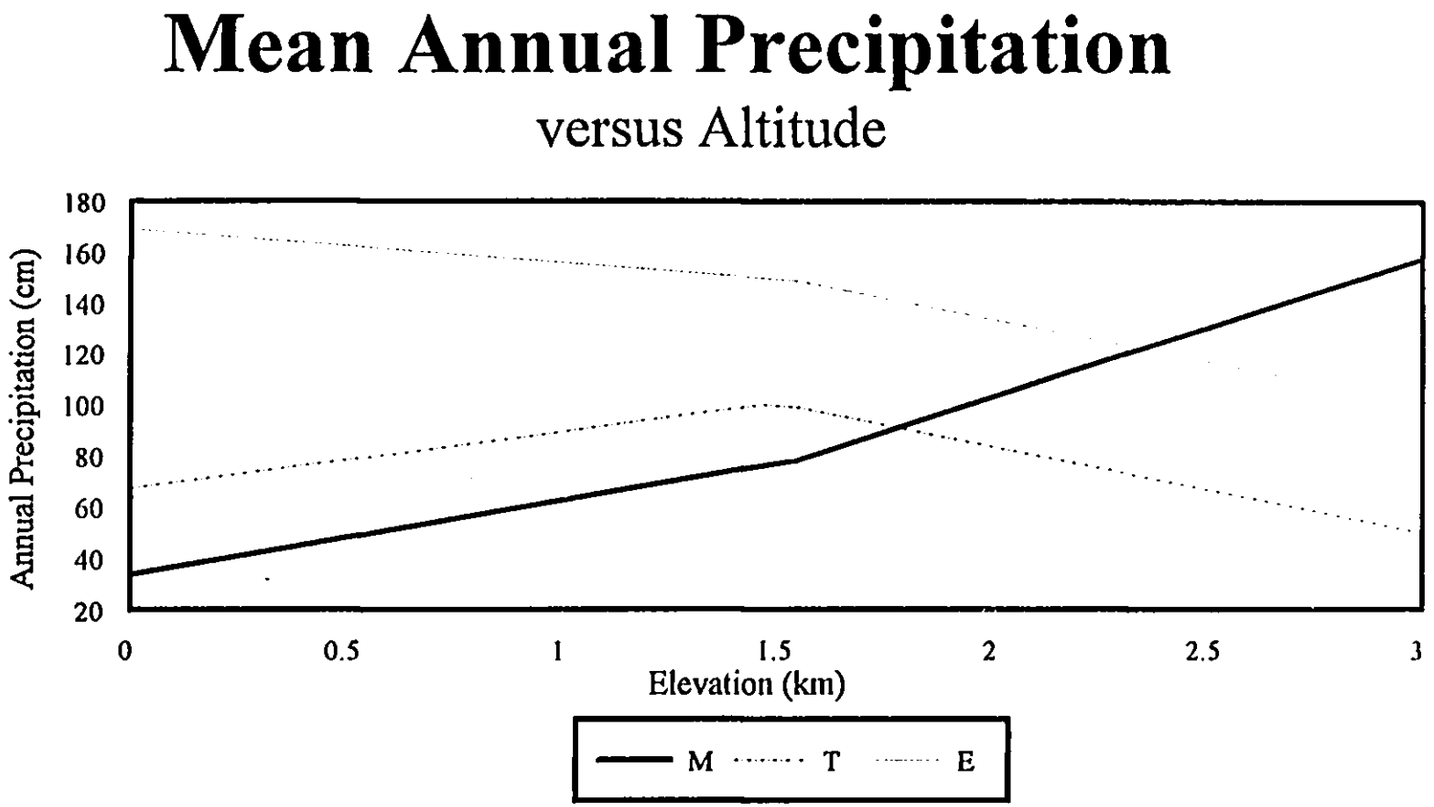

Figure 2.2 Mean annual precipitation versus altitude for the Middle latitudes (M), Tropical climates (T), and Equatorial Climates (E). Source: Barry, 1992 (after Lauscher, 1976).

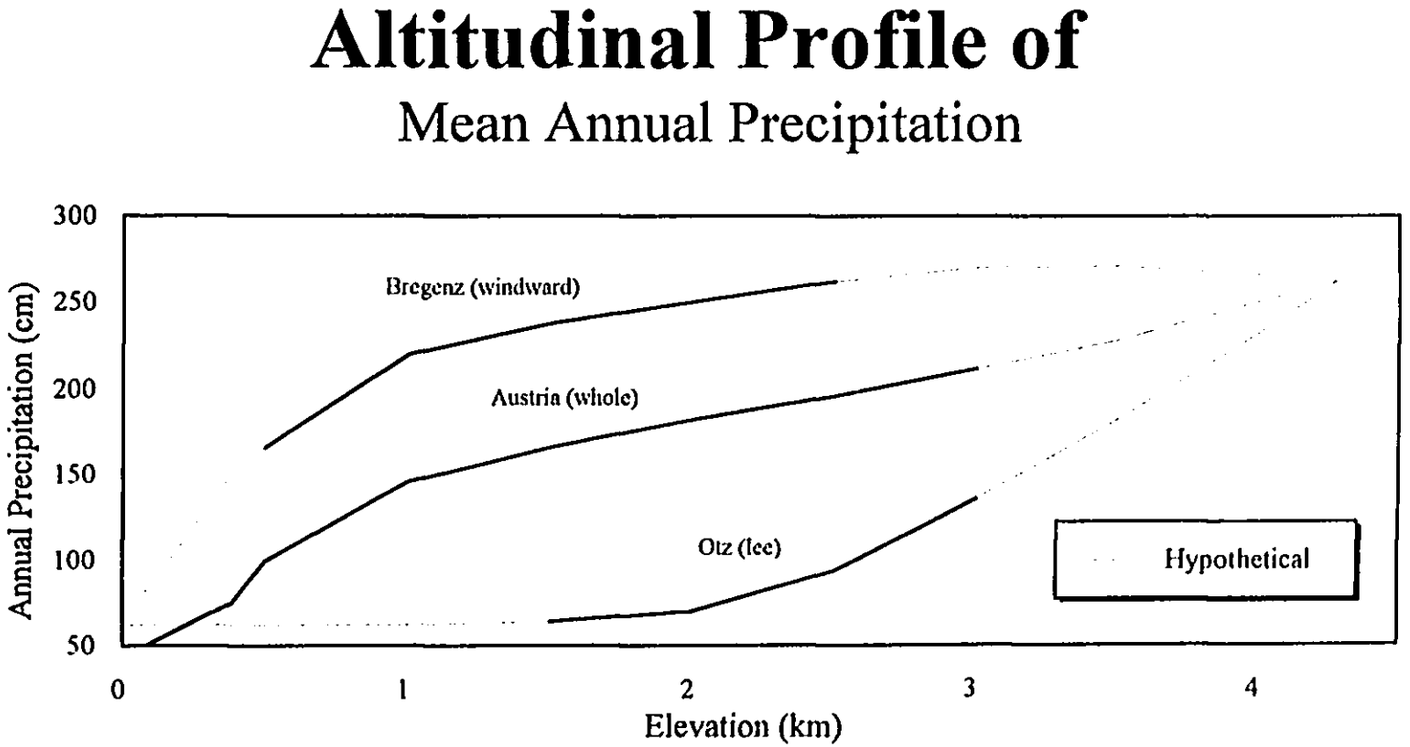

Figure 2.3 Altitudinal profile of mean annual precipitation for two sites in Austria compared with the country as a whole. Bregenz represents a windward location while Ötz is a lee location. Source: Barry, 1992 (after Laucher, 1976).

Canadian watersheds. One particular area they looked at was Marmot Creek Basin which is similar in many ways to the upper Oldman Basin (compare to Table 3.1). It is located on the west side of Kananaskis Valley and just east of the Continental Divide. The elevations range from 1585 to 2805 metres with an average slope of 39 percent and a general easterly aspect. Unlike the Oldman Basin, however, Marmot Creek has one of the densest precipitation gauge networks outside urban areas in Canada. Based on data from 33 sites, they performed a stepwise regression analysis on the mean rainfall. Table 2.1 summarizes the regression results for elevation, slope, aspect, and combinations thereof versus rainfall. The equations described by Storr and Ferguson are as follows:

Summer Precipitation,

$$R = -1.88 + 0.0939H \quad (1)$$

$$R = 1.29 + 0.0909H + 0.169\theta \quad (2)$$

South facing gauges,

$$R = -17.47 + 0.1027H \quad (3)$$

$$R = -10.03 + 0.0975H + 0.160\theta \quad (4)$$

East facing gauges,

$$R = 7.59 + 0.0883H \quad (5)$$

$$R = 1.44 + 0.927H - 0.499\theta \quad (6)$$

Where, R = rainfall (mm)
H = elevation (m)
θ = slope (°)

The results indicate that although the inclusion of slope and aspect increase the correlation coefficient, it also tends to increase the standard error. The authors illustrate, however, that actual isohyetal maps differ significantly from the elevation contour pattern. This confirms that not all variation is determined by elevation alone. Using data from nine storage gauges and two recording gauges they formulate the relationship shown in Figure 2.4. As expected with fewer data points, the correlation is lower and the standard error larger, but the results

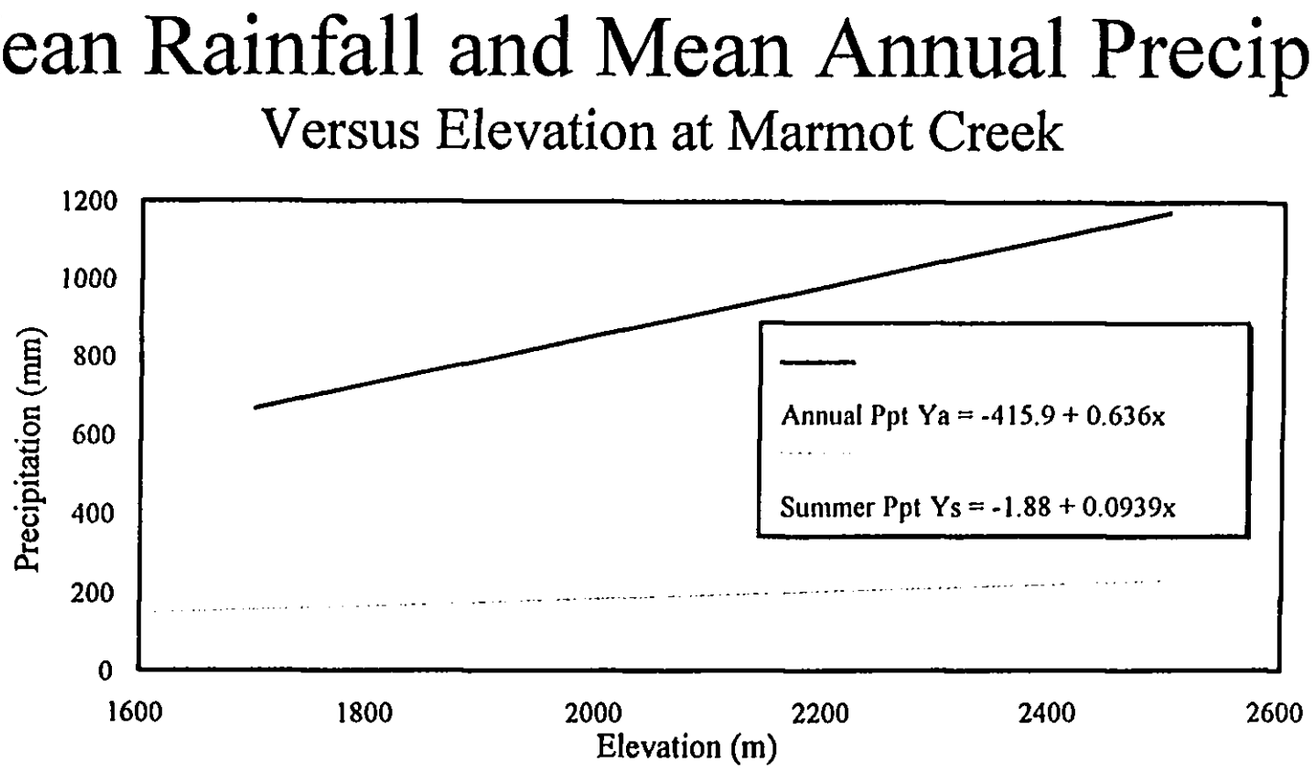

Figure 2.4 Mean rainfall and mean annual precipitation versus elevation at Marmot Creek. Source: Storr and Ferguson, 1972.

are informative regarding several precipitation functions.

Table 2.1 Summary of Marmot Creek regression analysis (Storr and Ferguson, 1972).

Independent Variable(s)		Dependent Variable	r	Standard Error (mm)
Elevation	(1)	Precipitation	.905	10.51
Elevation, Slope	(2)	Precipitation	.906	10.61
Elevation, Aspect(south)	(3)	Precipitation	.948	9.61
Elevation, Aspect(south), Slope	(4)	Precipitation	.945	10.29
Elevation, Aspect(east)	(5)	Precipitation	.942	8.20
Elevation, Aspect(east), Slope	(6)	Precipitation	.941	8.92

Mistaya Basin, adjacent to the continental divide and approximately 120 km northwest of the Marmot Creek site, is the focus of yet another elevation-precipitation study by Loijens (1972). Loijens, like Storr and Ferguson (1972), finds near linear relationships between three years (1970-1972) of spring snow water equivalent measurements and elevation which ranges between 1500 and 2800 metres (see Figure 2.5). Elevation is shown to be responsible for approximately 80% of the variance over the three year period, with slope explaining 10% and 3% for 1970 and 1971 respectively. Slope orientation and forest stand density are found to be insignificantly related at the 95% probability level.

Garen (1995) identifies a similar precipitation-elevation relationship using mean annual precipitation over a ten year period. He uses seven stations ranging in elevation from 1795 to 2676 metres along with their respective data to construct a linear regression which he applies throughout the Wood River watershed in south central Idaho (see Figure 2.6). Taking

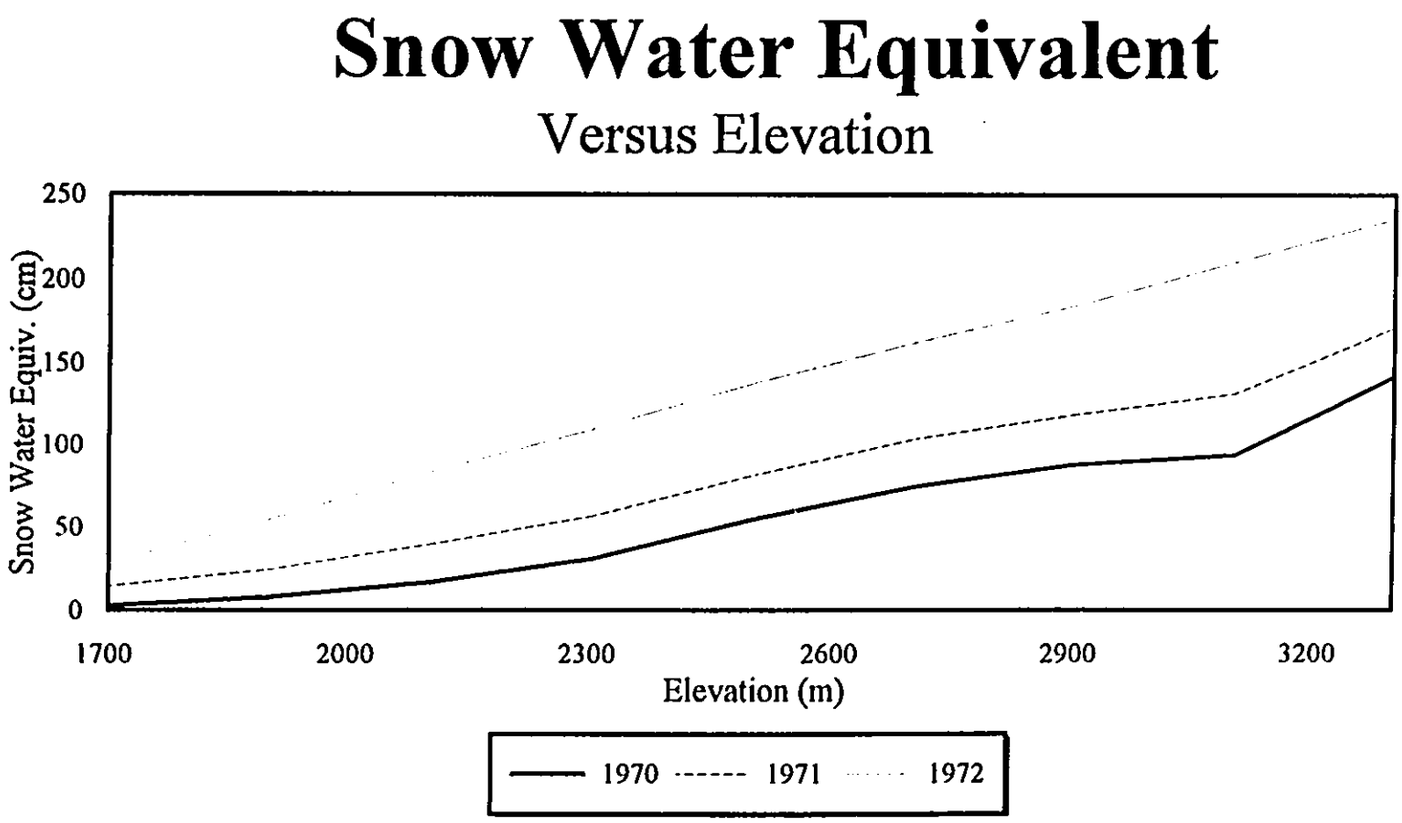

Figure 2.5 Snow water equivalent versus elevation at Mistaya Basin in Banff National Park for the years 1970-1972. Source: Loijens, 1972.

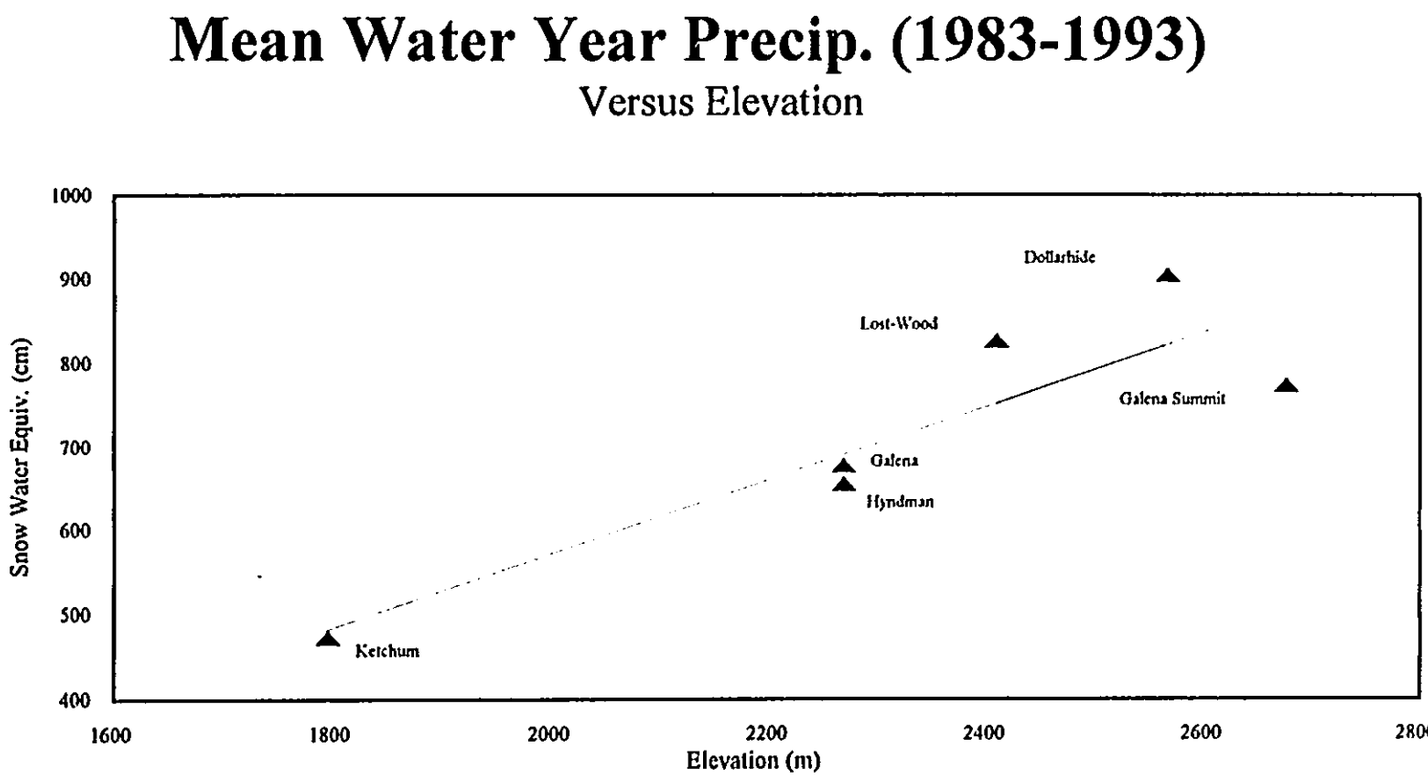

Figure 2.6 Mean water year precipitation (1983-1993) versus elevation for the Wood River watershed in south-central Idaho. Source: Garen, 1995.

into account that elevation is not the sole control, he uses detrended kriging as a means of deriving a weighting factor for each grid cell in the study area which is then employed to adjust estimated precipitation values. The results he presents use a 2.5 km grid cell resolution.

Tecle and Rupp (1995) simulate the spatial and temporal distribution of precipitation events across the Woods Canyon Watershed in north central Arizona. Temporal analysis produces a description of the time between events as well as the precipitation depths and durations of cold-season precipitation. Spatial analysis enables the estimation of event depth and duration across the entire watershed given the measured or simulated precipitation depth and duration at one point. To do this they use multivariate regression equations taking into account elevation, UTM easting, UTM northing, and aspect. Aspect is adjusted such that instead of designating north as 0°, the direction of the prevailing wind is assumed to represent 0° and the leeward direction is set to 180°. In addition, aspect is designed to increase positively both clockwise and counter-clockwise from the windward direction. With these adjustments and regression equations, they use the modelling capabilities of GIS to map the spatial distribution of event characteristics.

On the east slope of the Colorado Front Range, Barry (1973) discovered an almost perfectly linear relationship between mean annual precipitation and elevation from four ridge sites. Regression analysis on his data produces a correlation coefficient r=0.97 for the 1965-1970 mean (Figure 2.7).

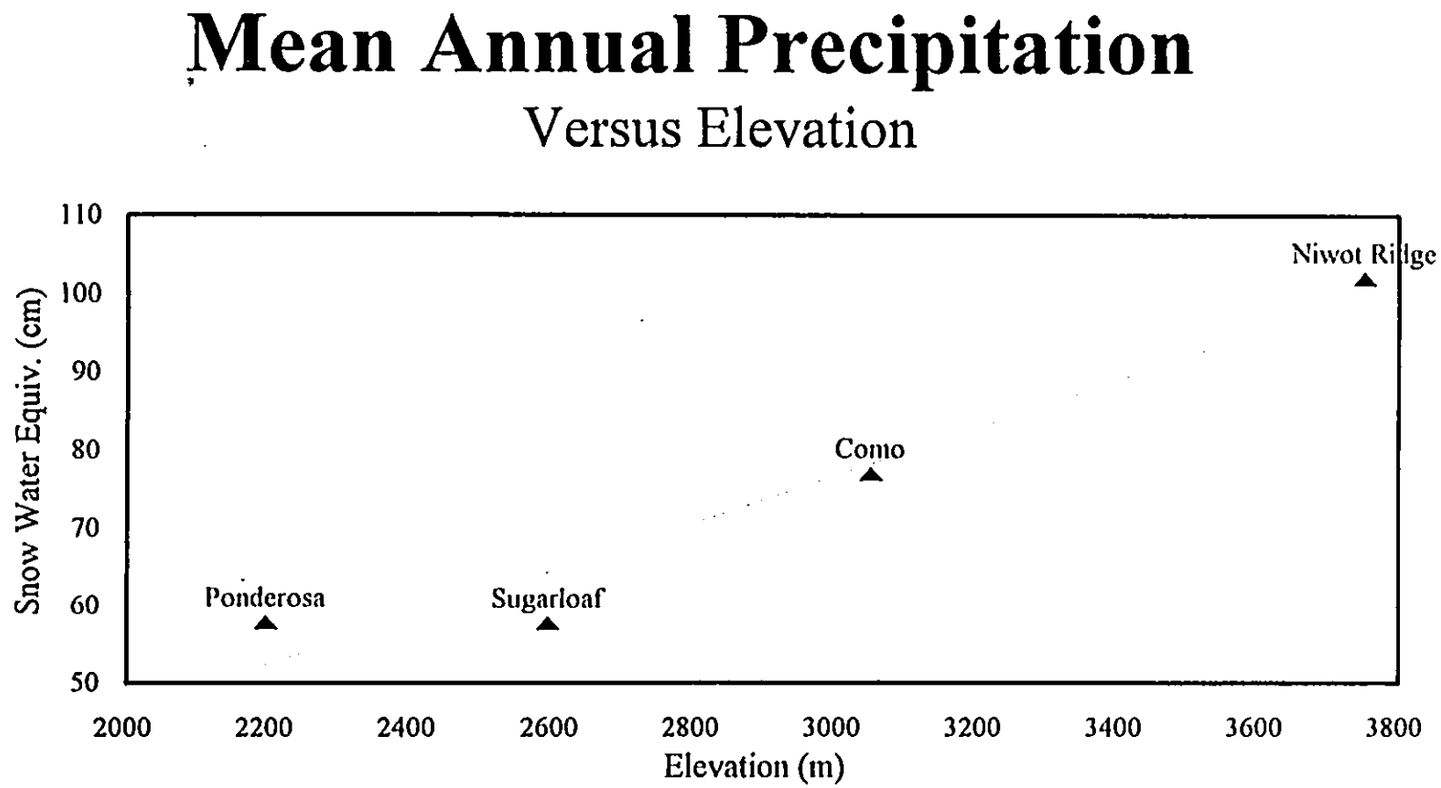

Figure 2.7 Mean annual precipitation versus elevation for the east slope of the Front Range, west of Boulder, Colorado. Source: Barry, 1973.

2.4 Snow Accumulation and Ablation in an Alpine Environment

Accumulation and melting of snow is heavily influenced by many of the same climate controls discussed in relation to both temperature and precipitation. The following sections will elaborate on some of the theories of snow accumulation and ablation as well as review some research which has lead to the formation of these theories. Not unlike total precipitation, relationships between snowcover and elevation, slope, and/or aspect vary from location to location.

2.4.1. Snow Formation

The controls on snowcover distribution and the physics of snow formation are reasonably well known. Input data with sufficient temporal and spatial resolution for accurate estimates are often unavailable, especially in remote areas. The role that each factor plays in determining snowpack amount and character has been investigated where adequate data are available. Gray and Prowse (1993) suggest that in order for snow to form in the atmosphere two conditions must be met: (i) there must be a presence of water vapor and ice nuclei, and (ii) the ambient temperature must be below 0°C. Both conditions are readily met in that most clouds have high percentage of ice crystals. However, whether atmospheric snow reaches the Earth as snow or rain is dependent upon the characteristics of layers of air through which it descends.

Previous discussion herein indicates that snow accumulation occurs earlier and in greater amounts with increasing elevation. Perhaps the best explanation for this phenomenon is the

drop in temperature associated with higher altitudes. As such, precipitation that forms in the atmosphere is more likely to fall as snow in the cooler mountainous regions. Gray and Male (1981) include a figure depicting the mean date of snowcover formation which shows earlier dates occurring in the northern regions of the continent with a finger extending southward along the approximate extent of the Rocky Mountains. According to Gray and Prowse (1993) the amount of snowfall resulting from an individual storm normally decreases with elevation, however, the seasonal snowcover usually increases higher up. The latter, they suggest, is the result of more precipitation events combined with a decrease in evaporation and melt at higher elevations. This also implies that precipitation is only one factor contributing to snow accumulations, the role of melt and sublimation at lower altitudes need also be considered.

As discussed with respect to elevation-precipitation relationships, Loijens (1972), finds near linear relationships between three years (1970-1972) of spring snow water equivalent measurements and elevation which ranges between 1500 and 2800 metres (Figure 2.5). With his dataset of 33 snow courses, he shows that elevation is responsible for on average 80% of the variance over the three year period. Slope appears to explain some of the variation for several years, but is still relatively unimportant overall. Other variables, azimuth and vegetation, he finds are statistically insignificant at the 95% probability level.

Although Gray and Prowse (1993) agree there is a strong linear relationship between elevation and seasonal snowcover, they do not so easily discount the other variables. They

discuss the occurence of major snow accumulations on the lee slopes and in abrupt depressions. As well they suggest a decrease in snow depth with increased upslope distance along slopes oriented in the direction of the prevailing wind. Such conditions certainly suggest that slope and aspect also play a role. The link between vegetation and snowcover distribution is manifested in several ways. First, vegetation modifies the roughness of a surface and, in turn, the wind speed. Combined, these factors effect snow erosion, transport, dispersion, and sublimation. Second, vegetation cover influences energy exchange at the surface. Finally, the amount of snowfall that reaches the ground is related to tree density and species. For example, interception of falling snow is much greater for conifers than for deciduous trees simply because the latter lose their leaves for the winter.

In an attempt to compute mountain snowpack accumumulation and depletion, Wyman (1995) describes an algorithm requiring only daily maximum and minimum temperatures and precipitation. This simplified model responds to the problem of infrequent or nonexistent recorded data in many high altitude watersheds. Wyman essentially describes several mean daily temperatures which define breakpoints determining the composition of falling precipitation. All precipitation below 0.6°C is identified as snow, all precipitation above 3.6°C as rain, and in between as a proportional mix.

In a study correlating snowpack with topography and snowmelt runoff on the Marmot Creek Basin, it is discovered that the variables having the greatest effect on accumulation are elevation, topographic position, aspect, slope, and forest density (Golding, 1974). Forty-eight

percent of the variability in snow accumulation is accounted for in a multiple regression with these variables. The May 1 - June 30 streamflow appears to be most closely correlated with the March snow course water equivalent.

Of significance to any study of areal distribution of precipitation are the three spatial scales of variability outlined by Gray and Prowse (1993). Selection of an appropriate resolution is paramount in the examination if representative snow cover variability is to be identified. Areas up to 10^6 km^2 with distances of 10 to 1000 kilometres are classified as macroscale or regional. Examples of atmospheric effects of similar scale include standing Rossby waves in the atmosphere, directional flow around barriers, and lake effects. Linear distances of 100 metres to 1 kilometre are classed as mesoscale and include such things as snow distribution due to wind, avalanches, terrain variables, and vegetation cover. The final category, microscale, extends over distances of 10 to 100 metres and includes small-scale turbulence generated by the surface roughness and convection, dust devils, and small cumulus clouds. In order to detect and identify phenomenon of interest in this study, microclimate and snowcover, the lower limit of the mesoscale category (100 m) is used.

2.4.2. Measurement of Snowcover

Methods of measuring snowcover are described by Gray and Prowse (1993) and Gray and Male (1981). In general the four types of information that may be measured are snow depth, snow density, areal coverage, and water equivalent. The type of data recorded is directly related to the method of measurement. Methods of measurement include snow ruler, snow pillows, snow surveys, radioisotope snow gauges, aerial markers, snowline flights, aerial

surveys, natural gamma radiation, airborne survey, microwave sensing of snowcover from aircraft, and satellite observations.

The simplest type of data, snow depth, may be obtained using a snow ruler which is pushed through the snow to the ground surface. In remote areas or along frequently read snow courses, snow markers are used. For the aerial marker, snow depth is observed from distant ground points or from aircraft by means of binoculars or telescope.

Snow pillows are pillows made from butyl rubber, neoprene rubber, sheet metal, or stainless steel. They are filled with an antifreeze mixture of methyl alcohol and water or a methanol-glycol-water solution having a specific gravity of 1.0. The fluid pressure inside responds to changes in the weight of snow on the pillow and is measured with a manometer or pressure transducer to provide a snow water equivalent (SWE) for the site. Pillows are most commonly found in the form of an octagon or a circle, but shape does not appear to affect accuracy. Size varies and is determined by estimates of snowcover depths. Generally, larger snow depths require larger pillows in order to provide accurate snow water equivalents (Gray and Male, 1981). Daily SWE is made available through automated onsite data collection and transmission via meteor burst telemetry to a collection office. This form of transmission uses ionized meteor trails as reflectors for VHF radio signals to overcome line of sight limitations (Lettenmaier and Wood, 1993).

Snow surveys are made at regular time intervals, usually every 2-4 weeks depending on

accessibility, and at designated locations throughout the winter to determine depth, vertically integrated density, and water equivalent of a snowcover. A snow course is a permanently marked traverse where snow surveys are conducted (Gray and Male, 1981).

Radioisotope snow gauges are capable of measuring the total water equivalent and/or provide a density profile. They work on the basic principle that water in any state attenuates radiation. Snow accumulates between a radiation source and a detector such that as it accumulates, the count rate decreases in proportion to the water equivalent (Goodison, *et al.*, 1981). Similar technology includes the use of natural gamma radiation which is detected by sensors mounted on aircrafts. Again, the water/snow attenuates the radiation proportionately.

Microwave sensing systems mounted on aircrafts may be either active or passive. Passive systems detect natural radiation emitted by objects while active systems emit radiation and then measure that which is reflected. Since microwave emission changes with depth and wetness of snow, it is possible to derive water equivalents. A major advantage of either of these systems is the ability of microwave radiation to penetrate cloud cover. Examples of microwave systems are discussed by Rango (1990) and Wankiewicz (1990).

The final method of measurement is satellite observation. Satellites such as Landsat, NOAA, and GOES provide, for the most part, areal extent of snowcover. The multispectral capabilities of Landsat, however, also allow for the interpretation of such snow characteristics as dryness, wetness, or whether or not it has been metamorphosed (Goodison, *et al.*, 1981).

2.4.3. Snow Melt

A snowpack is considered "primed" to produce melt when it is at a temperature of 0°C throughout and individual snow crystals are coated with a thin film of water. As well, small pockets of water may be found in the interstices between adjacent grains such that they amount to between 3 and 5% of the total snow by weight. When these conditions are met, the input of any additional energy results in the production of melt water which subsequently drains to the ground.

Detailed analysis of snowmelt runoff characteristics is extremely difficult given the complex internal structure of snow which significantly influences the retention and movement of melt water through the pack. However, during most of the melt period the total melt water produced is governed by energy exchanges at both the upper and lower snow surfaces.

The amount of snow-melting energy available on a daily basis can be calculated using the energy flux equation. This equation is described similarly by both Gray and Prowse (1993) and Gray and Male (1981) as follows:

$$Q_m = Q_{sn} + Q_{ln} + Q_h + Q_e + Q_g + Q_p - \Delta U / \Delta t$$

Where,
Q_m = energy flux available for melt ($kJ/m^2 \cdot d$),
Q_{sn} = net shortwave radiation flux absorbed by the snow,
Q_{ln} = net longwave radiation flux at the snow-air interface,
Q_h = convective or sensible heat flux from the air at the snow-air interface,
Q_e = flux of the latent heat (evaporation, sublimation, condensation) at the snow-air interface,
Q_g = flux of heat from the snow-ground interface by conduction,
Q_p = flux of heat from rain, and
$\Delta U / \Delta t$ = rate of change of internal energy per unit area of snow cover.

While the net longwave radiation and convective heat transfer processes are restricted to the snow-air interface, the net shortwave radiation exchange does penetrate in small amounts into the pack. The latter is strongest, however, also at the upper interface. Melt as a result of the normally modest ground heat flux at the lower surface is generally small. Melt water is produced at this lower interface only when the snow reaches 0°C and the pack is holding its maximum amount of liquid. Rain penetrating into the snowpack results in a more uniform distribution of heat throughout than does the other sources, but energy exchanges at the snow-air interface remain the principal source of melt water.

Although these detailed calculations of energy flux are available, unfortunately input data necessary are not always available. Overall energy balances (Saunders and Bailey, 1994) and specific calculations to determine energy available for melt (Gray and Prowse, 1993) have been proposed for mountainous regions. Saunders and Bailey (1994) summarize some of the research on radiation and energy budgets of alpine tundra environments in North America. They suggest that difficulties ensue when attempting to define generalized alpine radiation and energy balances because of the myriad of possible combinations of slope, aspect, and surface type that may arise.

Once the energy flux available for melt (Q_m) has been calculated it is possible to determine the total daily snowmelt water equivalent using the following equation (Gray and Male, 1981):

$$M = Q_m/(\rho H_f B)$$

Where, M = snowmelt water equivalent (cm/d),
Q_m = energy flux available for melt (kJ/m^2·d),
H_f = latent heat of fusion (kJ/kg),
ρ = density of water (kg/m^3), and
B = thermal quality or the fraction of ice in a unit mass of wet snow.

Latent heat of fusion and the density of water under normal melt conditions equal 333.5 kJ/kg and 1000 kg/m^3 respectively. Inserting these values into the formula results in a further reduction of the equation to:

$$M = Q_m / (3335\ B)$$

The thermal quality or the fraction of ice in a unit mass of wet snow relates back to the statement regarding the percentage of water in a snowpack. It was mentioned previously that a primed snowpack normally contains 3-5% interstitial water of the snow by weight. Thermal quality for such a pack is 0.95 - 0.97.

The physics of snow melt are quite complicated and variation is dependent on the availability of energy. The UBC watershed model accounts for energy resulting from convective heat transfer at the snow-air interface, net radiant energy gain from short and longwave radiation exchanges, and latent heat fluxuations as a result of condensation and evaporation at the snow surface (Pipes and Quick, 1977). A simplified melt calculation uses estimates of these energy sources based on the more readily available air temperature. The mean daily temperature is taken to represent the convective heat transfer while net energy gain is represented by the range between maximum and minimum temperatures. Assuming that the minimum temperature approximates the dew point, condensation and evaporation are functions of the temperature difference between the dewpoint and the freezing point.

Wyman (1995) uses the UBC model to carry out similar calculations of snow melt. Energy sources are the same as those discussed in the previous paragraph so will not be reiterated. Other important parameters mentioned include snow albedo, sublimation, and wind speed. Wyman's model assumes that ground melt and heat from raindrops are negligible in deep mountain snowpacks, thereby simplifying the calculations. When the mean daily temperature is less than 2°C, melt is assumed negligible. Therefore, water equivalent melted during a given day (m_i) is calculated as:

$$m_i = p_m (t - 2)$$

Where, p_m = the point melt factor in millimetres per day per °C
t = the mean daily temperature in °C

The amount of snow melt that can be absorbed by the underlying snow and the changes in snowpack density are also considered.

2.5 MTCLIM Microclimate Simulator

MTCLIM was developed at the Intermountain Research Station in Ogden, Utah as a means of generating climate data for use in fire models, ecological models, insect and disease models, or aiding in the development of silviculture prescriptions (Hungerford, *et al.*, 1989). This section describes the results from linear regression analysis between observed daily solar radiation, air temperature, relative humidity, and precipitation and those simulated by the MTCLIM model for a number of mountainous sites in western Montana.

Solar Radiation:

Recorded solar radiation data is available for only three of the nine test sites. The regression analysis of simulated to actual values produces three regression lines, all with slopes less than

1.0 and all with intercepts greater than zero thereby implying a general overestimation of lower values and underestimation of higher values. R^2 values fall between 0.50 and 0.55. Table 2.2 summarizes the regression results obtained for those Montana sites.

Table 2.2 Predicted vs Observed solar radiation comparisons for three sites in Western Montana (after Hungerford *et al.*, 1989).

Site	Intercept	Slope	r^2	Standard Error of the Estimate	n
Ambrose S.	102	0.78	0.55	102	174
Ninemile S.	143	0.65	0.50	104	146
Coram 12	5.6	0.74	0.50	4.4	184

Although the authors admit the results are not as good as desired, they attribute at least part of the blame to variations in cloud cover between the higher altitude mountain sites and the base stations which are generally found in valley bottoms. They found that the MTCLIM model tended to overestimate for cloudy days and underestimate for clear days. The overestimation could be attributed to the fact that on days when it was partly cloudy in the valley bottoms, the mountain sites were likely to be cloudier. Underestimation occurred on days when the weather was changing, thereby producing a small temperature amplitude. This, in turn, resulted in a lower predicted radiation because the model was simulating for cloudy skies when actually they were clear. The overestimation aspect could be significantly improved using a base station in close proximity to the site as a means of reducing the amout of cloud variation between the two locations.

Daylight Average Temperature:

For simplicity, evaluation of the three predicted temperature values is done separately by the

MTCLIM authors. The first of these, daylight average temperature, is available at all nine stations so is tested most extensively. The results of the regression analysis between predicted and observed values is shown in table 2.3 below. It is obvious that temperature simulations, in general, are very good as R^2 ranges from 0.87 to 0.93 and intercepts from 0.5 to 2.3 °C. The statistics again indicate a slight tendency to overestimate low temperatures and underestimate high temperatures. The authors suspect this phenomena is a reflection of the choice of lapse rate (3.5°F/1000 ft or 6.4°C/1000 m). However, they suggest this to be the best compromise for their study area.

Table 2.3 Predicted vs Observed daylight average temperature comparisons for nine sites in Western Montana (after Hungerford *et al.*, 1989).

Location	**Year**	**Intercept °C**	**Slope**	**r^2**	**Standard Error of the Estimate °C**	**n**
Lubrecht	1980	2.3	0.89	0.92	1.6	131
Coram 14	1976	1.5	0.98	0.89	1.6	160
Coram 33	1976	1.6	1.03	0.88	1.9	174
Coram 12	1976	1.5	0.93	0.87	1.8	163
Ambrose N.	1983	0.5	0.89	0.89	2.1	174
Ambrose S.	1983	1.1	0.91	0.89	2.1	174
Ninemile N.	1983	1.7	0.92	0.89	2.0	146
Ninemile S.	1983	1.0	0.97	0.90	2.0	146
Schwartz N.	1983	0.8.	0.83	0.93	1.6	172

Daily Maximum Temperature:

Unlike daylight average, daily maximum temperature is available at only five of the nine test sites. However, the regression analysis between observed and simulated daily maximum indicates the same tendency to overestimate lower and underestimate higher temperatures as does the daylight average analysis which again the authors attribute to the lapse rate used (MAXLAP). Intercepts range from -0.69 to 2.6 and slopes lie between 0.91 and 1.03. R^2 values are between 0.86 and 0.94. A summary of the regression results may be found in table 2.4 below.

Table 2.4 Predicted vs Observed daily maximum temperature comparisons for five sites in Western Montana (after Hungerford *et al.*, 1989).

Location	Year	MAXLAP °F/1000ft	Intercept °C	Slope	r^2	Standard Error of the Estimate °C	n
Lubrecht	1980	4.5	0.56	0.94	0.94	1.6	131
Coram 33	1976	4.5	2.6	0.92	0.89	2.1	175
Coram 12	1976	4.5	2.1	0.91	0.86	2.3	172
Coram 14	1983	4.5	2.0	1.03	0.92	1.7	173
Ambrose S.	1983	4.5	-0.69	0.96	0.89	2.4	174

Daily Minimum Temperature:

The final temperature value to be simulated, daily minimum, produces slightly less desireable results than the previous two. It appears that due to the effect of frost pockets, cold air drainage, and temperature inversions, prediction is difficult. Simulation accuracy depends on the relative locations of the base and the site. When the base is located in a basin or creek bottom locations, cold air tends to be trapped and a higher lapse rate is required in some

cases. Predictions on mountain slopes tend to require a lower lapse rate and simulate more closely to observed values. Table 2.5 describes the regression analysis results where two lapse rates are tested at each site. Coram 33 and Lubrecht test a minimum lapse rate of 10°F/1000ft because they represent a creek bottom station and a basin location respectively. Another factor found to influence lapse rate is season. The authors determined that minimum temperatures on the slopes are generally warmer than in valley bottoms during the months of September and October due to temperature inversions which they did not account for in their simulations. This effect could likely be offset simply by using a different lapse rate for those months than the rest of the simulation period (May 1 to September 1).

Table 2.5 Predicted vs Observed daily minimum temperature comparisons for five sites in Western Montana (after Hungerford *et al.*, 1989).

Location	Year	MINLAP °F/1000ft	Intercept °C	Slope	r^2	Standard Error of the Estimate °C	n
Lubrecht	1980	10.0 2.0	0.10 3.70	1.05 1.05	0.91 0.91	1.5 1.5	131 131
Coram 33	1976	10.0 2.0	-1.10 3.28	0.98 0.98	0.70 0.70	2.1 2.1	116 116
Coram 12	1976	2.0 0	0.76 2.29	0.76 0.76	0.56 0.56	2.8 2.8	118 118
Ambrose N.	1983	2.0 0	-0.39 2.7	0.77 0.77	0.61 0.61	3.3 3.3	174 174
Ninemile S.	1983	2.0 0	-1.50 0.95	0.97 0.97	0.75 0.75	2.7 2.7	145 145

Relative Humidity:

Relative humidity is evaluated with only three sites since it is not recorded at the other test stations. Regresssion analysis produced intercepts between 19.7 and 23.9, slopes from 0.50

to 0.59, and r^2 values from 0.43 to 0.60 (Table 2.6). Once again the lower values tend to be overestimated while higher values are underestimated. Hungerford *et al.* (1989) suggest this is a reflection of the model's tendency to overpredict lower temperatures and underpredict higher temperatures. Since temperatures at the high end of the scale are lower than observed, relative humidity is simulated higher than observed. The reverse is also true for the overestimation of lower temperatures which causes the relative humidity to be lower than observed. This effect, which is typical of any iterative process, is an example of how minute errors introduced into a model can propagate throughout until subsequent calculations are eventually affected.

Table 2.6 Predicted vs Observed relative humidity comparisons for three sites in Western Montana (after Hungerford *et al.*, 1989).

Location	Intercept °C	Slope	r^2	Standard Error of the Estimate °C	n
Lubrecht N.	19.7	0.59	0.59	9.6	174
Ninemile S	21.4	0.50	0.43	10.9	176
Schwartz N	23.9	0.55	0.60	9.2	176

Precipitation:

Analysis of precipitation prediction is carried out on five different mountainous sites for which data are available. Linear regression is again used to compare observed against simulated daily precipitation for a number of scenarios. First, a comparison is performed to determine the impact of using one or two precipitation base stations and second, analysis is run against simulations for which the site to base isohyet ratios use either 30-year average annual or 5-year May through October average. When two base stations are used, R^2 values range from

0.47 to 0.69, intercepts from 0.01 to 0.03, and slopes from 0.65 to 1.01. However, when only one precipitation base is used, R^2 drops to between 0.23 and 0.57 and the standard error of the estimate increases (Table 2.7). In general, use of two base stations that are in reasonably close proximity to the site will significantly improve simulations. In addition to proximity, base stations should ideally be located at opposite ends of and possess similar prevailling weather paths to the site. Also evident in table 2.7 is the slight improvement of R^2 and reduction of the standard error of the estimate when May through October ratios are applied.

Table 2.7 Predicted vs Observed precipitation comparisons for five sites in Western Montana. The results are given using 1 and 2 base stations, the annual and May through October ratios of precipitation between site and base stations (after Hungerford *et al.*, 1989).

	30-Yr Annual Ratio				5-Yr May-OctRatio			
Location	Intercept	Slope	R^2	SEE[1]	Intercept	Slope	R^2	SEE[1]
Garnet								
1 base	0.03	0.84	0.30	0.22	0.03	0.70	0.30	0.19
2 base	0.02	0.80	0.47	0.15	0.02	0.77	0.49	0.14
Bozeman I2NE								
1 base	0.02	1.04	0.35	0.32	0.02	0.72	0.35	0.22
2 base	0.02	1.04	0.50	0.23	0.02	0.72	0.51	0.16
Summit								
1 base	0.05	0.73	0.23	0.27	0.03	0.49	0.23	0.18
2 base	0.03	0.84	0.54	0.16	0.02	0.65	0.59	0.11
Deception Creek								
1 base	0.03	0.94	0.57	0.22	0.03	0.78	0.57	0.18
2 base	0.03	0.89	0.68	0.17	0.03	0.73	0.68	0.14

	30-Yr Annual Ratio				5-Yr May-OctRatio			
Location	Intercept	Slope	R^2	SEE[1]	Intercept	Slope	R^2	SEE[1]
Garnet								
1 base	0.03	0.84	0.30	0.22	0.03	0.70	0.30	0.19
2 base	0.02	0.80	0.47	0.15	0.02	0.77	0.49	0.14
Bozeman I2NE								
1 base	0.02	1.04	0.35	0.32	0.02	0.72	0.35	0.22
2 base	0.02	1.04	0.50	0.23	0.02	0.72	0.51	0.16
Pierce								
1 base	0.01	0.94	0.57	0.18	0.01	0.89	0.57	0.17
2 base	0.01	0.83	0.68	0.12	0.01	0.84	0.69	0.12

[1] Standard error of the estimate

Chapter 3

STUDY AREA

3.1 Description

For the purposes of this research, it was decided that the study area would be the upper Oldman River basin. The lower bound of this drainage basin is defined by the hydrometric gauging station near the intersection of the Oldman River and Highway #22 (South-western Alberta). To the west, the basin is bounded by the continental divide separating British Columbia and Alberta. The Whaleback Ridge marks its extent to the east. Coleman and Blairmore are located just south of the basin while Pekisko lies to the north. (Figure 3.1)

The basin covers an area of approximately 1445 square kilometres, most of which is covered by needleleaf evergreen boreal forest. The boreal forest of North America is composed mainly of evergreen conifers such as spruce and fir (Strahler and Strahler, 1979). The rugged mountainous terrain with slope angles as high as 68° ranges in elevation from 1267 metres at the outlet to 3099 metres at Tornado Mountain. Table 3.1 summarizes the basin land use and physiographic characteristics as percentages of total area. Figure 3.2 illustrates the average monthly meteorological conditions for the Pekisko climate station.

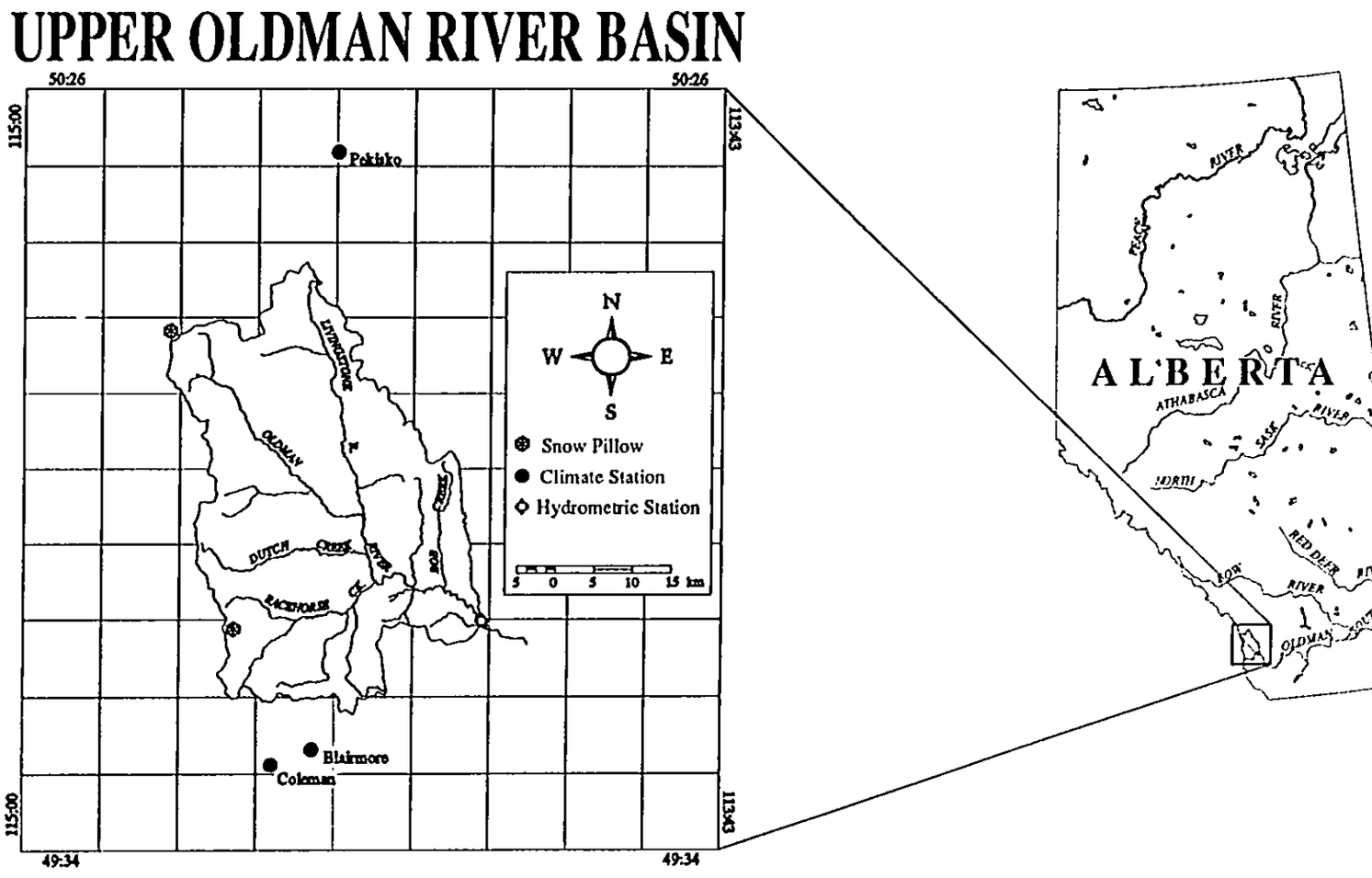

Figure 3.1 Upper Oldman river basin study area location, southwestern Alberta

Table 3.1 Summary of Land Use and Topography for the Upper Oldman River Basin.

MAP LAYER	% OF TOTAL AREA
Land Use	
Forested	80.43
Non-forested	19.43
Water	0.14
Slope (%)	
0 - 42	74.94
43 - 102	23.93
103 - 250	1.13
Elevation (m)	
1200 - 1400	2.75
1401 - 1600	14.21
1601 - 1800	26.03
1801 - 2000	28.82
2001 - 2200	19.04
2201 - 2400	7.02
2401 - 2600	1.72
2601 - 2800	0.36
2801 - 3000	0.05
3001 - 3200	0.003
Aspect	
North	20.00
South	21.00
West	25.00
East	34.00

TOTAL BASIN AREA = 1445 km^2

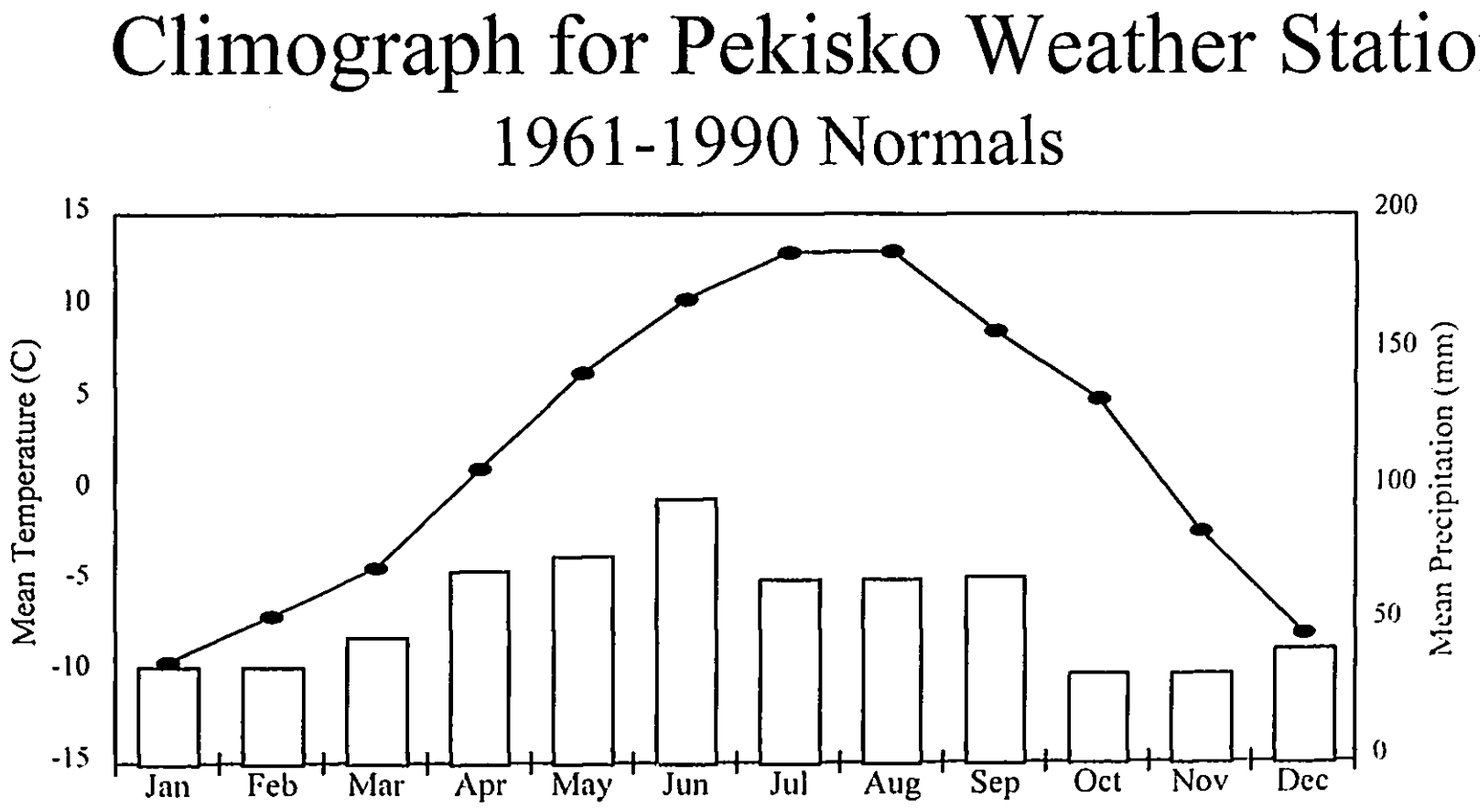

Figure 3.2 1961-1990 normal meteorological conditions for Pekisko, Alberta. Derived from daily data recorded at the AES-operated climate station.

The streamflow gauging station is described by Environment Canada's Water Resources Branch as the Oldman River near Waldron's Corner, Station no. 05AA023; 49° 48' 50" N latitude, 114° 11' 00" W longitude (Environment Canada, 1985).

3.2 Data Availability

This project is founded on the integration of multiple data sources in such a way as to improve simulations in alpine regions. The following sections describe the individual datasets as they have been employed here.

3.2.1 1:50000 National Topographic Series

Initially, some consideration was given to the possibility of using 1:20000 scale NTS maps because of their relatively high positional accuracy. However, upon investigation it was found that because of its relatively large expanse, the drainage basin falls on six 1:50000 NTS mapsheets which translates into approximately twelve 1:20000 mapsheets. The larger scale may have provided a higher level of accuracy, but the cost of time dedicated to manual digitizing would greatly outweigh the potential benefits. In addition to the time, individual file size and total hard disk space required would be less manageable.

Another reason for going with the smaller scale is related to the nature of the phenomena being modeled. A major focus of the study deals with hydrologic and meteorologic phenomena. Since these are rarely small scale, discrete entities, it was decided that the 1:50000 scale maps would suffice. Reference back to the discussion in Chapter 2 indicates that these effects generally take place at the scale described as mesoscale. Mesoscale events

are characterized by areal extents between 100 metres and 1 kilometre.

The key point is that the environmental conditions of interest in this case, namely alpine temperature and precipitation, fall well within the category identified as mesoscale, if not macroscale. As a result, very little is lost by going with the smaller scale maps. Table 3.2 provides the particulars regarding the NTS mapsheets utilized.

Table 3.2 NTS Mapsheets obtained from Maps Alberta.

SHEET NO.	TITLE	SCALE	PRODUCTION DATE
82G/9	BLAIRMORE	1:50000	1967
82G/10	CROWSNEST	1:50000	1980
82G/15	TORNADO MOUNTAIN	1:50000	1980
82G/16	MAYCROFT	1:50000	1970
82J/1	LANGFORD CREEK	1:50000	1980
82J/2	FORDING RIVER	1:50000	1975

3.2.2 Digital Elevation Model

Raw digital elevation data was purchased from Alberta Environmental Protection, Land Information Division in Edmonton. The X, Y, Z data is extracted to a file such that it is formatted into fixed-width columns. It is then imported into the geographic information system where a digital elevation model (DEM) is created.

Digital elevation data are available at a scale of 1:20000 with optional grid spacings of 25, 50,

and 100 metres. In addition to the regular grid of X,Y,Z information, it contains spot heights and breaklines. The data is an ASCII file which conforms to the Digital Map Data Format (DMDF) (Alberta Environmental Protection, 1988).

For reasons similar to those mentioned in the previous section, detail is sacrificed somewhat in order to keep data as simple as possible. For this model it has been decided to utilize the 50 metre grid as it is not so generalized that significant detail is lost, yet there is not such an overwhelming volume of data as with the 25 metre grid. Also, given that manual digitizing is done from 1:50000 mapsheets, any spacing less than 50 metres is difficult to resolve and is within a margin of error associated with manual digitizing.

3.2.3 Historic climate station data

Historic climate data are supplied by Atmospheric Environment Service (AES) in the form of daily or monthly averaged temperature and precipitation. Table 3.3 summarizes the data availability for both Coleman and Pekisko observation stations. Beaver Mines is a possible alternate base station to the south of the basin since it too has recorded temperature and precipitation. Unfortunately, Beaver Mines is further from the basin than Coleman and MTCLIM simulation is dependant on the horizontal distance between base station and site.

Table 3.3 Climate Station Summary

STATION ID	NAME	LAT (dd:mm)	LONG (dd:mm)	ELEV(m)	LENGTHO F RECORD	DATA TYPE (T / P)
3051720	Coleman	49:38	114:35	1341	1965-1989	T,P (daily)
3055120	Pekisko	50:22	114:25	1439	1905-1989	T,P (daily)
3050600	Beaver Mines	49:28	114:10	1286	1935-1989	T,P (daily)

3.2.4 Snow Data

Recorded snow pillow and snow course data that fall within the study area is sparse. In consultation with Dick Allison at the Lethbridge office of Alberta Environment's Technical Services Division, it was discovered that only two snow pillows fall either inside or within close proximity of the basin. They include the Racehorse Creek pillow located at 49° 49' N latitude, 114° 38' W longitude and the Lost Creek pillow located at 50° 10' N latitude, 114° 43' W longitude. The Racehorse pillow has been in operation from 1983 to present while the Lost Creek pillow has only been in operation since 1987. Snow course data also exist for these two points.

Chapter 4

METHODOLOGY

4.1 Use of a Geographic Information System

It was decided early in the program that a geographic information system (GIS) would be ideally suited to the task of modelling basin hydrometeorology in mountainous terrain. As described in the Alpine Hydrology section, the hydrologic cycle is driven primarily by such influences as temperature and precipitation which are, among other things, a function of elevation, latitude, and time of year. In the context of this research project, GIS is a computer-based system capable of capture, management, manipulation, analysis, modelling, and display of spatially referenced data. Since the distribution of temperature and precipitation are inherently spatial, GIS lends itself as an excellent tool to aid analysis.

In the initial stages, PAMAP GIS is used primarily for data collection. PAMAP is a vector-based software with raster data handling capabilities. Its strengths lie in natural resource applications as it was originally developed for such purposes. This characteristic was key in the decision to use PAMAP instead of some other GIS package.

As with any project of this sort, the most time-consuming task is the creation of a spatially referenced database for the area of interest. This is achieved by manually digitizing topographic, hydrographic, and land use information from paper maps. Many of these data are available in digital format, but the costs are prohibitive. Therefore, it was decided to digitize as much as possible. A major drawback with manual digitizing is not only that it is a time consuming process, but also that it introduces positional errors into the database. These errors are practically impossible to eliminate given the physical limitations of human dexterity and thus are also included in commercially available datasets. However, it is hoped that data sold commercially is systematically scrutinized for accuracy and consistency.

One of the first layers to be collected is the hydrography. Included in these data are rivers sufficiently large that they are described as double-sided, their tributaries, and lakes (figure 4.1). The double-sided rivers and lakes are stored as polygonal information while the narrower tributaries are defined strictly as vector data. In addition to the water bodies, the boundary defining the drainage basin is also captured. It too is stored in polygon format. The final layer to be digitized is the land cover polygons. For lack of another source for this information, the general distinction between forested and non-forested land found on 1:50000 NTS maps is used. It was decided that for the spatial scale at which calculations are performed, these data are sufficient. The ideal alternative would, of course, be to use classified satellite imagery but the cost for such information is prohibitive at this time and may easily be incorporated at a later date.

Hydrographic Network

Upper Oldman Basin

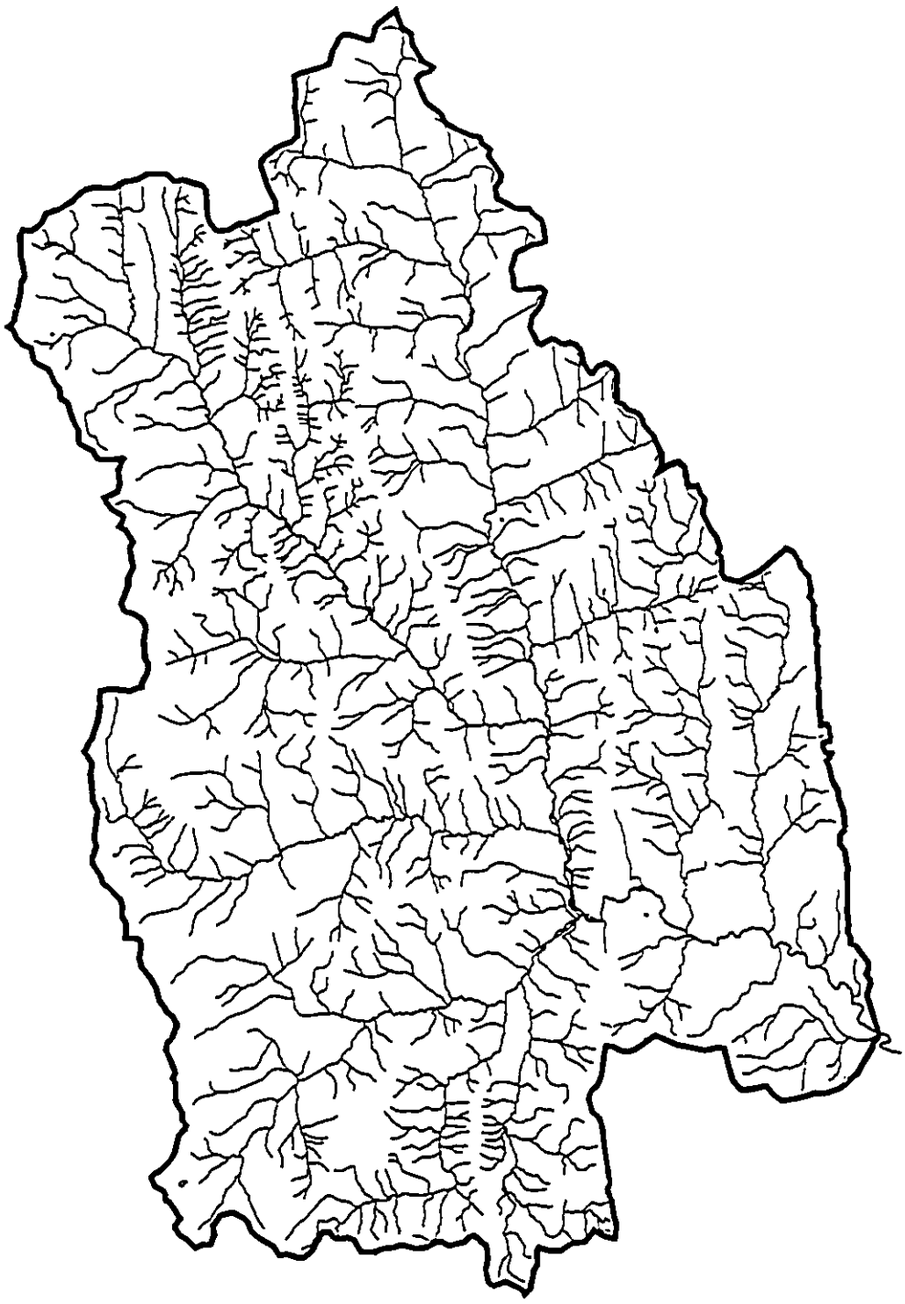

Figure 4.1 Double and single-sided rivers, major lakes, and drainage basin boundary as digitized from 1:50000 NTS mapsheets.

Before further discussion of data layers is provided, it is important to make a distinction between the two ways of representing areal information in PAMAP GIS. A surface is composed of a series of regularly spaced pixels with each pixel having only a single value assigned to it. Surface levels are used to represent elevation, slope, aspect, or proximity buffers, for example. Like the surface, a polygon cover too is composed of regularly spaced pixels. Each pixel on a polygon level, however, is linked to a particular polygon and its associated database. While a surface can have only one attribute value (ie. elevation), a polygon can have up to 100 attributes including those inherent to the GIS (ie. Record Number, X_Coord, Y_Coord, etc). Also, each pixel on a surface represents an average, be it weighted or non-weighted, of surrounding point information within a specified scan radius. Each pixel on a polygon coverage is categorized as being either inside or outside an area enclosed by vectors.

As mentioned in the data sources section, the raw digital elevation data for the area was purchased from Alberta Environmental Protection thus saving many hours of painstaking work. From the 50 metre spaced point data, was derived a digital elevation model (DEM) surface in PAMAP. Each pixel in the basin received a value for elevation in metres that represents a weighted average of surrounding points. Since point density is every 50 metres, each pixel uses a number of surrounding point values on which to base its interpolated elevation. From the DEM surface may be derived two other related physiographic surfaces, slope and aspect. Because of the microclimate simulator requirements, slope is derived as a percent slope and aspect is derived as an azimuth from 0°-360° (0° = north facing and 180 °

= south facing). Maps of the DEM, slope, and aspect surfaces are illustrated in figures 4.2 through 4.4 respectively. Figure 4.5 depicts the land cover polygons. The yellow areas represent non-forested land or open alpine meadow. The remainder of the basin is forested with evergreen tree species.

4.1.1 Grid-Point Spacing

Originally, it was believed it would be necessary to generate an evenly spaced grid of points over the study area and from it create a point database. These points were to be used as the study sites described later in the microclimate simulation section. Once a point database had been defined, it would be overlaid with the DEM, the slope, the aspect, and the land cover layers in order to append their respective attributes. The point database would then be exported to an ASCII file with the information necessary for use as input into the microclimate simulation model.

However, PAMAP can quite easily export a surface or polygon coverage with the Topographer/Report utility. Grid point spacing is dependant upon pixel size (ie. a point is output for each pixel containing data). For this study, DEM surfaces have been created at pixel sizes of 100, 200, and 500 metres. Since slope and aspect are derived from the DEM, their respective pixel sizes are also 100, 200, and 500 metres. The result is a series of ASCII files containing *easting, northing, and attribute,* where *attribute* is one of elevation, percent slope, aspect, and percent forest coverage.

4.1.2 Relating the Information

After exporting the surface information from PAMAP, it is necessary to merge the individual

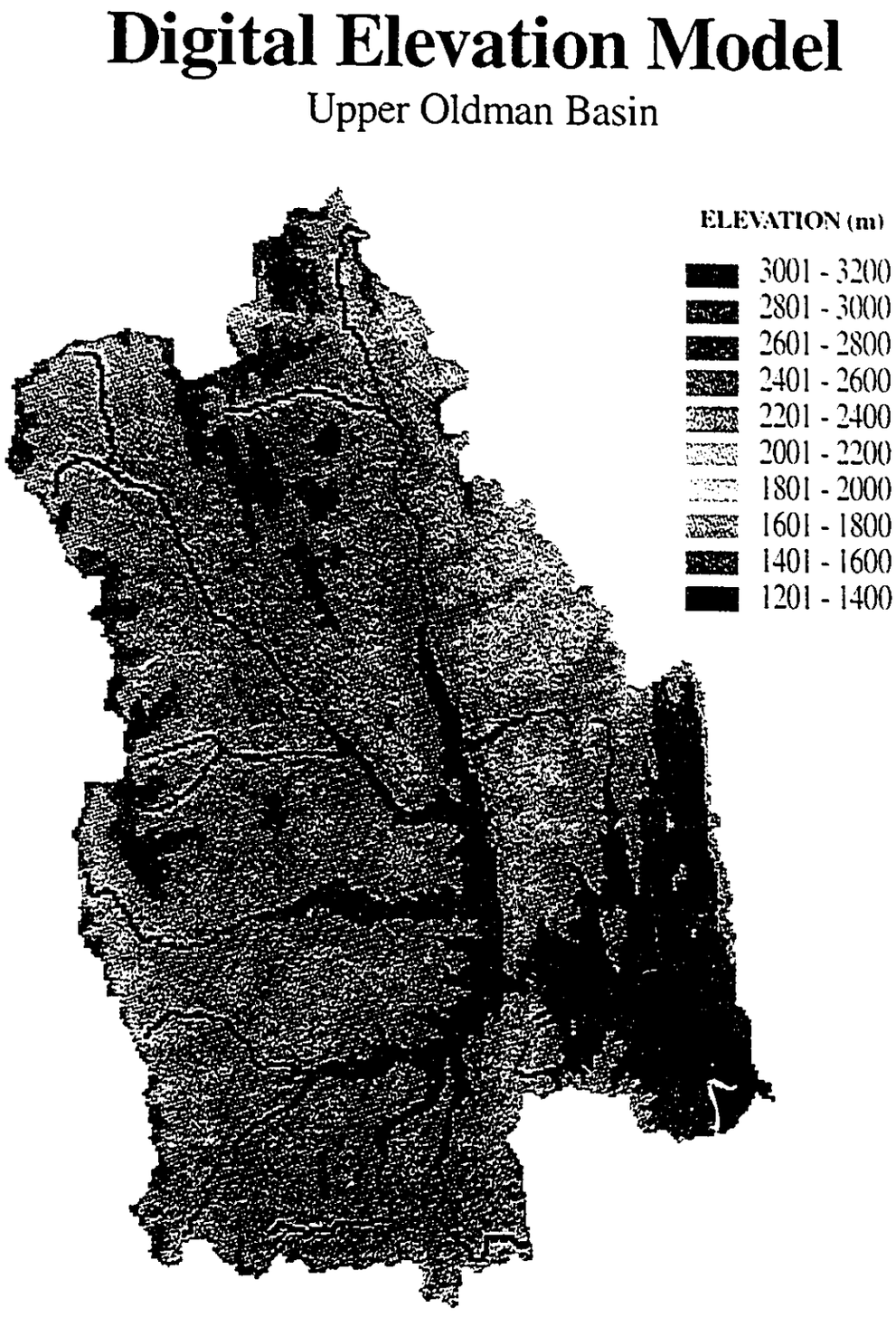

Figure 4.2 Digital Elevation Model (DEM) created using 50 metre regular space grid from Alberta Environmental Protection. Pixel size is 100 metres.

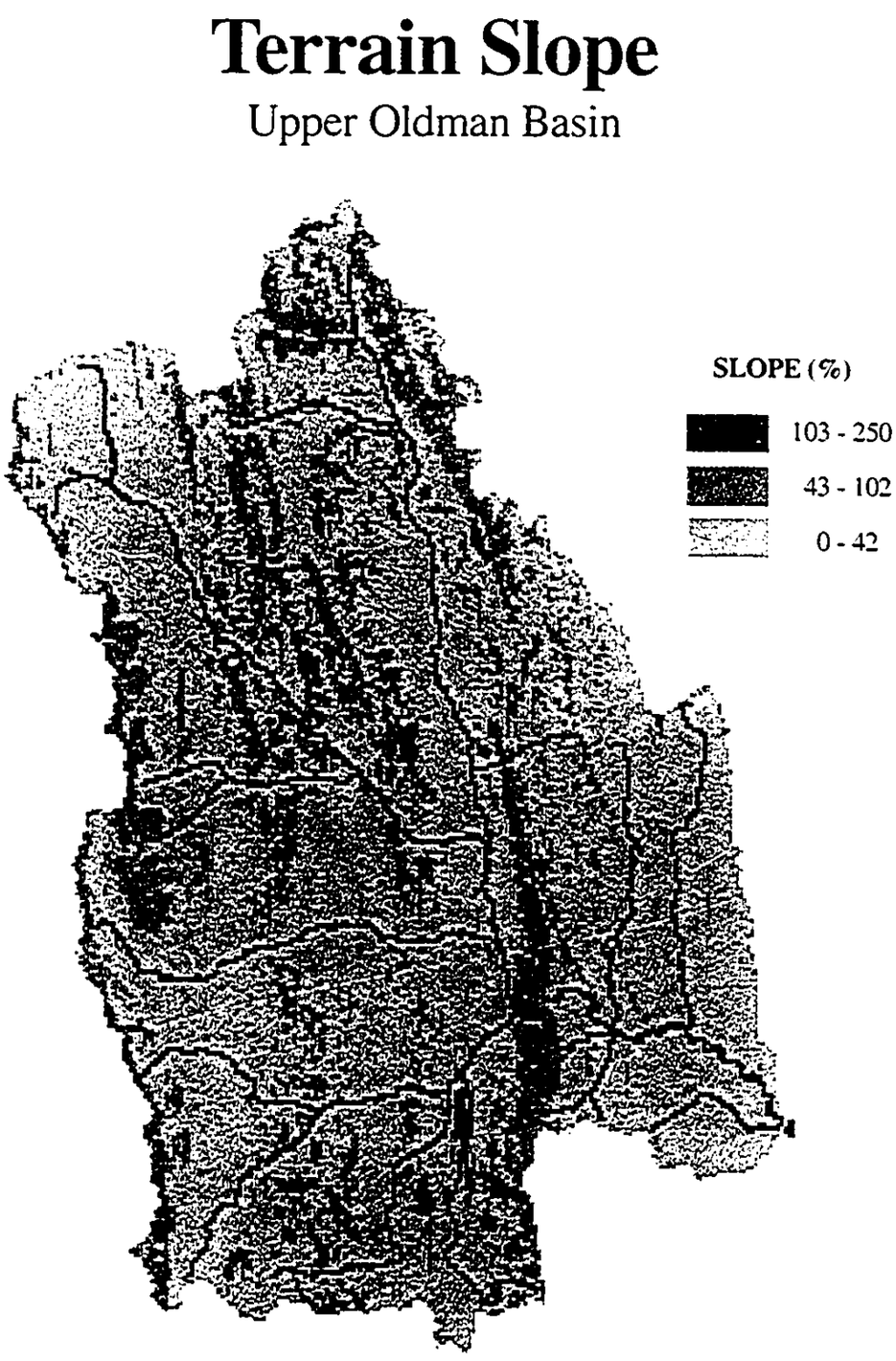

Figure 4.3 Terrain slope as derived from the digital elevation model (DEM). The three classes represent approximately 23° slope each. Pixel size is 100m.

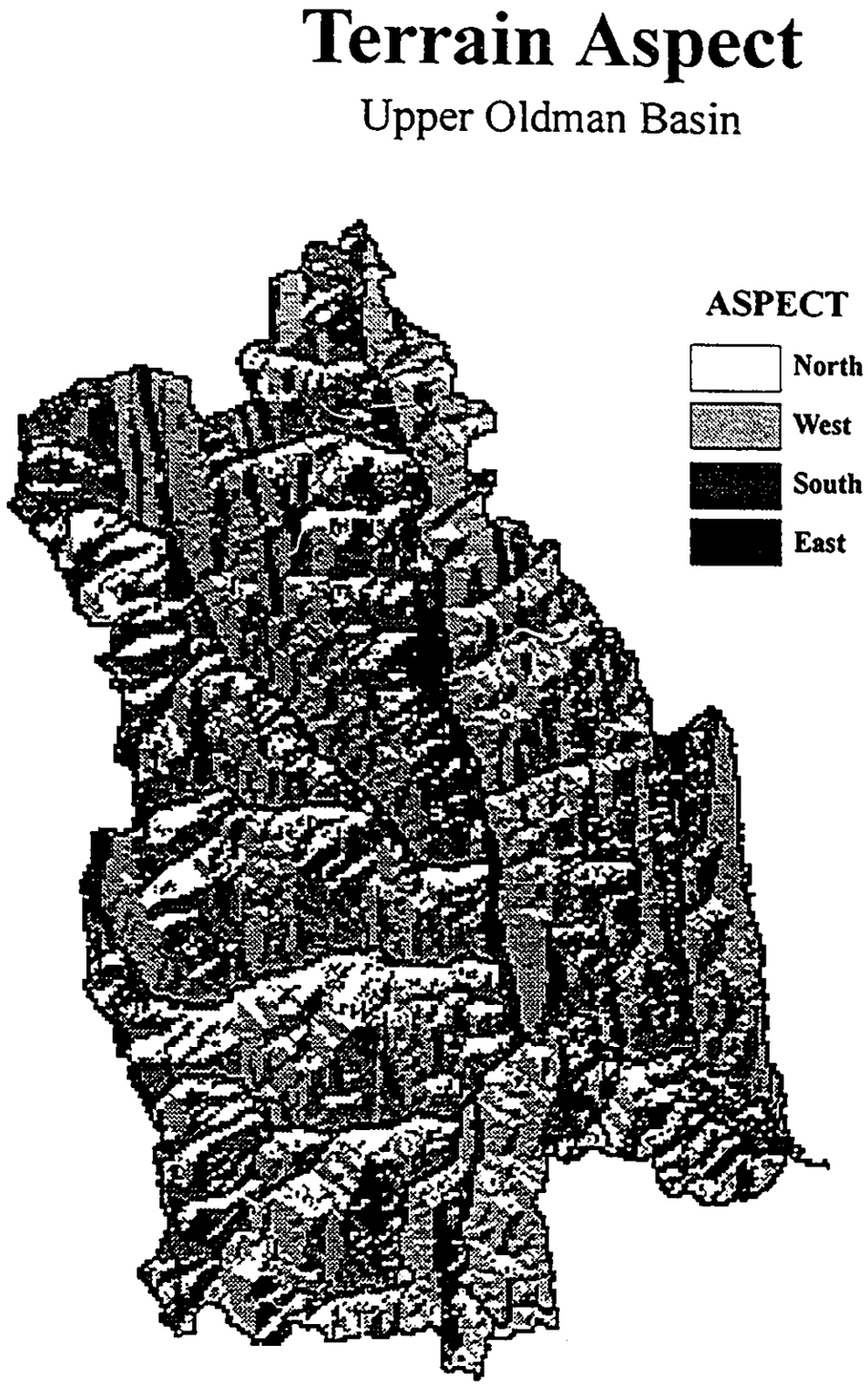

Figure 4.4 Terrain aspect as derived from the digital elevation model (DEM). Pixel size is 100m.

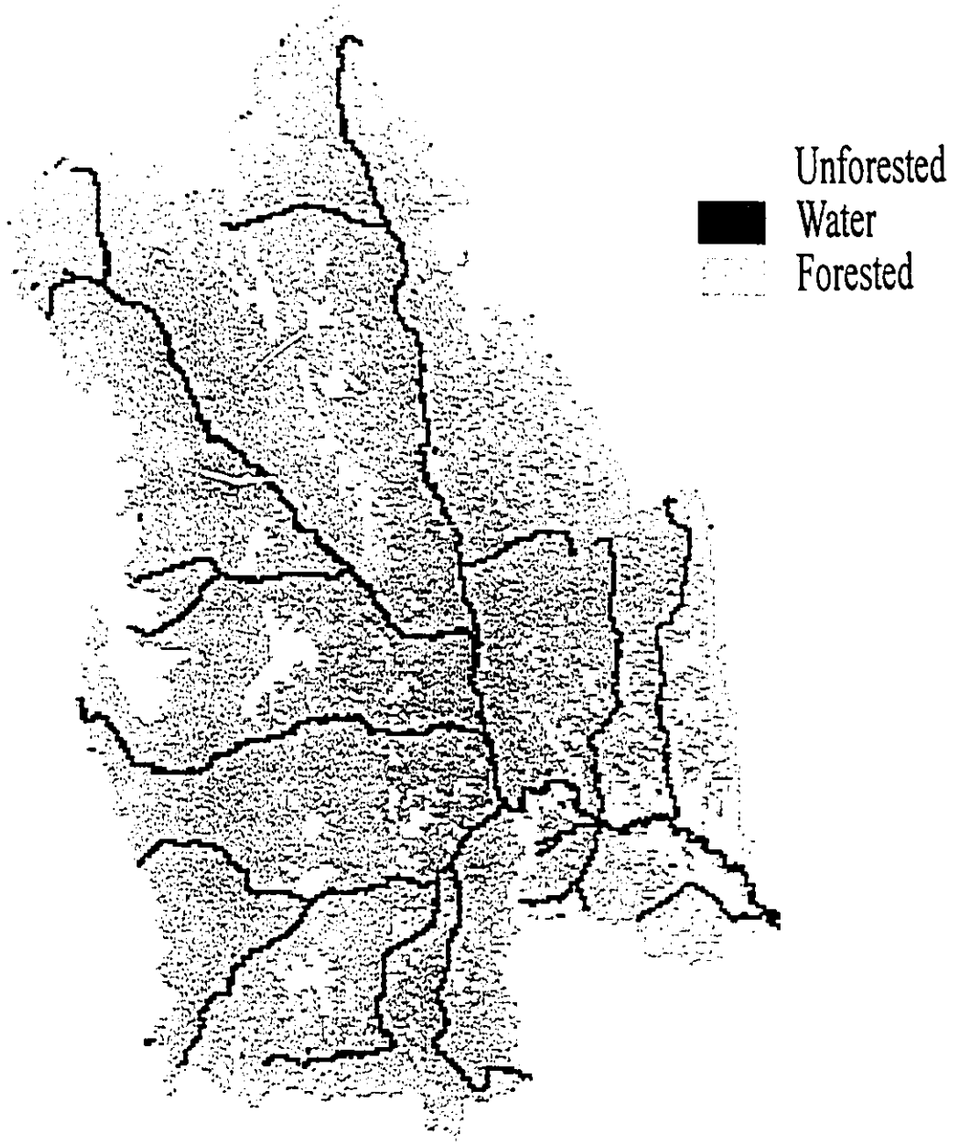

Figure 4.5 Land cover as digitized from the 1:50000 NTS mapsheets. Pixel size is 100m.

attributes into a single file for simplification of later calculations. Dbase IV provides the tool by which to join the surface and polygon data into one file. First, three database skeletons are set up to accommodate X,Y coordinates along with their attribute values (one file for each of elevation, slope, and aspect). The ASCII files are then appended into their respective database skeletons. Finally, the newly created databases are related by easting and northing at which point they are merged into yet another database skeleton called SITES.DBF. Appendix B illustrates the specific structure definition used in SITES.DBF. It should be noted that field type and size definitions are unchanged from those used in the individual databases prior to merging.

A noteworthy advantage of dBase is its direct link with PAMAP. The version of PAMAP used for this study has been setup such that dBase is designated as the external database management system for handling point, line, and polygon databases. Another important advantage is dBase's ability to quickly and easily summarize numeric information (ie. mean, min, max, SD, sum, etc.) through reporting utilities.

4.2 Single-Site Microclimate Simulation

The basis for microclimate simulation is founded in the Fortran program, MTCLIM, developed at the Intermountain Research Station in Ogden, Utah (Hungerford *et al.*, 1989). Roger Hungerford was a research forester at the Intermountain Fire Sciences Laboratory in Missoula, Montana, while Ramakrishna Nemani, Steven Running, and Joseph Coughlan all

were part of the University of Montana's School of Forestry. Their code and documentation is used extensively in the early stages of algorithm development for dealing with multi-site simulation. The following few sections describe the theory, data requirements, and overall workings of the original program.

4.2.1 Model Theory

The primary function of MTCLIM is the extrapolation of meteorological conditions for a single point of interest from another point at which conditions are recorded. In MTCLIM terminology, the location to be simulated is referred to as the *SITE* and the station for which records exist is known as the *BASE*. Generally speaking, this is accomplished by making corrections to *BASE* meteorologic data for changes in elevation, slope, and aspect between the two points.

Figure 4.6 is a flowchart of the model subroutines as adapted from Hungerford *et al.* (1989). As the figure shows, included in the program are subroutines to calculate daily air temperature, incoming solar radiation, humidity, and precipitation.

Air Temperature

MTCLIM calculates three air temperature values per day for each *SITE*: daily maximum, daily minimum, and daylight average. The first two are obviously the highest and lowest temperatures for a day. The third represents the temperature averaged over the daylight hours. Since it is assumed that the daily minimum occurs sometime near sunrise, daily maximum around midday, and sunset to occur somewhere in between, the model utilizes a sine wave to approximate the daylight average temperature. The equation used to calculate

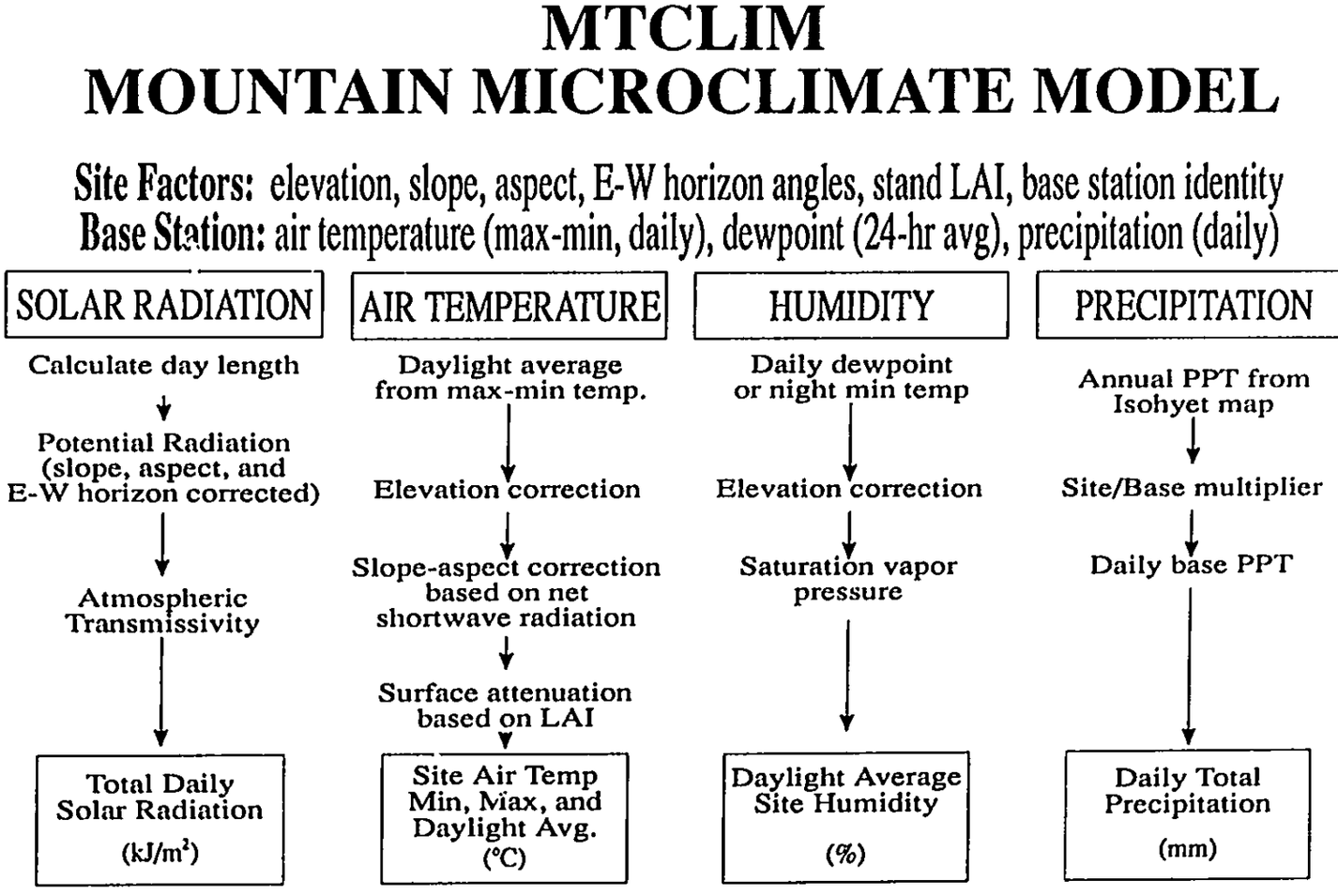

Figure 4.6 Flowchart of the MTCLIM model (after Hungerford, *et al.*, 1989).

the daylight average is:

$$T_{ave} = TEMCF * (T_{max} - T_{mean}) + T_{mean}$$

where,

T_{ave} = weighted average daylight air temperature for the *BASE*,
TEMCF = coefficient to adjust daylight average temperature (0.45 in MTCLIM),
T_{max} = daily maximum temperature
T_{mean} = arithmetic mean for the day $[(T_{max} + T_{min})/2]$

The weighted average daylight temperature is next corrected for elevation, cloud cover, and aspect. The elevational lapse rate used for western Montana is 6.4°C/1000 metres (or 3.5°F/1000 feet). This value is increased by ten percent on clear days and decreased by ten percent on cloudy days. According to simulation test results reported later in this chapter, the lapse rate of 6.4°C/1000 metres also appears to be appropriate for southern Alberta. Theoretically, this should be the case since southern Alberta and western Montana are alike in many ways. Both fall on the east slopes of the Rocky Mountains with similar terrain variation, both experience a similar climate, and they are in relatively close proximity to one another. Finally, aspect determines whether temperature is increased (south facing slopes) or is decreased (north facing slopes) according to the following formulae:

South aspects:

$$T_{site} = T_{ave} - T_{lap} ((SE-BE)/1000) + (RADRAT * (1-(SLAI/MLAI)))$$

North aspects:

$$T_{site} = T_{ave} - T_{lap} (SE-BE)/1000 - (1/RADRAT) * (1+(SLAI/MLAI))$$

where,

T_{site} = final calculated *SITE* temperature,
T_{ave} = BASE station daylight average air temperature as above,
T_{lap} = elevational lapse rate correction,
SE = *SITE* elevation,
BE = *BASE* elevation,
RADRAT = ratio of slope radiation/flat surface radiation,

SLAI = *SITE* leaf area index,
MLAI = maximum leaf area index is 10.

Solar Radiation

The equations for calculating the daily solar radiation are extremely complex. Considered are many parameters, some of which are calculated by MTCLIM and others of which must be provided by the user. Important in determining solar radiation reaching the Earth's surface is the clear sky atmospheric transmittance which is first corrected for elevation and, in turn, is used to calculate atmospheric transmittance at the location as a function of daily maximum and minimum temperature range. This atmospheric transmittance value is then used in the following set of equations to derive the potential incoming radiation on a sloped surface.

$$Q_s = Is_s + D_s$$

where,

$Is_s = \cos\phi(R_o N * T_t^{AM})$
$AM = 1/\cos\theta + 1.0 * 10^{-7}$
$T_t = A(1-\exp(-B\Delta TC))$
$A = TRANCF + (SELEV)\ (0.00008)$
$\cos\phi = -\sin S*\sin AZ*\sin H*\cos\delta + (-\cos AZ*\sin S*\sin L + \cos S*\cos L)*\cos\delta$
$*\cos H + (\cos AZ*\sin S*\cos L + \cos S*\sin L)*\sin\delta$
$D_s = D_f * \cos(S/2)^2$
$D_f = ((\cos\theta\ R_o N)^2 T_t^{AM})^{0.5} * (1-\cos\theta\ R_o N T_t^{AM})^{0.5}$
$\cos\theta = \cos\delta*\cos L*\cos H + \sin\delta*\sin L$

and where,

Q_s = total incoming radiation on a sloping surface
Is_s = direct beam radiation on a sloping surface,
$\cos\phi$ = cosine beam slope angle,
$\cos\theta$ = cosine zenith sun angle,
R_o = solar constant,
N = time interval for calculation in seconds,
T_t = atmospheric transmissivity constant,
AM = optical air mass,
A = maximum clear sky atmospheric transmittance,
B = empirical coefficient (-0.0030 in MTCLIM),

C = empirical coefficient (2.4 in MTCLIM),
TRANCF = clear sky transmittance equivalent to sea level (0.65 for western Montana,
SELEV = elevation of the *SITE* in metres,
ΔT = daily range of temperature,
S = slope in degrees,
AZ = aspect of *SITE* in degrees,
H = hour angle of sun from solar noon,
L = latitude of site in degrees,
D_s = diffuse radiation on a sloping surface,
D_f = diffuse radiation on a flat surface,

Relative Humidity

SITE humidity calculations are based on BASE station dew point and simulated SITE daylight average temperature. Where recorded dewpoint is not available for the BASE, night minimum temperature is assumed to be approximately equal. The original authors of MTCLIM tested this assumption with datasets from both western and central Montana producing an average $R^2 = 0.87$ and a regression line slope very near 1.0. The average daylight temperature, calculated by MTCLIM, is the same as that described previousiy and referred to as STEMP in the program. SITE dewpoint is estimated by correcting the BASE dewpoint according to an elevational lapse rate of 2.7 °C/km (or 1.5 °F/1000 ft). The final SITE dewpoint is combined with air temperature to produce a value for daylight average relative humidity. The formulae are as follows:

$$SRH = (ES/ESD) * 100$$

where,

$$ES = 6.1078 * e^{(17.269*SDEW)/(273.3+SDEW)}$$
$$SDEW = BDEW - DLAPSE * (SELEV-BELEV)/1000$$
$$ESD = 6.1078 * e^{(17.269*STEMP)/(273.3+STEMP)}$$

and where,

SRH = day average *SITE* relative humidity in percent,

ES = saturation vapor pressure at dewpoint,
SDEW = dewpoint at the *SITE*,
BDEW = dewpoint at the *BASE* station,
DLAPSE = the humidity lapse rate (2.7°C/1000 metres elevation),
ESD = saturation vapor pressure at the day average temperature,
STEMP = daylight average temperature at the *SITE* calculated by MTCLIM.

Precipitation

Given the highly variable nature of mountainous precipitation, accurate simulation is not possible, especially at shorter time scales. For this reason, MTCLIM uses a simplified algorithm that applies the ratio between BASE to SITE annual average precipitation to the daily BASE station values. Hungerford *et al.* (1989) suggest these may be obtained by averaging the recorded data at the BASE and estimated from annual isohyet maps for the SITE. Isohyet maps are available for Canadian locations from such publications as the Climate Atlas collection (Environment Canada, 1986) but their reliability is unstated and important information such as point density is unknown.

More specifically, precipitation at an unknown location or site is derived from one of the following equations, depending on whether or not the optional second precipitation base station is available:

One precipitation station:

$$P_s = P_{b1} * A_s/A_{b1}$$

Two precipitation stations (optional):

$$P_s = (P_{b1} * A_s/A_{b1} + P_{b2} * A_s/A_{b2})/2$$

where,

P_s = daily precipitation at the *SITE*,
P_{b1} = daily precipitation input from the first or only base station,
P_{b2} = daily precipitation input from the second base station,

A_s = long-term average annual precipitation at the *SITE*,
A_{b1} = long-term average annual precipitation at the first *BASE*,
A_{b2} = long-term average annual precipitation at the second *BASE*.

4.2.2 Model Input

Input requirements include terrain features, vegetation characteristics, and meteorological information for the SITE of interest. For the BASE, requirements include basic terrain features and meteorological information only. These variables plus several others relating to temperature and dewpoint lapse rates, enable MTCLIM to output simulated daily values for solar radiation, temperature average and extremes, relative humidity, and precipitation. Specific requirements for each module are discussed below.

Physiographic features include elevation, slope, aspect, and east-west horizon angles. Inclusion of elevation is generally provided with a description of climate stations and may easily be obtained for the SITE using a topographic map or onsite survey using such technology as a global positioning system (GPS). Slope and aspect, required only for the SITE, may also be obtained using either a topographic map or by traditional survey techniques at the location. In its original form, MTCLIM, requires that slope be provided as a percentage while aspect must be in the form of degrees clockwise from north (zero). East-west horizon angles are angles to the east and west horizon which are used to truncate direct solar illumination due to blocking by ridges and/or other obstructions at the SITE, be they natural or otherwise. These parameters may be measured onsite or, as with the previous factors, from maps using the equation:

$$\theta = \arctan h/d$$

where,

θ = the horizon angle,
h = the elevation difference between the SITE and the top of the obstruction,
d = the horizontal distance from the SITE and the top of the obstruction.

The only terrain variable required for the BASE is the location's elevation.

Vegetation characteristics include Leaf Area Index (LAI) and the associated albedo. The LAI is a value which describes the leaf area per square metre of ground surface. In other words, it is an estimate of canopy coverage. Hungerford, *et al.* use an LAI of 1.0 and suggest it as being appropriate for a Northern Rocky Mountain coniferous forest. Associated not only with vegetated surfaces but also with non-vegetated ones is a measure of the reflective characteristics at the location to be simulated. This value, known as albedo, represents the percentage of solar radiation reflected by a surface. Reflection redirects radiation with no change in wave length or frequency. Forest canopies reflect approximately 10-20 %, grass 20-25 %, and rock about 10-30 % of incoming radiation back into the atmosphere. Given these estimates, it can be assumed that remaining incoming energy is absorbed. MTCLIM requires that albedo be in decimal format so, for example, 20% is entered as 0.20.

In order for the model to function, certain meteorological information describing the BASE is needed. First, the long-term average annual precipitation is required in the precipitation calculations. According to the World Meteorological Organization (WMO), long-term average is defined as the arithmetic average over a 30-year period. It is more commonly known as the "normal". Second, and more important, are the daily climate records.

Minimum requirements include daily maximum and minimum temperature and daily total precipitation at a single weather station. Optionally, the model makes use of daily dewpoint records when available. When dewpoint is unavailable, the program uses the minimum daily temperature. As well, MTCLIM provides the option of improving precipitation simulation by allowing the inclusion of data from a second precipitation base. Total daily precipitation is defined as being the sum of both rain and snow where rain, as recorded by AES, is given in millimetres and snow in centimetres. Given the accepted approximation of a 10:1 ratio between snow depth and snow water equivalent (SWE), the snow readings essentially represent SWE in millimetres and can therefore be added directly to the rain readings to give total daily precipitation in millimetres (Goodison, *et al.*, 1981). All that is required for the SITE in terms of climate is the long-term average annual precipitation. It is important that this value be derived from the same time period for both BASE and SITE stations since they are applied as a ratio between the two locations.

Appendix A includes sample datasets as described above. They are excerpts from the files used to test MTCLIM for microclimate simulation in southwestern Alberta.

4.2.3 Model Output

MTCLIM output consists of the simulated microclimate for a single site based on the data from one or two nearby weather recording stations. The units (ie. SI or English) supplied by the base station data determine the format of output. For example, the data obtained from AES use SI units, therefore all output temperatures are in degrees Celsius and all precipitation depths are in millimetres.

The output file is similar in form to the sample provided in Appendix A.1 (OUTPUT). The file begins with a regurgitation of the initialization file as a means of easily identifying the input values for each run of the program, followed by a tabular display of the daily weather conditions for the time period supplied. The first column contains the julian day for each day whose microclimate is simulated. Column two is the daily total solar radiation in kiloJoules per metre squared (kJ/m^2). Columns three through five hold site temperatures in C. STEMP, the first of these, is defined as the daily temperature averaged over the daylight hours (sunrise to sunset). The second and third temperature columns are the daily maximum and daily minimum temperatures respectively, also in °C. Column six is the relative humidity expressed as a percentage, averaged over the daylight hours. The seventh and final column holds the total daily precipitation in millimetres of water equivalent irrespective of form.

4.2.4 Simulation Test Results

The following sections describe how the microclimate simulator output is tested against observed data. First is a brief review of the findings presented by the original authors of MTCLIM, followed by an evaluation of the Upper Oldman Basin simulations. In both cases, results are compared using simple linear regression analysis with observed versus simulated daily data as the independent and dependent variables respectively. The original MTCLIM evaluation employs nine sites in Western Montana. Since regression analysis for the Oldman basin is restricted to temperature and precipitation, the same will be applied to the Montana analysis. Discussion of the other simulated variables and detailed results is addressed in the literature review and so will not be repeated.

Montana

Comparison is carried out for the three simulated temperature values in Montana; daylight average, daily minimum, and daily maximum. The least accurate simulations occur for the daily minimum temperature which has an average $r^2 = 0.706$. The MTCLIM authors suggest this to be a result of frost pockets, cold air drainage, and temperature inversions which make prediction difficult. One possible solution suggested is the use of a higher lapse rate when the base station is located in a basin or creek bottom. Daylight average and daily maximum temperatures each produce an average $r^2 = 0.90$ with the latter having slightly higher y-intercepts and standard error of the y-estimates. Overall, temperature simulations are very acceptable.

Comparison of precipitation simulations with observed data for five mountainous sites in western Montana indicates significantly less reliable output from the model than is the case for temperature. Analysis carried out to determine the value of including a second precipitation base strongly recommends inclusion when another is available. Further, proximity to and relative positioning of the two precipitation bases greatly influences simulations. A single base produces average r^2 values equalling 0.404 while use of two bases results in an average $r^2 = 0.583$.

Upper Oldman Basin

Evaluations of Upper Oldman basin simulations are restricted to the analysis of temperature and precipitation only. At present, these variables are of primary concern since they provide sufficient information to predict snowpack, which in turn may be used to predict runoff from

the study area. The temperature simulations are very close to observed values and appear to produce consistent results. Precipitation, on the other hand, leaves room for improvement so analysis is carried out using two different techniques for determining site and base isohyets.

AES operated weather stations are sparse in the study area so the microclimate for one station is simulated using data from two other stations. In the case of this study, Coleman and Beaver Mines, south of the basin, are utilized to simulate climatic conditions for Pekisko which lies to the north of the basin. The base stations are separated from the SITE station by approximately 70-80 kilometres which itself could be responsible for some of the variation produced. Pekisko is located at an elevation of 1439 metres while Coleman and Beaver Mines are at 1341 and 1286 metres respectively. Table 4.1 is an example of the initialization

Table 4.1 Initialization file, INIT.INI, used to simulate climate for Pekisko using Coleman and Beaver Mines as Base stations one an two respectively.

```
********** MTCLIM DATA FILE FOR INITALIZATION DATA **********
* SIMULATE PEKISKO CLIMATE FROM COLEMAN & BEAVER MINES TO CHECK VALIDITY *
VALIDATE.TP     INPUT DATA FILE     {COLEMAN(PPT1) & BEAVER MINES(PPT2)}
VALIDATE.OUT    OUTPUT DATA FILE    {PEKISKO} - 1989
N               DEW POINT TEMPERATURE SUPPLIED [Y OR N]
2               NO. OF PPT STATIONS [1 OR 2] IF 2 THEN USE 2 ISOHYETS BELOW
N               USE THRESHOLD RADIATATION [Y OR N]
T               TOTAL OR AVERAGE RADIATION [T OR A]
Y               USE YEARDAY (JULIAN) IN PLACE OF MONTH & DAY [Y OR N]
365             NDAYS - INTEGER VARIABLE; ALL THE REST ARE REAL
49.6            LATITUDE OF BASE STATION        {COLEMAN}
1439.0          SITE ELEVATION (METRES)         {PEKISKO}
1341.0          BASE ELEVATION (METRES)         {COLEMAN}
330.0           SITE ASPECT  0 TO 360 DEGREES (0=NORTH; 180=SOUTH)
19.8            SITE SLOPE (PERCENT)
1.0             SITE LAI (ALL SIDED)
651.8           SITE ISOHYET (TOTAL ANNUAL PRECIPITATION..MM)
546.4           BASE ISOHYET STATION 1 (TOTAL ANNUAL PRECIPITATION..MM){Coleman}
605.1           BASE ISOHYET STATION 2 (OPTIONAL) SEE NO. OF PPT STATIONS.{ Blairmore}
0.0             SITE EAST HORIZION (DEGREES)
0.0             SITE WEST HORIZION (DEGREES)
0.2             SITE ALBEDO  (0.2 = 20%)
0.65            TRANCF (SEA LEVEL ATMOSPHERIC TRANSMISSIVITY)
0.45            TEMPCF (TEMPERATURE CORRECTION FOR SINE APPROX)
6.4             TEMP LAPSE RATE (DEG C/1000 M)
8.2             LASPE RATE FOR MAXIMUM TEMPERATURE (DEG C/1000 M)
3.8             LAPSE RATE FOR MINIMUM TEMPERATURE (DEG C/1000 M)
2.7             DEW LAPSE RATE (Deg C/1000 m)
```

file used for model validation which describes the other variable settings .

The MTCLIM model appears to work equally well for the mountainous regions of south-western Alberta as it does for western Montana, especially for temperature predictions. Table 4.2 outlines the results from linear regression analysis between observed and predicted daily average temperature and daily total precipitation for Pekisko. For these purposes, daily average temperature is defined as being the mean of daily minimum and maximum temperature and total precipitation is the total daily water equivalent irrespective of form.

Table 4.2 Predicted vs Observed temperature and precipitation for Pekisko, Alberta (1989). Results are given using the 30-year average annual isohyets and the 5-year Dec.1-Mar.31average (1985-90).

ISOHYET METHOD	TEMP				PRECIP			
	Intercept	Slope	R^2	SEE[1]	Intercept	Slope	R^2	SEE[1]
30-yr Annual Average	0.33	0.92	0.94	2.52	1.45	0.53	0.21	4.22
5-yr Dec.1 - Mar.31 Average	0.22	0.92	0.94	2.51	1.18	0.42	0.20	3.41

[1] Standard error of the estimate

Results for temperature simulation are promising with an R^2=0.94, a slope very close to 1 (0.92), andY-intercepts ranging between 0.33 and 0.22. As was the case for the Montana tests, there appears to be a slight overestimation of lower temperatures and underestimation of higher temperatures. Again, this is likely a side-effect of the choice in lapse rates, however, the statistics are sufficiently good to accept current parameters as laid out in table 4.1 and Appendix A.1. Figures 4.7 and 4.8 illustrate a typical scatter plot and comparison plot of observed to simulated temperature respectively. It is evident from the scatter of points

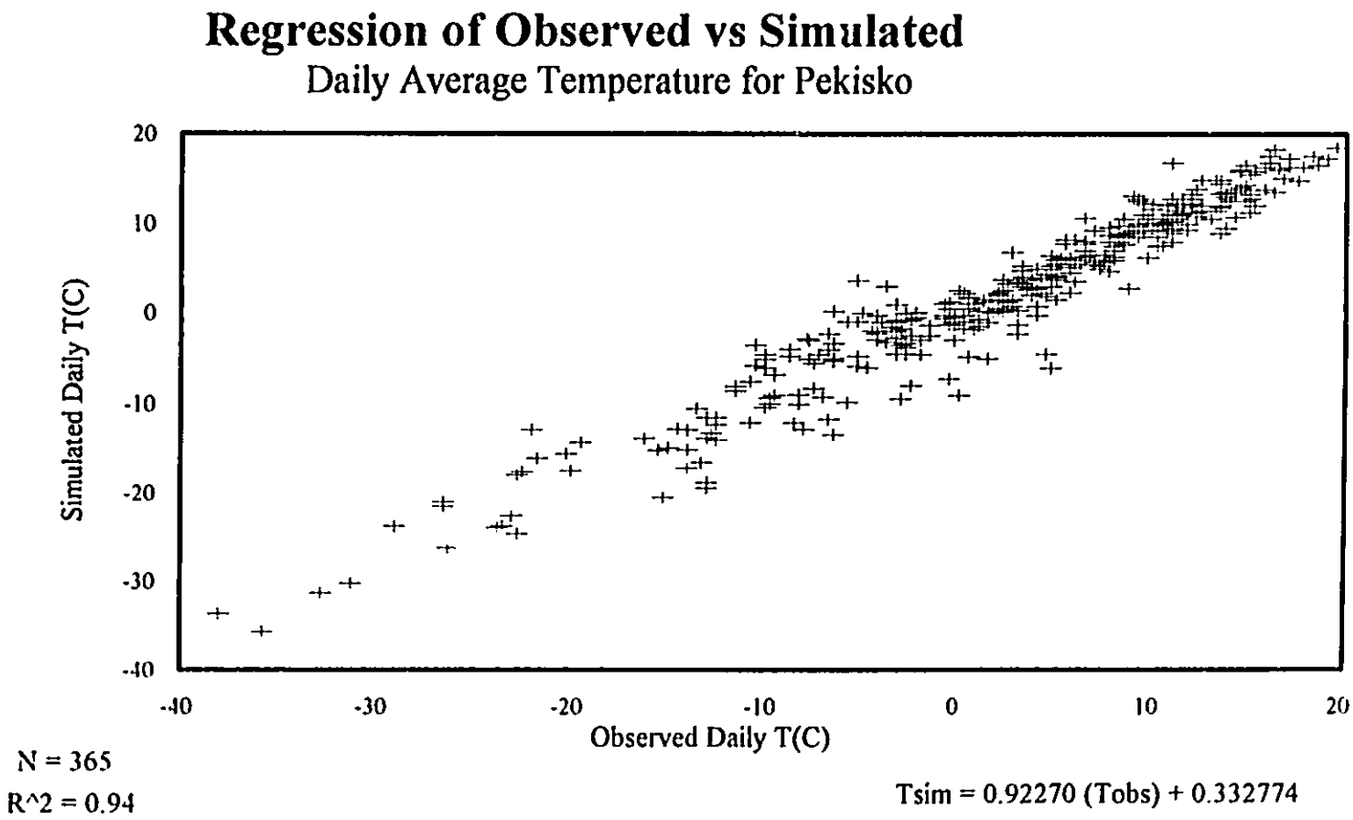

Figure 4.7 Typical scatter plot of observed versus simulated temperature for Pekisko, Alberta 1989.

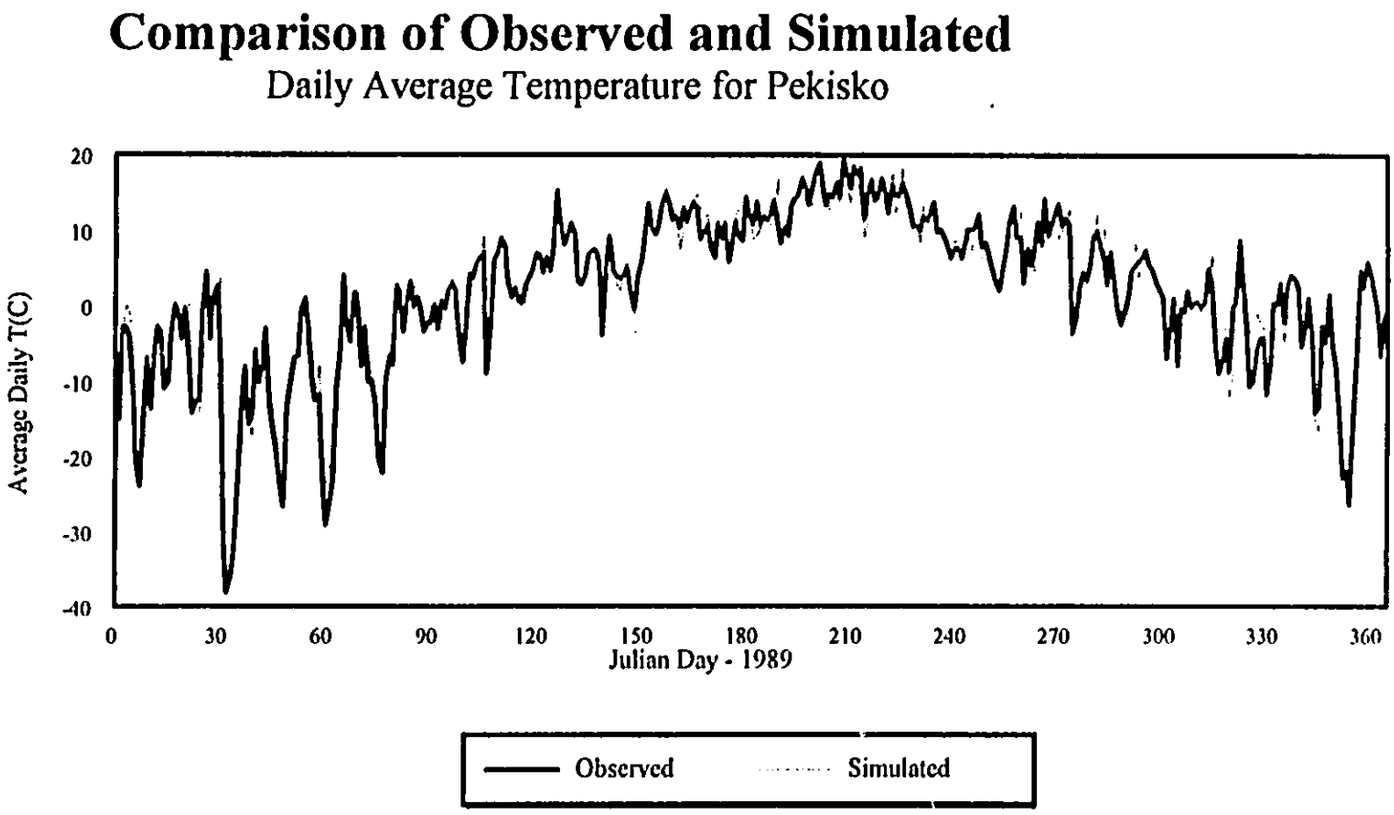

Figure 4.8 Typical comparison plot of observed versus simulated temperature for Pekisko, Alberta 1989.

in figure 4.7 that a truly linear relationship exists between the two variables. This implication is strengthened in figure 4.8 which shows only slight deviation of the daily simulated values from the observed.

Linear regression analysis between simulated and observed daily precipitation indicates a statistically less significant relationship than did the temperature. Table 4.2 shows regression results for two sets of analysis, one using the 30-year annual average isohyet and another using the 5-year Dec.1 to Mar.31 average isohyet. Regardless of which is used, results are somewhat weak (figures 4.9 and 4.10). The 30-year average method produces a slope closer to one and a slightly better R^2, but the 5-year winter average method produces a lower standard error of the estimate and an intercept which lies closer to the origin. Although it is tempting to proceed with the 30-year average method because of its slight improvements over the December to March method, winter precipitation is more important for this study and was therefore chosen as more representative of local hydrologic conditions. The reason for using the winter precipitation becomes more evident in later discussions of site isohyet estimation.

Figures 4.11 and 4.12 demonstrate a much improved relationship when the simulated data are summarized as monthly totals and compared with data from the Race Horse automated meteorological station (DACQ). R^2 is improved to 0.66 and the regression line slope of 1.17832 is well within acceptable limits of statistical significance. Most notable in both plots is the presence of an outlier occurring in September. The MTCLIM model appears to have greatly overestimated the precipitation for this month, possibly due to the use of winter

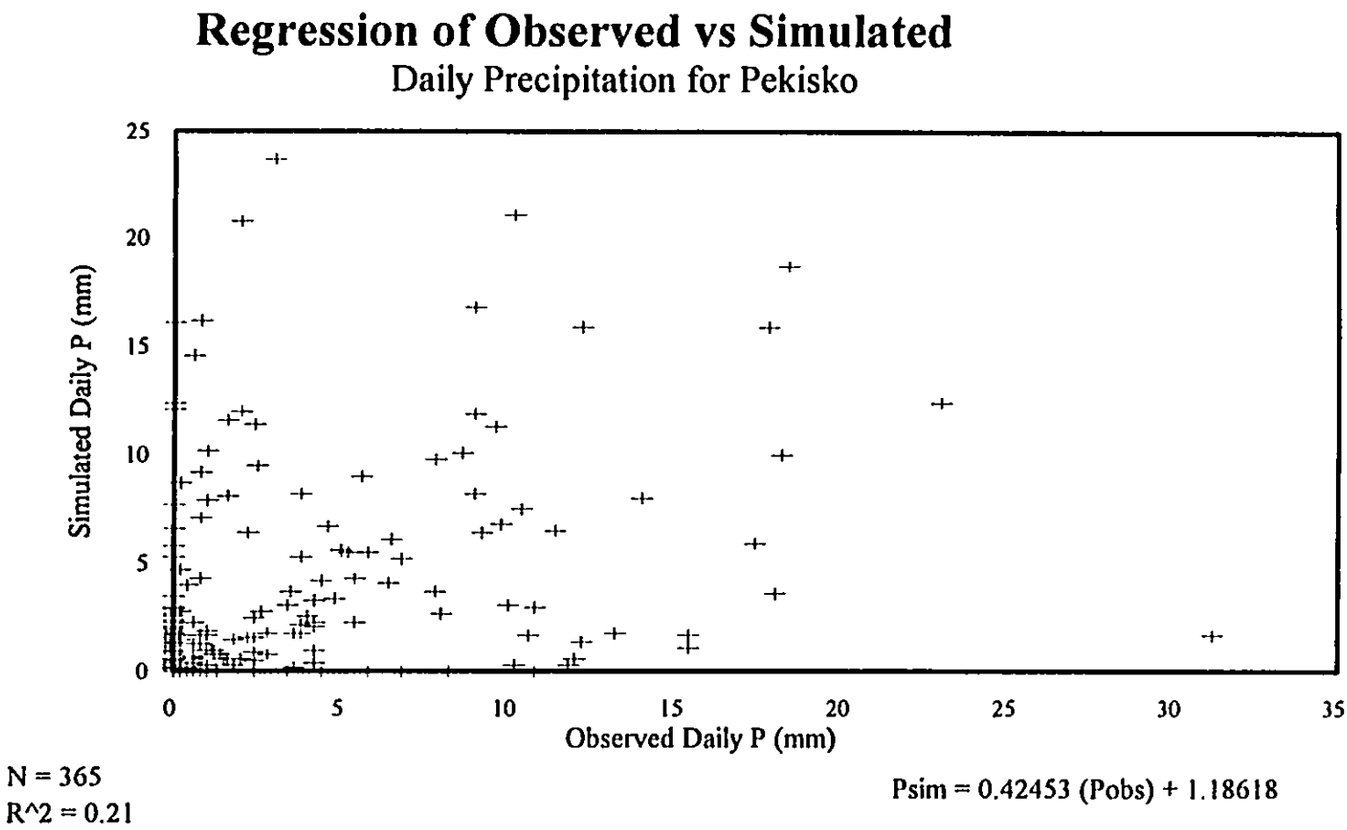

Figure 4.9 Typical scatter plot of observed versus simulated precipitation for Pekisko, Alberta 1989.

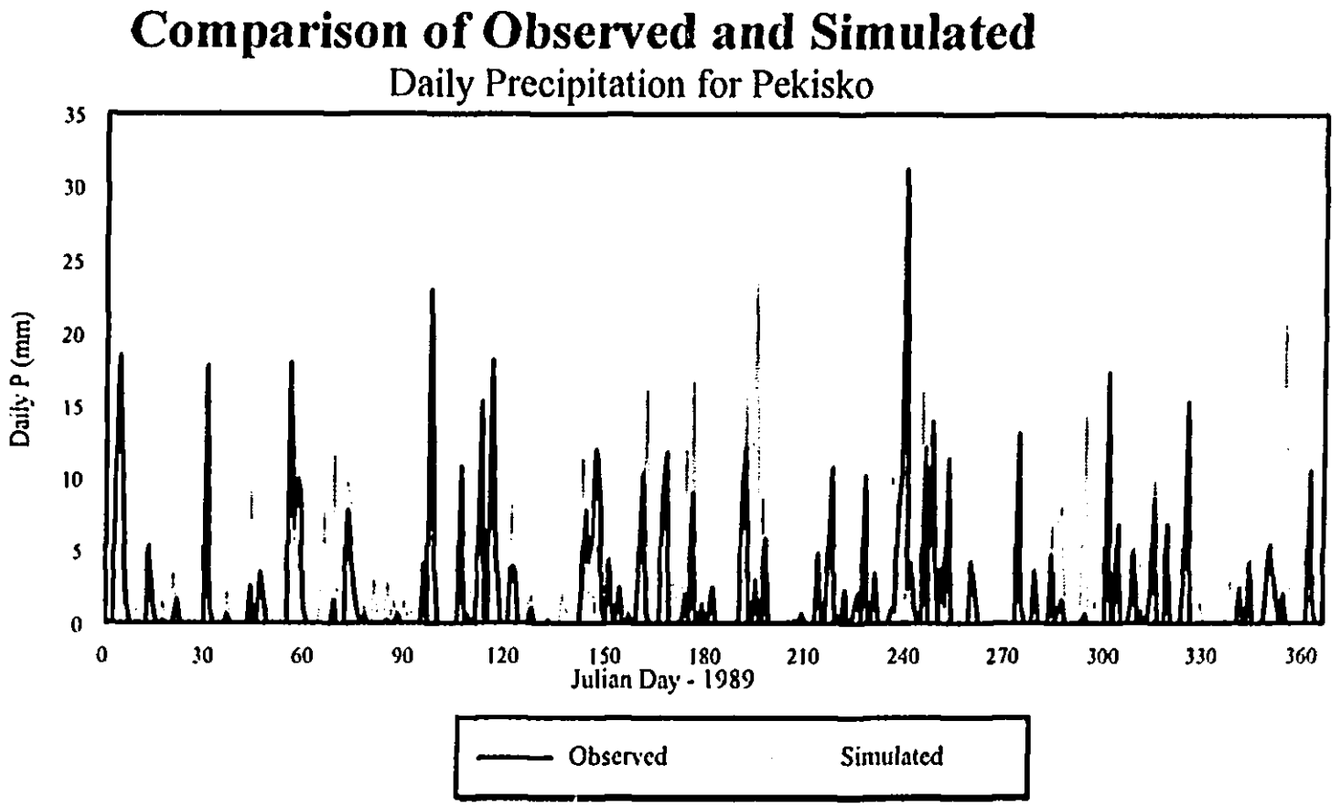

Figure 4.10 typical comparison plot of observed versus simulated precipitation for Pekisko, Alberta 1989.

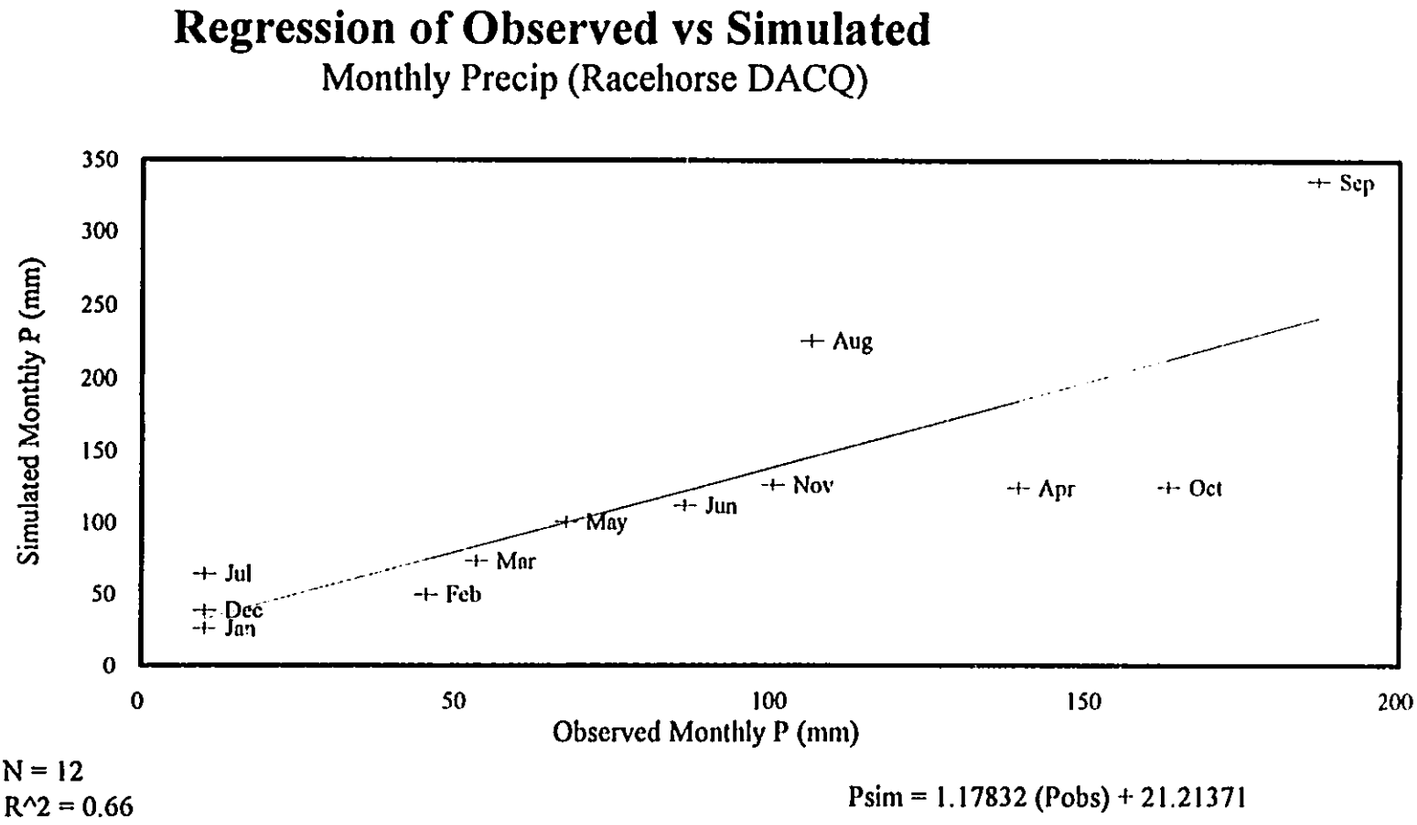

Figure 4.11 Scatter plot of observed versus simulated monthly total precipitation for the Racehorse Creek active meteorological station with telemetry (DACQ).

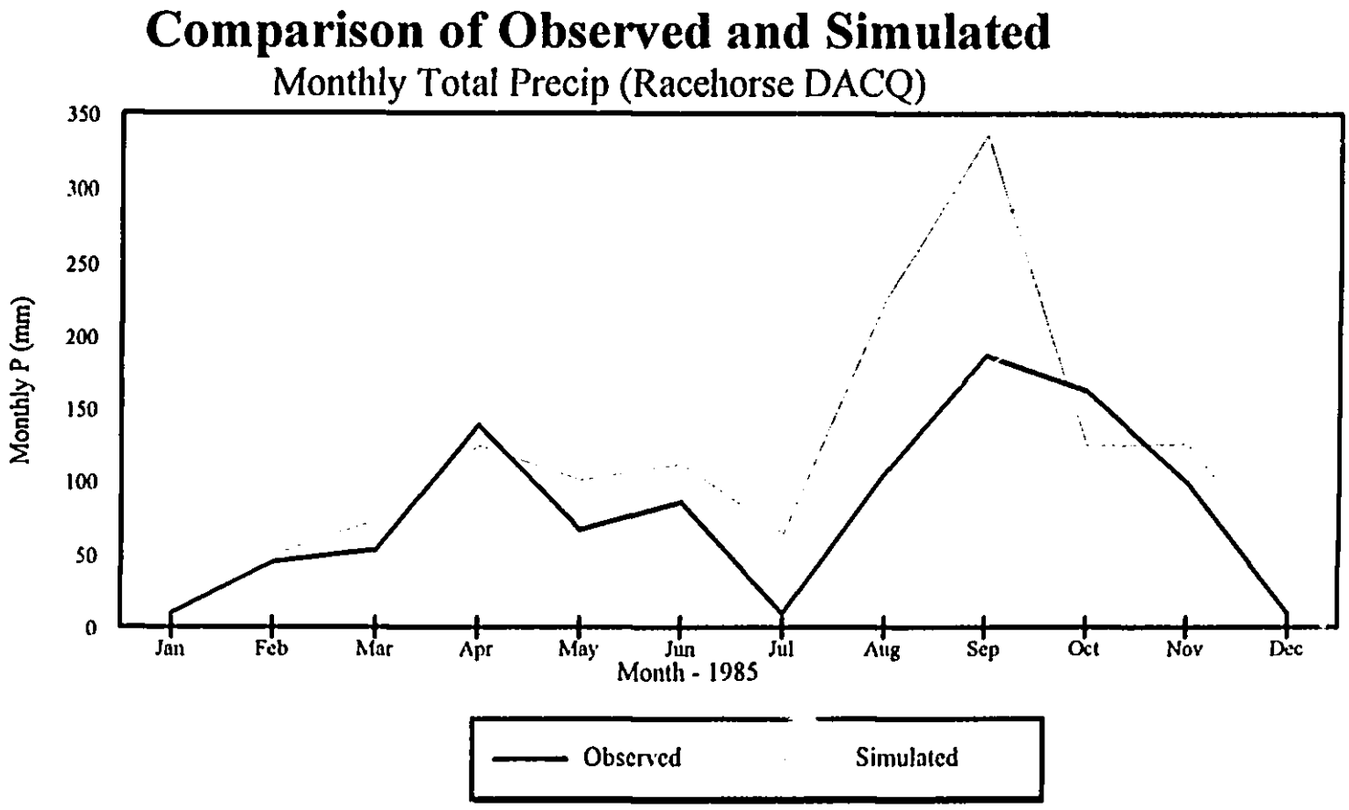

Figure 4.12 Observed versus simulated monthly total precipitation for the Racehorse Creek active meteorological station with telemetry (DACQ).

average isohyet for both base and site. Choice of isohyet averaging period impacts simulation results since it is influenced directly by changes in seasonal weather patterns.

4.2.4 Sensitivity Analysis of the Model

Due to the highly variable nature of terrain throughout the study area, it is necessary to uncover ways of simplifying site characteristics. The most difficult parameters to categorize are the east and west horizon angles since these would be unique to each and every point in the basin. To review, the horizon angle is the angle above the horizon from the SITE to the top of the highest visible obstruction, be that surrounding treecover, a building, or a mountain ridge. The following section attempts to identify the significance or insignificance of horizon angles for this study. Also considered is the influence of site slope on simulations.

Analysis of horizon angles indicate that changing the east and/or west angles does not have a great impact on temperatures nor precipitation output by the model. The 1989 Pekisko simulation used for testing model validity is used here as the basis for assessment. It is determined from a 1:50000 NTS map that the east horizon angle for Pekisko is 2.2 and the west horizon angle is 4.0. When these values are changed to 0.0 and 0.0 or to 45.0 and 45.0, simulated temperatures did not change at all. However, the simulated solar radiation value is affected. Solar radiation values are significantly higher when east and west horizon angles both set to zero and lower when the horizon angles are set to ninety. In other words, when horizon angles are set to zero, it is implied that there exists no obstruction between the site and the horizon and so incoming solar radiation is not truncated. When horizon angles are set to ninety, it is implied that the only radiation reaching the site is that received from directly

overhead. Since the purpose of horizon angles is to adjust for times during the day when the direct sunlight is blocked by natural or man-made obstructions, this is not unexpected. The results are provided in table 4.3.

Table 4.3 Analysis of model sensitivity to changes in *SITE* East and West Horizon Angles. For simplicity, both horizon angles are set to 0°, 45°, and then 90°.

SITE	0°			45°			90°		
FEATURE	MAX	MIN	AVG	MAX	MIN	AVG	MAX	MIN	AVG
SOLAR RADIATION (kJ/m^2)	33292	69	12934	24048	69	8456	10167	69	4856
DAY AVERAGE TEMPERATURE (°C)	24	-37	5	24	-37	5	24	-37	5
MAXIMUM TEMPERATURE (°C)	30	-35	10	30	-35	10	30	-35	10
MINIMUM TEMPERATURE (°C)	13	-44	-5	13	-44	-5	13	-44	-5
HUMIDITY (%)	98	10	51	98	10	51	98	10	51
PRECIPITATION (mm)	35	0	2	35	0	2	35	0	2

Using the same dataset, the role of site slope is investigated by running the simulator for three different values. From the digital elevation model created in the GIS, slope was found to range from 0 to 250 percent (0° to 68°). This range is broken into three classes of approximately 23° each with the exact breakdown described in table 4.4. Table 4.5 describes the simulation results for the three slope values. As expected, the solar radiation is affected simply because as the ground angle increases, there is a reduction in direct solar incidence. Also evident with an increased slope is a slight drop in daylight average and maximum

temperatures. Inversely related to the drop in temperature is a rise in relative humidity. Minimum daily temperature appears not to be affected.

Table 4.4 Breakdown of the three classes of slope as they are used for simulation.

Class	Range (°)	Mid-Point (°)	Slope (decimal)	Slope (%)	Range (%)
1	0-23	11.4	0.20	20.0	0-42
2	23-46	34.2	0.68	68.0	43-102
3	47-68	57.0	1.54	154.0	103-250

Table 4.5 Analysis of model sensitivity to changes in *SITE* slope. East and West horizon angles are both set to zero.

SITE	11.4°[1]			34.2°[1]			57.0°[1]		
FEATURE	MAX	MIN	AVG	MAX	MIN	AVG	MAX	MIN	AVG
Solar Radiation (kJ/m^2)	32028	68	12130	26183	63	9537	19531	53	7089
Day Average Temperature (°C)	24.0	-37.0	5.1	24.0	-37.0	4.7	23.0	-37.0	4.2
Maximum Temperature (°C)	30.0	-35.0	9.4	30.0	-35.0	9.0	29.0	-35.0	8.5
Minimum Temperature (°C)	13.0	-44.0	-4.6	13.0	-44.0	-4.6	13.0	-44.0	-4.6
Humidity (%)	99.0	10.0	51.4	99.0	11.0	52.6	100.0	11.0	54.3
Precipitation (mm)	35.0	0.0	2.0	35.0	0.0	2.0	35.0	0.0	2.0

[1]Approximate mid-points of the three equal classes as described in table 4.14.

4.3 Multi-Site Microclimate Simulation Model

Simulation of microclimate for multiple sites is achieved through a modification of the MTCLIM program in conjunction with output from the GIS. The modified program is currently referred to as SIMGRID in order to differentiate it from the original. The calculations described in previous sections are applicable and will therefore not be repeated. Some emphasis will, however, be placed on illustrating the difference and additions to the original techniques. Also explained are some generalizations and assumptions that must be accepted in order for model development to proceed.

4.3.1 Model Input from the GIS

In section 2.4.1 is a discussion of the spatial scale of snow cover variability as described by Gray and Prowse (1993). In it, horizontal distances of one hundred metres to one kilometre are classified as mesoscale and include such phenomena as snow distribution due to wind, avalanches, terrain variables, and vegetation cover. This appears to describe phenomena of concern in this study so it was decided to lean toward the lower end of the scale and employ a 100 metre grid over the entire basin. This increases the likelihood of simulations being more representative of actual field conditions.

Inputs from the GIS include coordinate information, elevation, percent slope, and aspect. Within the GIS, each of these is represented by a separate surface layer for which pixel size is user-defined. Use of a 100 metre pixel size results in the generation of 144,558 pixels in total covering the basin. This corresponds to the total basin area of 1445 square kilometres described in chapter 3. The information contained on each of the three GIS surfaces is first

exported to ASCII files such that one record containing UTM easting, northing, and pixel value is output for each of the 144,558 pixels. The separate files are then related and combined into one file using a database management system.

Due to the large number of sites for which the microclimate must be simulated, it is necessary to categorize terrain variables such that calculations are greatly simplified, yet still representative. Elevations in the basin range from 1267 metres at the river gauging station to 3099 metres at Tornado Mountain and are broken into ten elevation bands of 200 metres each starting at 1200. The slope values are broken into three classes ranging from flat (0 percent) to reasonably steep (250 percent). Although this appears at first to be a wide range, in effect the maximum slope is only 68° above the horizon and each class represents approximately 23°. As discussed just previous, site slope does affect the amount of incident solar radition and relative humidity, but plays only a minimal role in daily temperature extremes and precipitation (table 4.5). Finally, aspect is divided into the four groups of 90°, each representing the general compass directions of north, south, west, and east. See table 3.1 for details on the individual categories and their respective percentages of total land area in the basin.

The result is a maximum possible number of combinations equalling 120 (10 x 3 x 4). This represents a huge improvement in computational efficiency because the number of sites is essentially reduced from 144,558 to 120 points (0.08% of the original). Given that each point is accessed for every day in the user-defined period, this can make quite a noticeable

difference.

4.3.2 Simulation of Site Isohyet

In order for the multi-site microclimate simulator to run, each grid point in the basin requires an isohyet value. Again due to the severe lack of recorded data for the higher altitudes along the eastern slopes of the Canadian Rockies on which to base such values, it is necessary to develop a method to estimate the annual isohyet. Initially it was hoped that data from eight nearby weather stations (figure 4.13) could be used to determine a 30-year average annual precipitation value for each. This was done using a database management system (DBMS) to sum daily precipitation values by year for the 30 year period. The 1960-1989 period was chosen for calculations since it was common to all available datasets. Combining the calculated 30-year average precipitations with known station elevations provided the basis for a crude linear regression between precipitation and elevation. The results of the analysis, shown in Figure 4.14, indicates a somewhat weak relationship ($r^2 = 0.54$), but it provides a starting point from which to progress. The following equation describes the linear relationship from that first attempt:

$$P = -6.53 + (0.42 * E) \tag{4.1}$$

where,
P = Precipitation,
E = Elevation

Consideration of this somewhat weak relationship prompted an investigation into ways by which it may be improved. Since the study area does lie on the eastern slopes of the Continental Divide, it was theorized that a great deal of the annual precipitation results not from westerly flows, but instead from easterly flows resulting when low pressure cells are

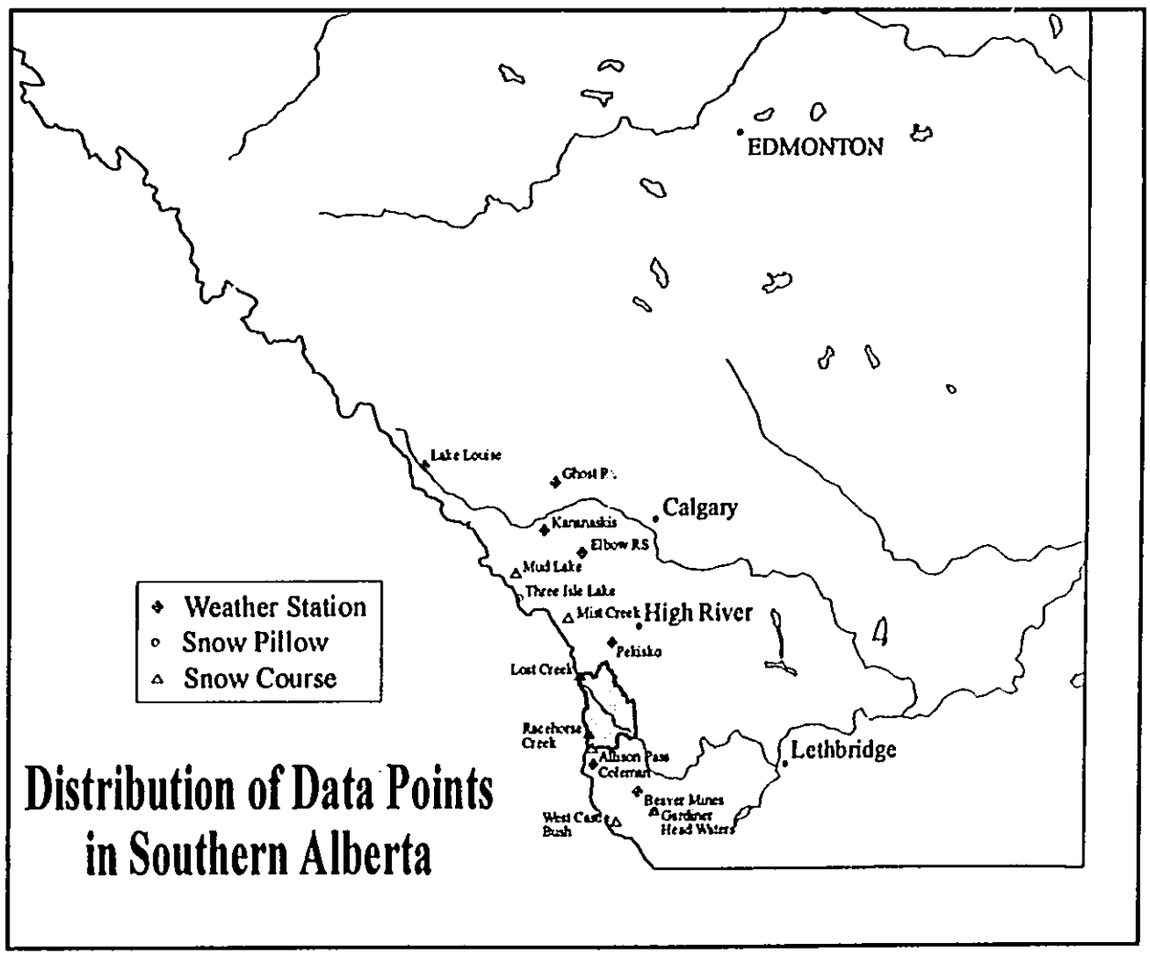

Figure 4.13 Location of the stations from which climate data is analyzed in creating an Elevation/Precipitation regression.

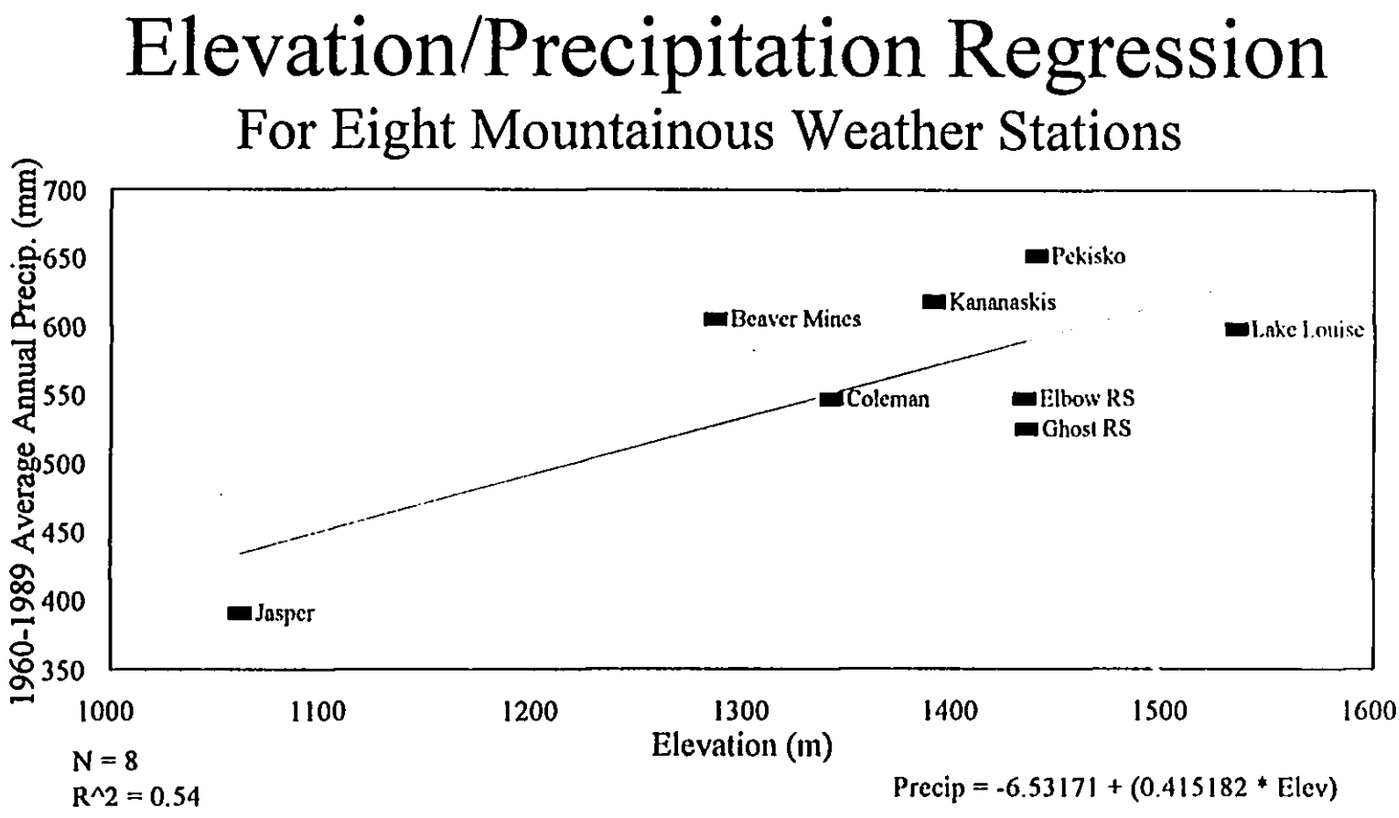

Figure 4.14 Elevation versus the 1960-1989 average annual precipitation for eight mountainous weather recording stations.

forced southward along the mountains. Easterly winds, resulting from a counter-clockwise rotation, rise up the slopes and precipitate moisture. This theory implies that aspect and slope both play a role in the amount of precipitation an area receives. A method was devised whereby both factors could be expressed as a positive value for high influence and a negative value for low influence. The range of aspect values is 0 - 360° with 0° and/or 360° indicating a north-facing slope while 180° indicates a south-facing slope. As mentioned previous, east-facing slopes (90° aspect) will theoretically receive greater amounts of precipitation, therefore it is assigned a positive one. Conversely, west-facing slopes (270° aspect) will receive lesser amounts of precipitation and therefore be assigned a negative one. Aspects to the north or south of either 90° or 270° vary proportionally. In other words, the simplified aspect value may be described as equal to SIN(ASPECT), where ASPECT is the bearing in degrees between 0-360°. A comparable adjustment of aspect was carried out by Tecle and Rupp (1995) as discussed in the literature review. A similar situation exists for the slope which, ignoring overhang cliffs, may range between 0° (flat) and 90° (vertical). Again, the SIN function may be applied to reduce degrees of slope to values ranging between 0, for a slope of 0° indicating little influence on the aspect and precipitation, and 1 for a slope of 90 indicating a strong influence on aspect and precipitation. The adjusted slope and aspect values are then multiplied to produce a single SLOPE/ASPECT coefficient for each station. Finally, a multiple regression is run with precipitation as the dependent variable, and elevation and the SLOPE/ASPECT coefficient as the independent variables. Unfortunately, the strength of the regression is improved only slightly with the inclusion of the slope and aspect parameters (r^2=0.55, only 0.01 better than the regression using only elevation as the

independent variable). The resulting equation is as follows:

$$P = (0.39*E)-(166.56*SAC)+25.78 \qquad (4.2)$$

where,

P = Precipitation,
E = Elevation,
SAC = Slope/Aspect Coefficient

The analysis did not provide any statistical support for the adoption hypothesis and related technique.

Other attempts at deriving an equation for site precipitation include dropping the Jasper data from the first set of values and also trying the 1951-1980 annual average precipitation. The first of these was done on the basis of distance from the basin. Jasper is much further from the basin than the other available stations and it was thereby assumed it could be omitted. Unfortunately, the result was an r^2 equal to 0.0009 indicating an almost non-existant relationship between elevation and precipitation. The second of these attempts involved running a regression between sixteen station elevations and their 1951-1980 average precipitation taken from the Climate of Alberta Report for 1983 (Alberta Environment, 1983). Again, the improvement in results was not significant. The r^2 of 0.48 is actually lower than the 0.54 valued obtained using equation (4.1).

Since a major portion of the research deals with the accumulation of snow, further analysis was directed at precipitation/elevation relationships using only average winter precipitation. For this purpose, winter precipitation is arbitrarily defined as that precipitation which falls

between December 1st and March 31st. Precipitation during this period was assumed to be snow. Using only this winter period allows for the inclusion of snow pillow and snow course data which not only adds more points, but more importantly, points at higher elevations. In order to overlap the period of record for weather station, snow pillow, and snow course data, the mean winter precipitation is calculated for the 1985-1990 values. In total, seven weather stations, seven snow courses, and three snow pillows ranging in elevation from 1286 to 2160 metres are employed. The regression improved to an r^2=0.71 (figure 4.15) and equation (4.3) is produced:

$$P = -485.22 + (0.45 * E) \qquad (4.3)$$

where,
P = Precipitation
E = Elevation

Obviously, the best results occur from the method using winter precipitation only. Therefore, equation (4.3) is chosen as the means by which to extrapolate grid point isohyets. Although slope and aspect in theory play a role in precipitation, the available datasets did not indicate any significant relationships. Perhaps this is partly due to the availability of only a few suitable data sources and may change for different areas.

4.3.3 Model Output

Like MTCLIM, SIMGRID output consists of simulated microclimate based on the data from several nearby weather recording stations. The difference with SIMGRID is the addition of two columns to the output file whose function is to identify the sites. The first of these is the category number (1-120) that describes a class of terrain variables to which it relates. The second column holds the two-digit year value (ie. "89") which is necessary since the program

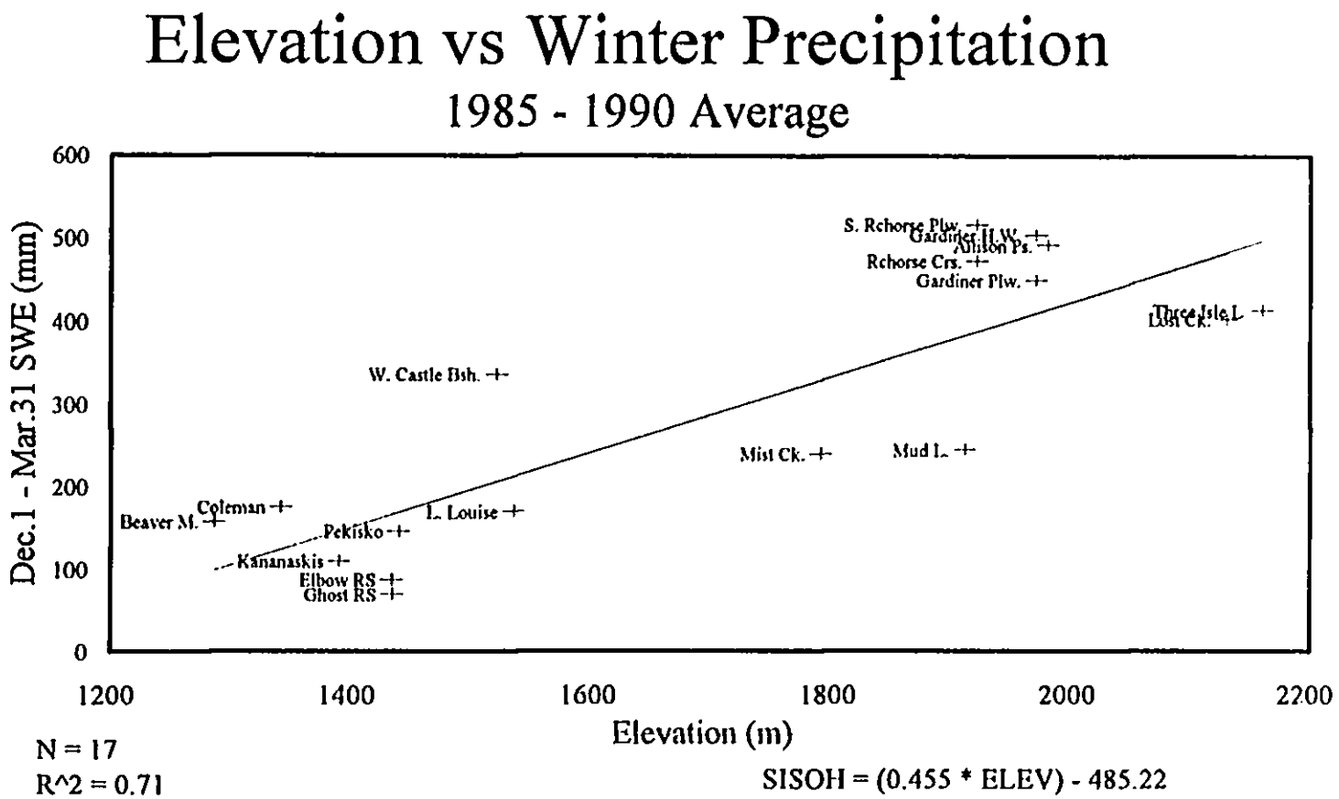

Figure 4.15 Elevation versus the 1985-1990 average winter precipitation. Points include AES operated weather recording stations as well as snow pillow and snow course data.

may be run for periods longer than a single year. That is certainly the case in this study where microclimate is simulated for a ten year time frame. Output is formatted such that microclimate is listed for all days in the user-defined period one category at a time. For example, given that microclimate is to be simulated for two categories from 1970 to the end of 1975, the following would represent sample output:

Cat	Yr	Jday .....plus the other variables (see Appendix A.1)
1	70	1 .....
1	70	2 .....
1	70	3 .....
.	.	.
.	.	.
1	75	365 .....
2	70	1 .....
2	70	2 .....
2	70	3 .....
.	.	.
.	.	.
2	75	365 .....

This format allows for relatively simple extraction of data based on category, year, and/or julian day. It also lends itself to elementary summation functions such as maximum, minimum, and mean for any of the calculated variables.

4.4 Snowpack Accumulation

The estimation of snowpack accumulation and ablation is accomplished through yet another program which incorporates the snowmelt algorithm from the UBC Watershed Model (Pipes and Quick, 1977) and an empirically-based accumulation model that describes the composition of precipitation based on temperature (Wyman, 1995). Both techniques are fairly simplistic in that they derive normally complex parameters strictly from daily air temperature extremes. Quite often air temperature is all that is available in alpine study areas.

The UBC snow melt technique takes into consideration three primary sources of snow melting energy. The first of these, convective heat transfer from warm air, is estimated as being equal to the mean daily temperature above freezing. Second, the net radiant energy gain from shortwave and longwave radiation exchanges is considered. It is represented simply as the daily temperature range. Finally, the latent heat gain from condensation or loss through evaporation at the surface is derived as a function of the range in temperatures between the dewpoint and the freezing point.

Snowmelt is dependent upon the ability of a snowpack to store cold. Pipes and Quick (1977) take into account a negative melt decay function in their cold storage equation which serves to limit the effect of daily temperature conditions to the previous ten days. The following is referred to as the negative melt formula:

$$TREQ_i = (ANMLTF * TREQ_{i-1}) + TMEAN_i$$

where,

$TREQ_i$ and$TREQ_{i-1}$ = snowpack cold storage on days i and i-1,
ANMLTF = the decay constant (set to 0.85),
$TMEAN_i$ = mean daily temperature on day i,

In order for melt to occur, the snowpack's cold storage must first be exhausted and when this happens open area melt takes place according the following formulae:

$$MELT_i = PTM * (TMAX_i + TCEADJ * TMIN_i)$$

where,

$MELT_i$ = melt depth in millimetres of water equivalent on day i,
PTM = point melt factor in millimetres per day per °C (Pipes and Quick give a PTM=3, a value of 1.8 is recommended by Wyman, 1995, and Byrne, 1990 used 1.0 for the prairies.),
$TMAX_i$ = daily maximum temperature on day i,

$TMIN_i$ = daily minimum temperature on day i,
TCEADJ =the energy partition multiplier.

and where,

$$TCEADJ = \frac{TMIN_i + T_r/2}{XTDEWP + T_r/2}$$

T_r = range of temperature over the particular day,
XTDEWP = reference dewpoint that controls energy partioning between melt and sublimation (set to 18 °C).

If falling precipitation is in the form of snow and temperatures are insufficient for melt to take place, then it is likely that existing snowpack will increase. The following formulae describe the criteria by which the distinction is made between precipitation that falls as snow and that which falls as rain (Wyman, 1995).

Daily snow water equivalent (SWE):

$$SNOW_n = PPT_n - RAIN_n$$

where,

$SNOW_n$ = precipitation that falls as snow on day n (mm SWE),
$RAIN_n$ = precipitation that falls as rain on day n (mm SWE),
PPT_n = total daily precipitation on day n (mm SWE),

and where,

$RAIN_n = 0$ if mean daily temperature < 0.6 °C,
$RAIN_n = PPT_n * (TMEAN_n/3 - 0.2)$ if mean daily temperature >0.6 °C and <3.6 °C,
$RAIN_n = PPT_n$ if mean daily temperature > 3.6 °C,
$TMEAN_n$ = mean daily temperature on day n.

In the basic equation, total snow on a given day, $SNOW_n$, is defined as the total daily precipitation amount minus the amout of precipitation which falls as rain. The amount of rain on a given day, $RAIN_n$, is dependent upon, TMEAN. When TMEAN is less than 0.6°C, $RAIN_n = 0$ because all precipitation is considered to be in the form of snow. When TMEAN is greater than 3.6°C, $RAIN_n$ = the total daily precipitation, because all precipitation is

considered to be in the form of rain. The case of TMEAN falling between 0.6 and 3.6°C is slightly more complex since the total daily precipitation is assumed to be a mix of snow and rain, the ratio of which is determined by the formula:

$$RAIN_n = PPT_n * (TMEAN_n/3 - 0.2)$$

The form precipitation takes determines the manner in which Wyman deals with its impact on the snowpack. Obviously, the addition of snow causes an increase in the depth of snow water equivalent held in the pack. The addition of rain, however, may do one of two things; 1. when the total rain added is less than that which the snowpack is capable of absorbing, the pack becomes more dense but no runoff occurs, 2. when the total rain added exceeds the pack's capacity to absorb water, additional rain and surface melt propogates through the pack where it contributes to runoff.

4.4.1 Input from the Microclimate Simulator

The microclimate simulator operating on a grid basis provides the much needed input into an attempt to model spatial variation in snowpack accumulation and ablation. The lack of an acceptable distribution and density of data collection stations in high altitude areas prompted the development of a technique to model the spatial and temporal distribution of snow from proxy conditions.

As mentioned in the previous section, the snowpack model, known as SNOPAC, operates on daily temperature extremes and daily total precipitation as basic inputs. These, of course, are available from the simulated data which provide daily maximum, minimum, and daylight average temperature as well as daily total precipitation. It is important to recognize that the

simulated precipitation is heavily dependent upon the elevation/precipitation regression developed early in the program. Although it is acknowledged earlier that this particular regression is somewhat weak, the actual procedures carried out are considered robust.

4.4.2 Simulation Test Results

Comparison of simulated and observed snowpack is very promising. Regression analysis on the Racehorse Creek snow pillow produced an r^2 of 0.8, a slope of 0.821, and an intercept of 39.0 for the 1983-84 season. Figure 4.16 illustrates a typical comparison plot for simulated and observed snowpack conditions. It is evident from the graph that the simulations closely reflect the short-term trends recorded at the site. However, there is some deviation in the first month of 1984 as well an undersimulated peak snowpack occurs at an approximate Julian date of 131.

Figure 4.17 is a comparison plot for the Lost Creek snow pillow versus the corresponding simulated snowpack. Regression analysis on this particular station for the 1988-89 season, produced an r^2 of 0.896, a slope of 1.11, and an intercept of 5.578. The left half of the graph indicates a very close relationship between observed and simulated data. However, after approximately one and a half months into the new year, the two lines begin to diverge with an apparent over simulation in the latter part of the snow season. Originally, it was suspected this was caused by a number of factors. The first of these is the over simulation of site precipitation at higher elevations as discussed earlier. Second, it is believed that there is a problem with certain coefficients in the SNOPAC program which control melt. Without sufficient data to investigate the first, emphasis focused on the latter.

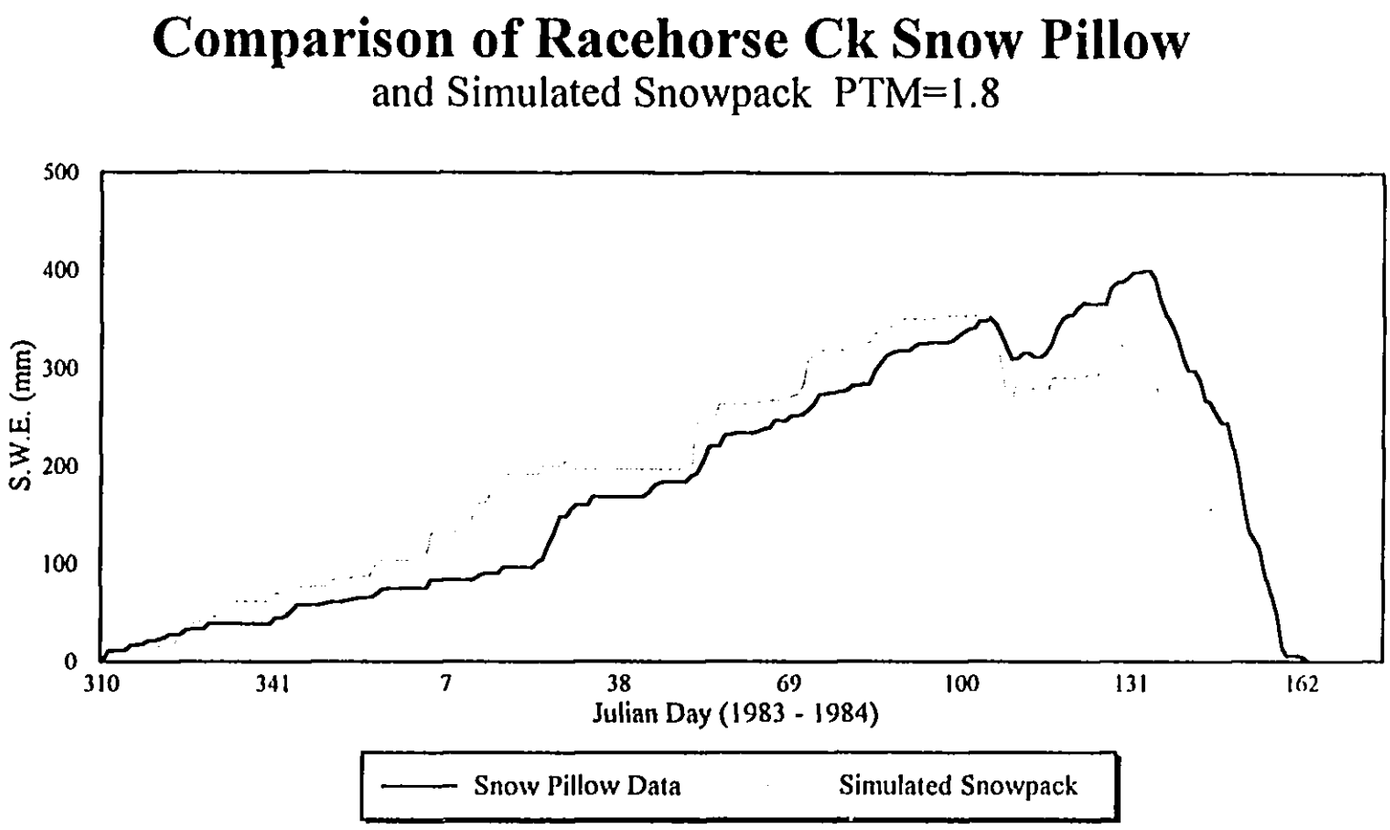

Figure 4.16 Comparison of snowpack model simulations with the Racehorse Creek snow pillow observed data for the 1983-198 snow season. A point melt factor (PTM) of 1.8 is used.

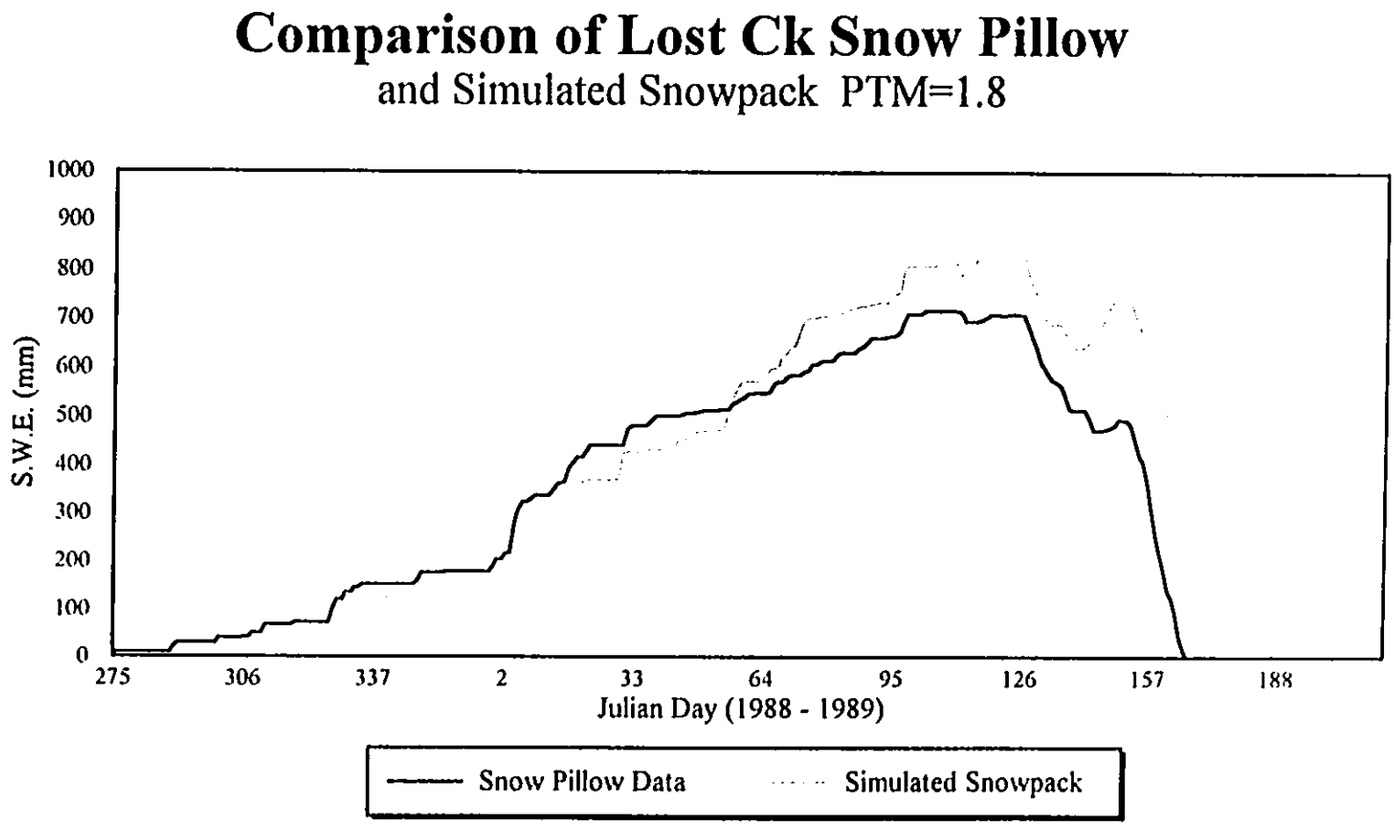

Figure 4.17 Comparison of snowpack model simulations with the Lost Creek snow pillow observed data for the 1988-1989 sno season. A point melt factor (PTM) of 1.8 is used.

The primary driving force behind snowmelt appears to be a variable know as the point melt factor (PTM). Its units are described in millimetres per day per °C. It is described by Wyman (1995) and Pipes and Quick (1977) as a necessary input into the UBC Watershed Model melt routines. Wyman suggests a PTM of 1.8 is suitable for the Canadian Rockies of British Columbia. For this reason, 1.8 is also employed in this study as a reasonable starting point. Figures 4.16 and 4.17 illustrate the results for two snow pillows using that point melt factor. Figure 4.18 represents the same period as figure 4.16 except that a PTM of 1.3 is used. A slight lag appears in the spring, but the peak snowpack is brought closer to the observed peak. This lower PTM results in an $r^2 = 0.9$ which is a small improvement over the previous simulation. Along the same lines, figure 4.19 illustrates an improved simulation over figure 4.17. The peak is still overestimated, but lag in spring melt is brought closer to the recorded data and r^2 is increased to 0.941. To accomplish this, a PTM of 2.2 is used. Perhaps an even higher PTM would bring the simulated and observed lines closer still.

Analysis indicates that the point melt factor is an important parameter in the snowmelt routine. Unfortunately however, it does not appear to be constant even within the study area. Without supporting field data, it is believed that the point melt factor is linked to elevation. In the previous discussion it is shown that for Racehorse Creek a PTM of 1.3 produces the best results while 2.2 appears more appropriate for Lost Creek. The main difference between the two sites is that Racehorse lies at 1920 metres while Lost Creek is at 2160 metres. With more snowpack recordings at varied elevations, this theory could be further investigated.

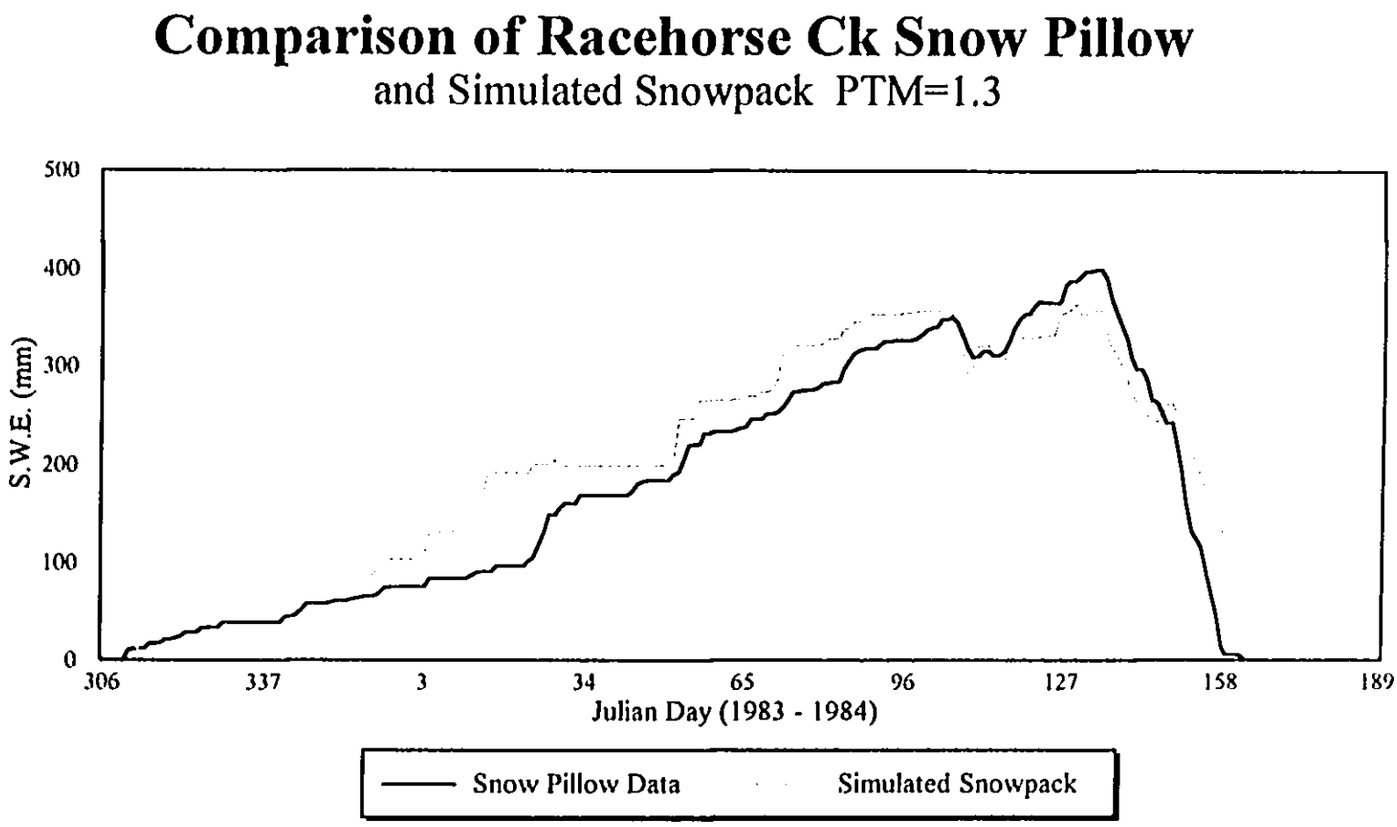

Figure 4.18 Comparison of snowpack model simulations with the Racehorse Creek snow pillow observed data for the 1983-198 snow season. A point melt factor (PTM) of 1.3 is used.

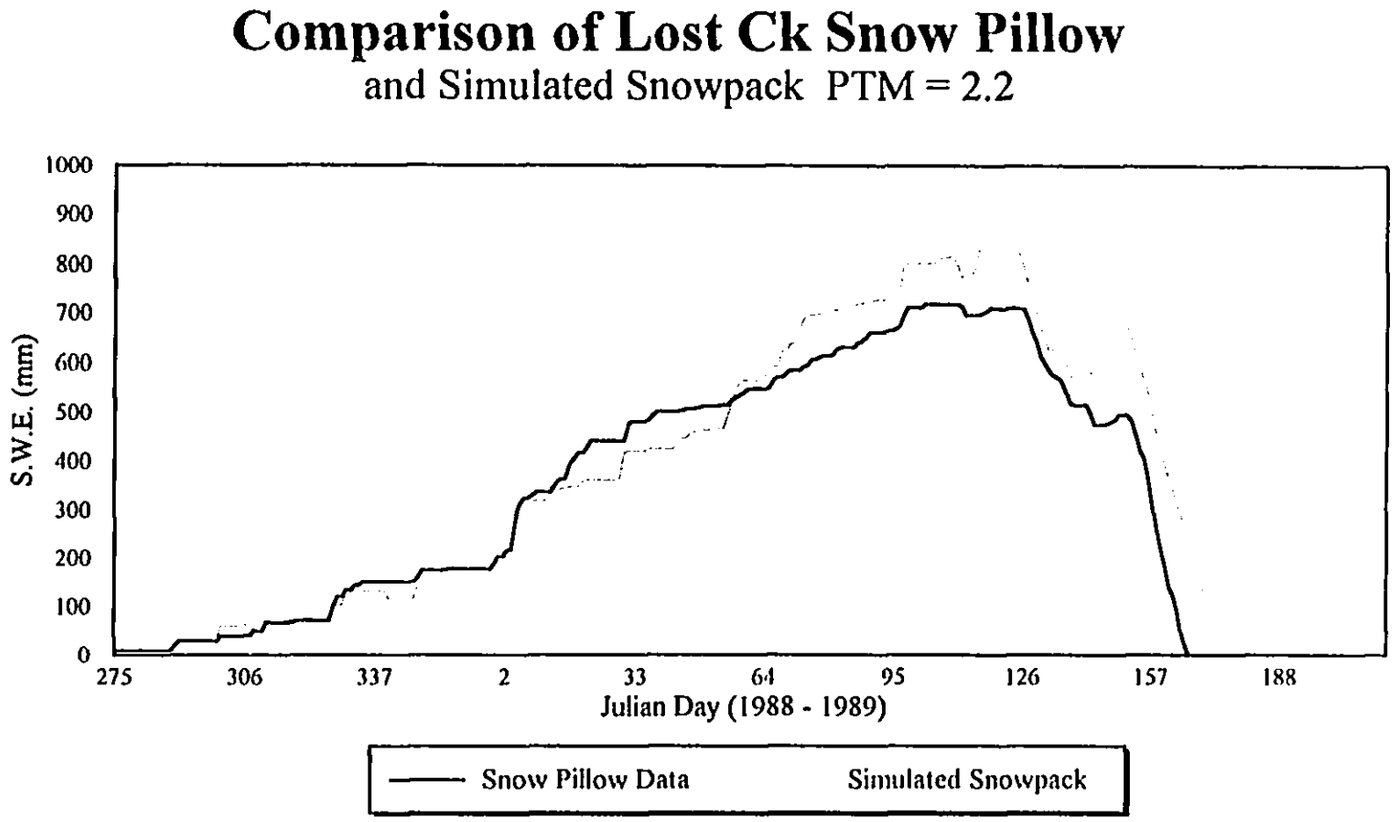

Figure 4.19 Comparison of snowpack model simulations with the Lost Creek snow pillow observed data for the 1988-1989 snow season. A point melt factor (PTM) of 2.2 is used.

Chapter 5

RESULTS

5.0 Overview

This chapter is a presentation of the findings of the project in the form of maps, tables, and statistical analysis. The early part of the chapter deals with output from the microclimate simulation model, SIMGRID, while the latter part illustrates the snowpack accumulation and ablation component derived from the gridded microclimate.

5.1 Microclimate Simulator

The following sections provide an overview of the microclimate as simulated by the SIMGRID model. The results have been imported into the GIS for map generation where several overlays and statistical analysis have been carried out. Where appropriate, shortcomings and/or problems which lend themselves to further investigation are discussed.

5.1.1 Temperature

All simulations in this study are reported at a daily interval. Such a data structure lends itself to a great deal of flexibility in terms of how the results are presented and analyzed. For example, any of the reported variables may be averaged in terms of daily, monthly, seasonally, and even long-term time periods.

For the purposes of illustration, two maps have been generated depicting temperature distribution throughout the study area. Figure 5.1, illustrates the spatial distribution of daily minimum temperature averaged over the ten year simulation period of 1970-1980. This figure does not reveal much new or surprising information, however it does indicate altitudinal controls exerted on temperature. As would be expected, the higher minimum temperatures occur at the lower elevations and decrease with increasing altitude. Generally, drainage of cold air to lower elevations is accompanied by adiabatic warming thus preserving the inverse relationship between altitude and temperature. The primary factor controlling the elevation/temperature function is the selection of lapse rates for use within the model (Appendix A). These are used to adjust the base station temperatures according to a calculated difference in elevation between it and the sites. Slope and aspect corrections do not appear to influence heavily the distribution of minimum temperature when averaged over the ten-year period. Table 5.1 summarizes the areal distribution of each two-hundred metre

Table 5.1 Areal extent of minimum temperature as a function of elevation in km^2.

Elevation Band	(°C) <-10	-10--9	-9--8	-8--7	-7--6	-6--5	-5--4	Total (km^2)	Weighted Mean (°C)
1200-1400	0.00	0.00	0.00	0.00	0.00	1.04	38.05	39.09	-4.53
1401-1600	0.00	0.00	0.02	0.00	3.30	199.70	0.40	203.42	-5.51
1601-1800	0.00	0.00	0.00	0.00	369.64	3.40	0.00	373.04	-6.49
1801-2000	0.00	0.01	0.00	5.52	407.08	0.00	0.00	412.61	-6.51
2001-2200	0.00	0.16	3.34	260.75	5.73	0.17	0.01	270.16	-7.49
2201-2400	0.00	1.59	90.70	3.10	0.36	0.11	0.06	95.92	-8.47
2401-2600	0.02	21.21	0.42	0.11	0.43	0.10	0.00	22.29	-9.40
2601-2800	0.11	3.79	0.01	0.03	0.16	0.01	0.00	4.11	-9.38
2801-3000	0.62	0.04	0.00	0.00	0.04	0.00	0.00	0.70	-10.21
3001-3200	0.05	0.00	0.00	0.00	0.00	0.00	0.00	0.05	-10.50
Total	0.80	26.80	94.49	269.51	786.74	204.53	38.52	1421.39	-6.68

Long-Term Average Daily Minimum Temperature

(1970-1980)

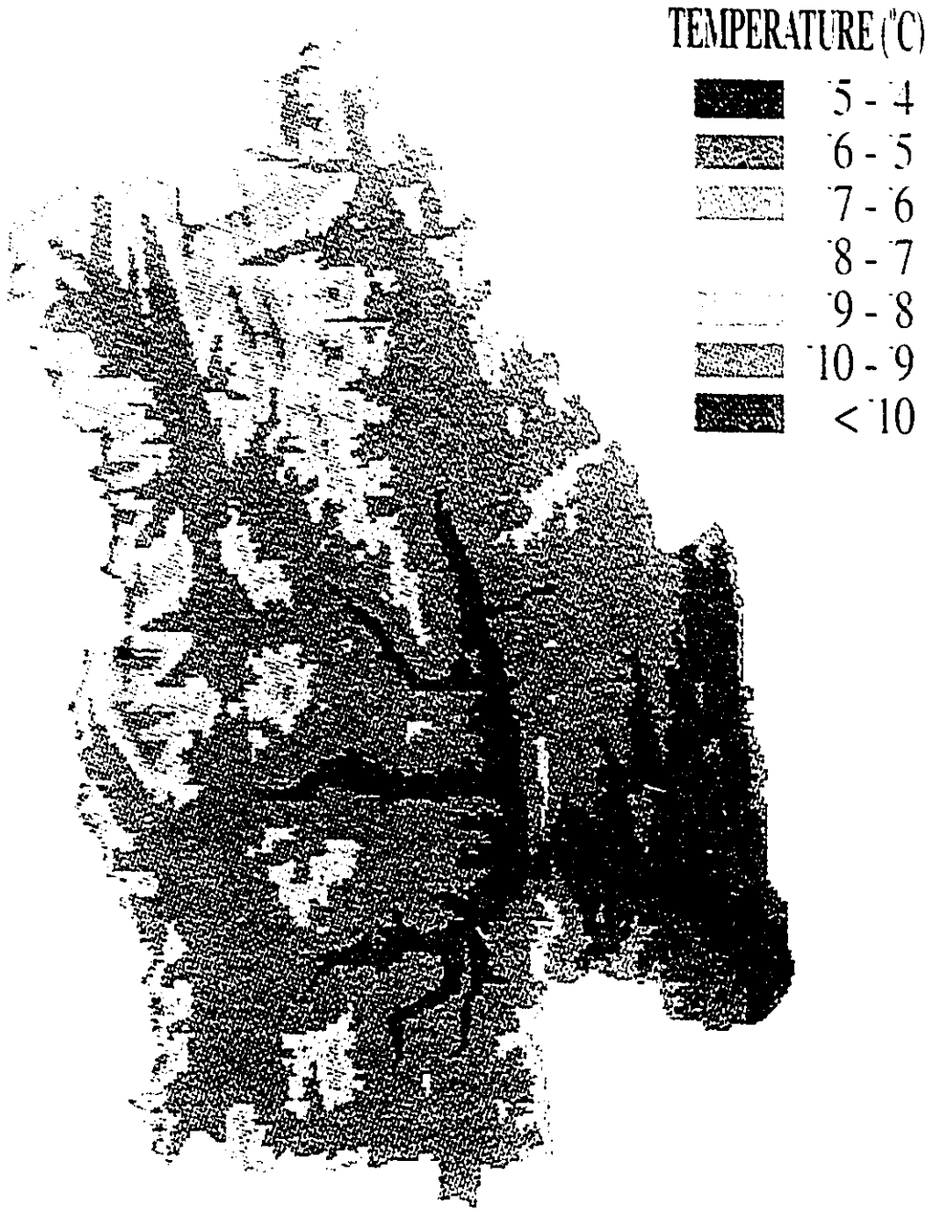

Figure 5.1 Long-term average daily minimum temperature for the 1970-1980 decade as derived from microclimate simulations. Pixel size is 100 metres.

elevation band in relation to the seven temperature classes and provides an area-weighted mean minimum temperature value for each elevation. The dispersion of data values representing area in km^2, indicates an obvious negative correlation between elevation and average minimum temperature. Areas in the "<-10" temperature class lie exclusively at the higher elevations while the warmer temperatures are generally found at lower elevations. There is a slight deviation from the linear distribution of points at either end of the temperature scale. Finally, the graph in figure 5.2 clearly illustrates the nearly linear negative relationship between elevation and the area-weighted mean minimum temperature. For reference purposes, figure 5.3 has been included to show the areal distribution of elevation in the study area.

Figure 5.4 demonstrates the spatial variability of the mean daylight temperature, described earlier as STEMP, averaged over the 1970 to 1980 simulation period. Unlike the previous map, mean STEMP is sensitive to aspect. A close inspection of the map reveals that the south-facing facets tend to be slightly warmer (generally by 1-2 °C). This is not surprising since daylight average temperature is driven, for the most part, by the interaction between incoming solar radiation and the reflective properties of ground features. This feature does not appear on the previous map because the daily minimum temperature is less sensitive to aspect. More specifically, the minimum daily temperature is most likely to occur during the non-daylight hours. The appearance of this differentiation between north and south-facing slopes reaffirms the selection of pixel size and therefore spatial resolution used in the model. It indicates that the model is detecting small scale variations consistent with established

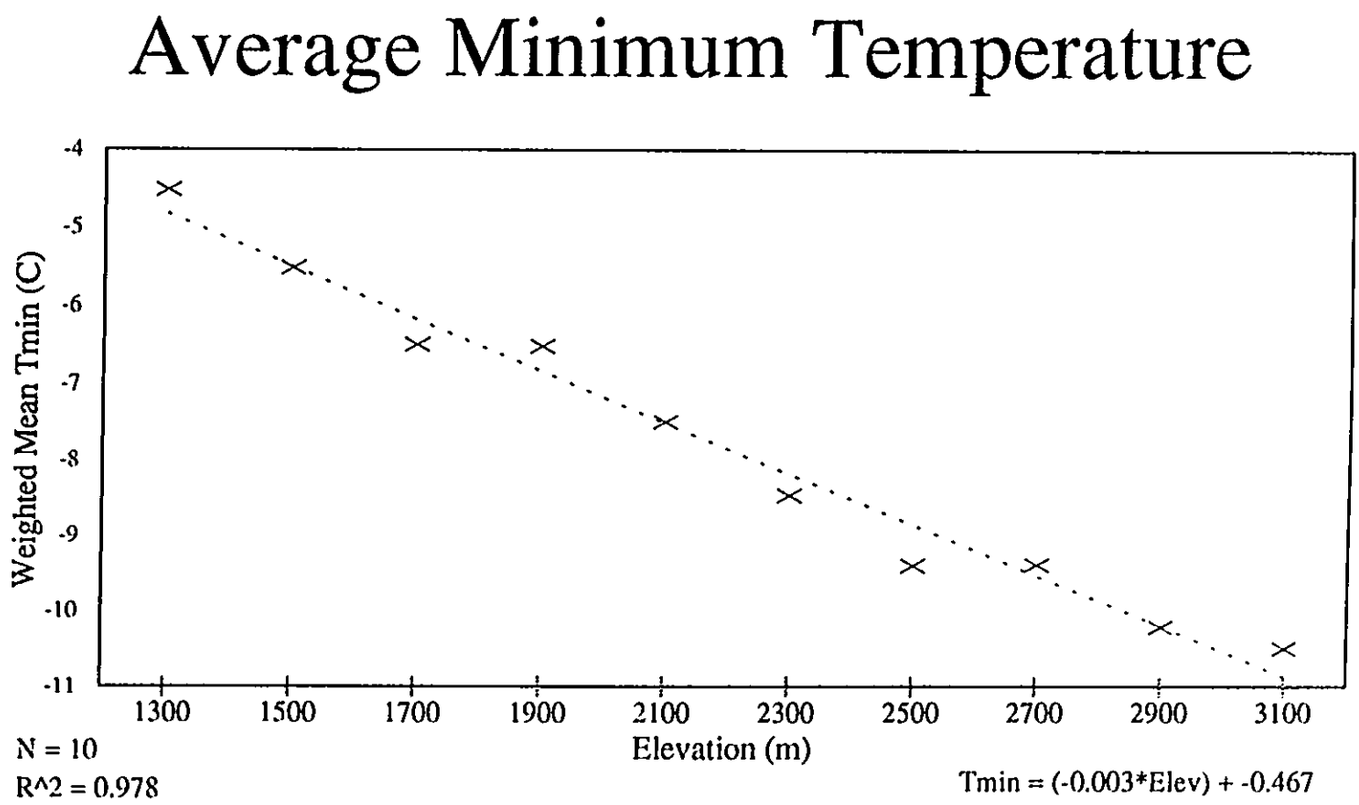

Figure 5.2 Area-weighted mean daily minimum temperature as a function of elevation.

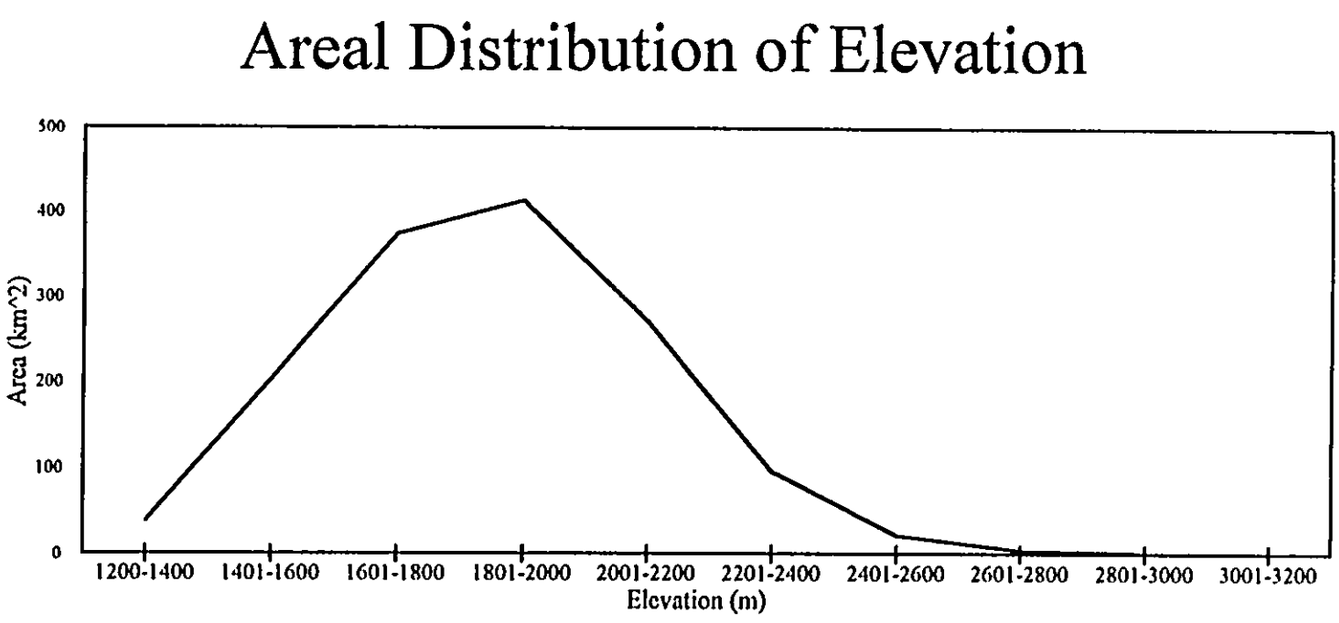

Figure 5.3 Areal distribution of elevation throughout the study area.

Long-Term Mean Daylight Average Temperature (STEMP) (1970-1980)

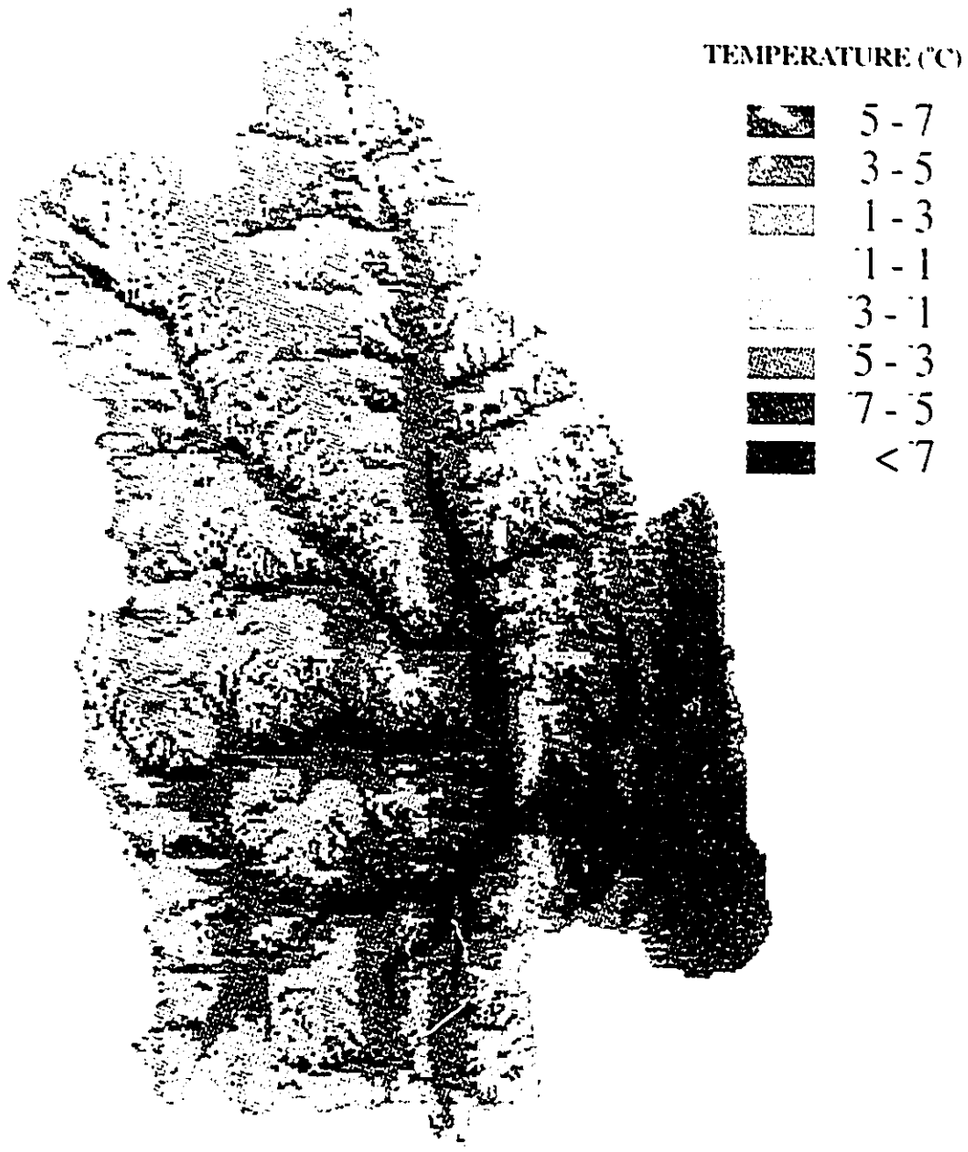

Figure 5.4 Long-term mean daylight average temperature (STEMP) for the 1970-1980 decade as derived from microclimate simulations. Pixel size is 100 metres.

general principles which would suggest differences due to slope orientation are likely to occur. Table 5.2 shows the total area in km^2 for each of eight temperature classes versus the ten elevation bands as well as the area-weighted mean STEMP. Once again, the strongly negative correlation between elevation and temperature is shown by the nearly linear dispersion of data values from the lower left of the table to the upper right. However,

Table 5.2 Areal extent of average STEMP (Average daylight temp.) as a function of elevation in km^2.

Elevation Band	(°C) <-7	-7--5	-5--3	-3--1	-1-1	1-3	3-5	5-7	Total (km^2)	Weighted Mean (°C)
1200-1400	0.00	0.00	0.00	0.00	0.00	0.00	28.30	10.79	39.09	4.55
1401-1600	0.00	0.00	0.00	0.02	0.00	3.28	156.24	43.88	203.42	4.40
1601-1800	0.00	0.00	0.00	0.00	6.91	278.11	87.53	0.49	373.04	2.44
1801-2000	0.00	0.00	0.01	0.00	320.51	29.36	62.73	0.00	412.61	0.75
2001-2200	0.00	0.00	0.10	3.40	210.64	55.79	0.23	0.00	270.16	0.39
2201-2400	0.00	0.00	0.50	73.84	21.18	0.22	0.15	0.03	95.92	-1.55
2401-2600	0.00	0.02	3.50	17.33	1.03	0.31	0.09	0.01	22.29	-2.14
2601-2800	0.00	0.11	2.55	1.25	0.13	0.06	0.01	0.00	4.11	-3.21
2801-3000	0.00	0.41	0.25	0.00	0.00	0.04	0.00	0.00	0.70	-4.83
3001-3200	0.01	0.04	0.00	0.00	0.00	0.00	0.00	0.00	0.05	-6.40
Total	0.01	0.58	6.91	95.84	560.40	367.17	335.28	55.20	1421.39	1.54

consideration of figure 5.5 implies that the mean daylight temperature is not related completely linearly to elevation as some deviation occurs in the 1700 -1900 metre elevation range.. Essentially, this implies that elevation, although very important, is not the only significant factor. Table 5.3 is similar to the previous table except that the temperature classes are reported as total areal extent within each of the four aspect categories. When the area-weighted mean STEMP for each aspect is plotted as in figure 5.6, it becomes evident that south-facing slopes do react differently than the others in that temperatures are

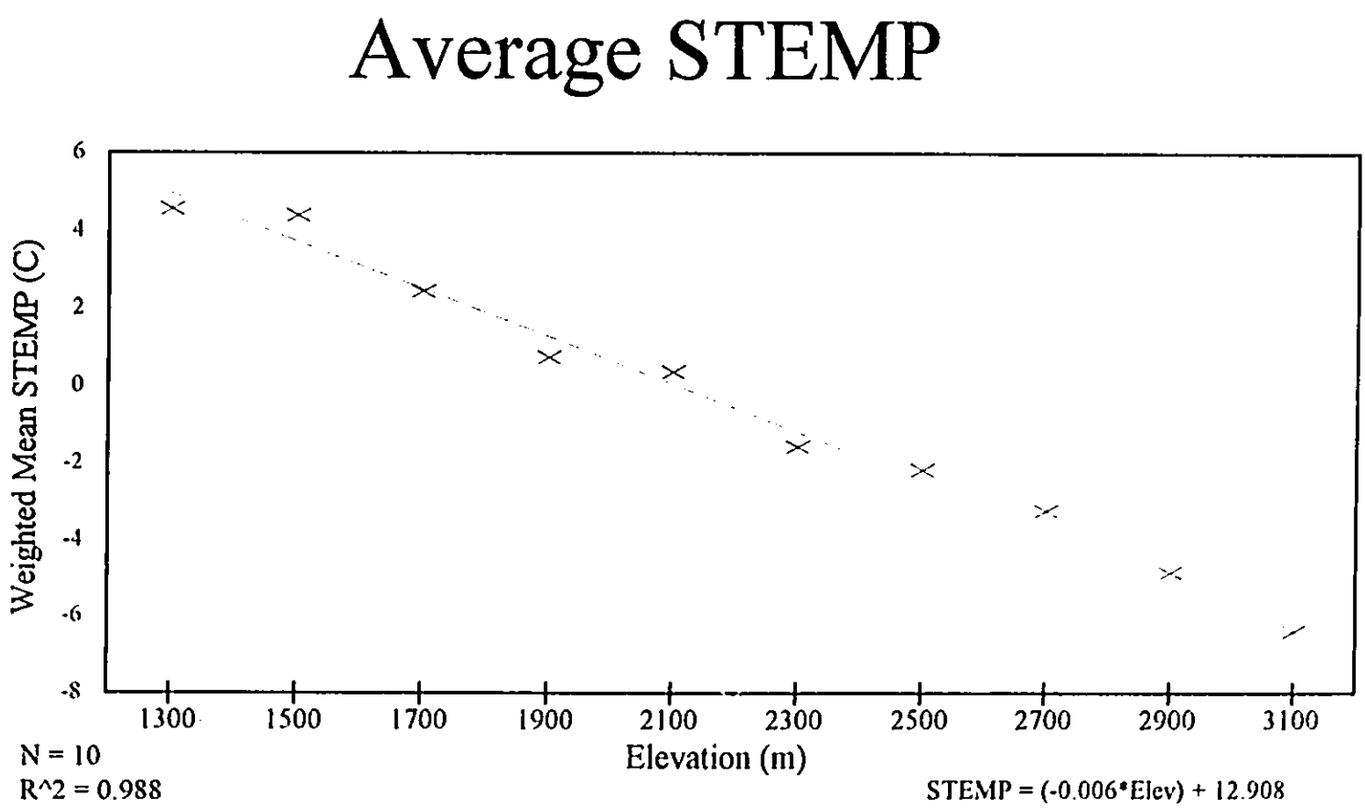

Figure 5.5 Area-weighted mean daylight average temperature as a function of elevation.

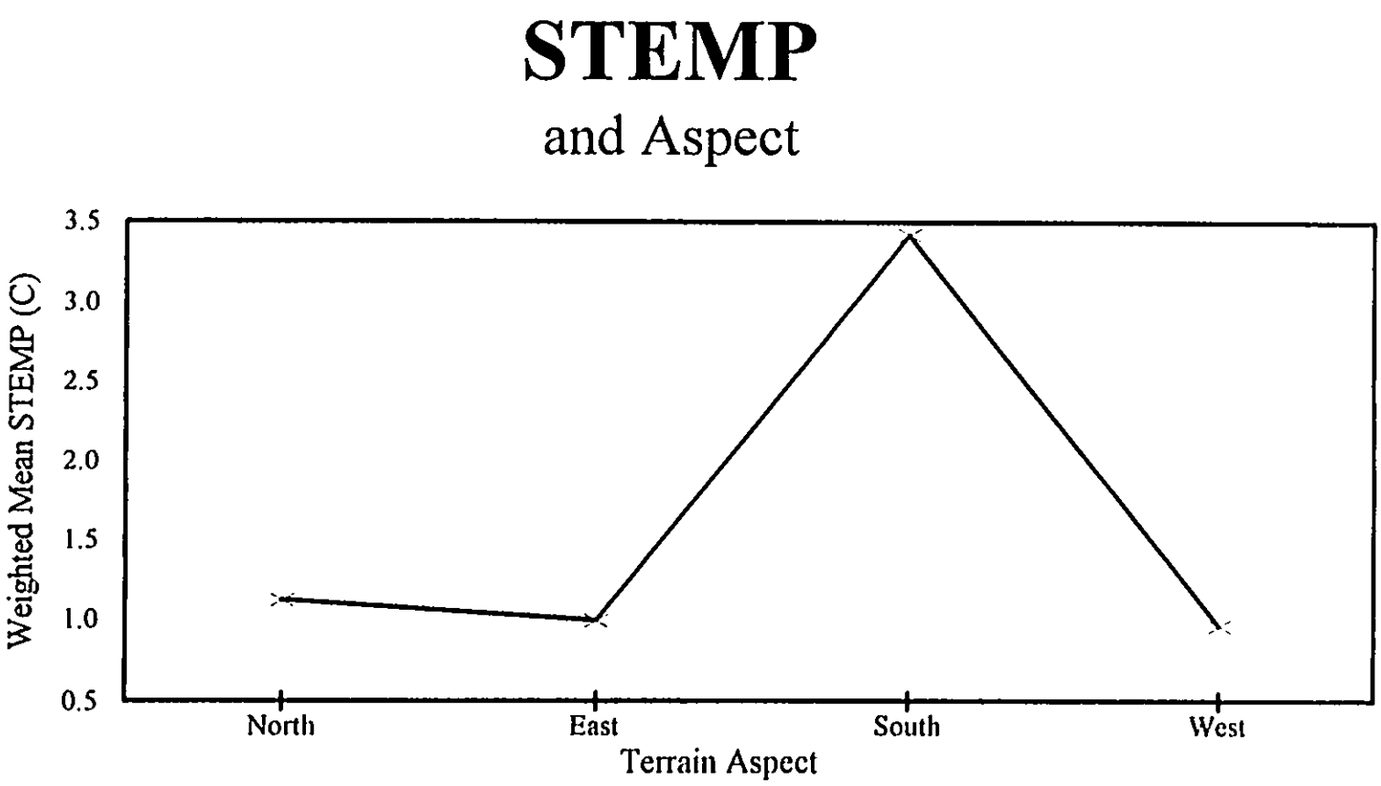

Figure 5.6 Area-weighted mean daylight average temperature as a function of terrain aspect.

Table 5.3 Areal extent of STEMP as a function of aspect in km^2.

Aspect	(°C)								Total	Weighted Mean (°C)
	<-7	-7--5	-5--3	-3--1	-1-1	1-3	3-5	5-7		
North	0.00	0.25	2.16	19.12	137.40	77.53	48.55	3.76	288.77	1.12
East	0.00	0.21	4.51	43.86	230.55	124.12	85.62	0.00	488.87	0.99
South	0.00	0.00	0.48	5.42	21.49	77.63	142.98	52.08	300.08	3.42
West	0.01	0.16	1.72	33.85	179.27	91.80	61.05	0.00	367.86	0.96
Total	0.01	0.62	8.87	102.25	568.71	371.08	338.20	55.84	1445.58	1.51

significantly higher. Finally, regression analysis presented in table 5.4 illustrates the influence of not only elevation but also aspect and slope on mean daylight temperature. According to simulation results, STEMP as a function of elevation alone produces an r^2 of 0.699 while aspect alone results in an insignificant r^2 of 0.001. Inclusion of aspect along with elevation results in a slight improvement. Slope does not appear to be significant on its own.

Table 5.4 STEMP regression analysis summary.

Independent Var(s)	Dependent Var	Constant	SEYE*	R^2	No. of Obs.	DOF*	X Coef(s)	SEC*
Elevation	STEMP	13.845	1.116	0.699	5782	5780	-0.0067	0.000058
Aspect	STEMP	1.332	2.035	0.001	5782	5780	0.0007	0.000270
Elevation	STEMP	13.712	1.114	0.701	5782	5779	-0.0067	0.000057
Aspect							0.0008	0.000148
Elevation	STEMP	13.614	1.113	0.701	5782	5778	-0.0066	0.000066
Aspect							0.0008	0.000148
Slope							-0.0023	0.000790

SEYE* = Standard Error of the Y Estimate
DOF* = Degrees of Freedom
SEC* = Standard Error of Coefficient

5.1.2 Precipitation

Due to the fact that precipitation is determined to be strictly a function of elevation with the limited datasets available for this study, the map of its distribution is very similar in appearance to the digital elevation model portrayed in chapter 4. Figure 5.7 depicts the ten-

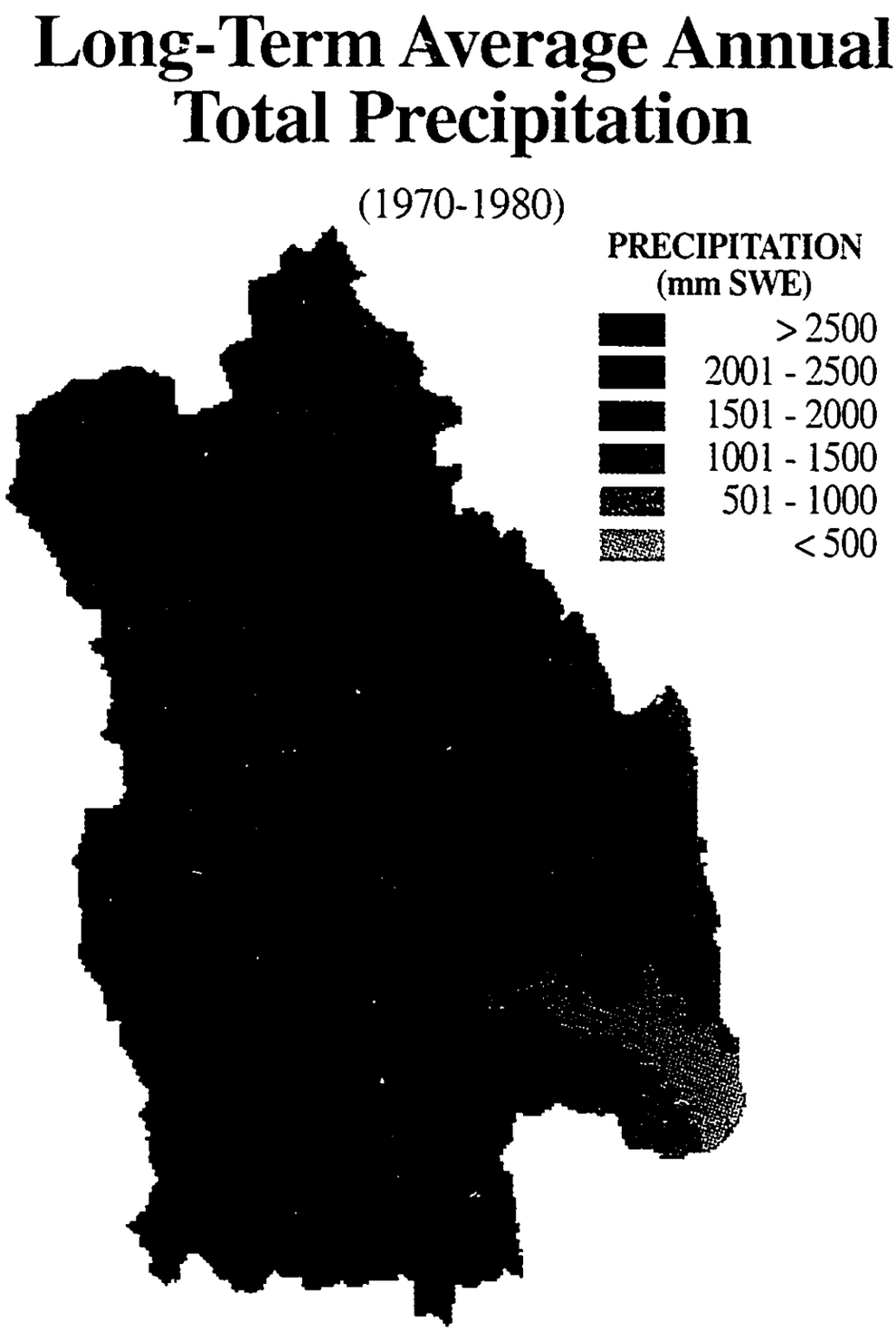

Figure 5.7 Average annual total precipitation for the 1970-1980 decade as derived from microclimate simulations. Pixel size is 100 metres.

year (1970-1980) average annual total precipitation in millimetres of snow water equivalent (SWE). The map implies that the greater annual precipitation occurs at the highest elevations while the areas near the gauging station receive the least amounts. Several other factors including slope, aspect, prevailing wind direction, and distance from the continental divide may also play roles. These, along with elevation, are identified in the literature as being important in determining the occurrence and quantity of precipitation (Price, 1981; Barry, 1992; Storr and Ferguson, 1972). However, these influences are not identified to be statistically significant with the datasets used.

Table 5.5 shows a breakdown of the areal extent of the precipitation classes as a function of elevation and the area-weighted mean annual precipitation. This time there is a positive relationship with precipitation becoming more abundant as elevation increases. The data values deviate only slightly from the upper left to the lower right diagonal. However, the graph in figure 5.8 implies a non-linear relationship between elevation and precipitation when the area-weighted mean is used. The graph suggests precipitation increases in a nearly linear fashion before approximately 2000 metres and then the rate at which it increases drops off. At approximately 2500 metres, the total annual precipitation levels off implying further elevation gain has no effect. This is likely a product of the insignificant area above 2500 metres (Table 3.1 and Figure 5.3).

Related to temperature and moisture is relative humidity which is the amount of water vapor in the air expressed as a percentage of the amount it can hold at a particular temperature and

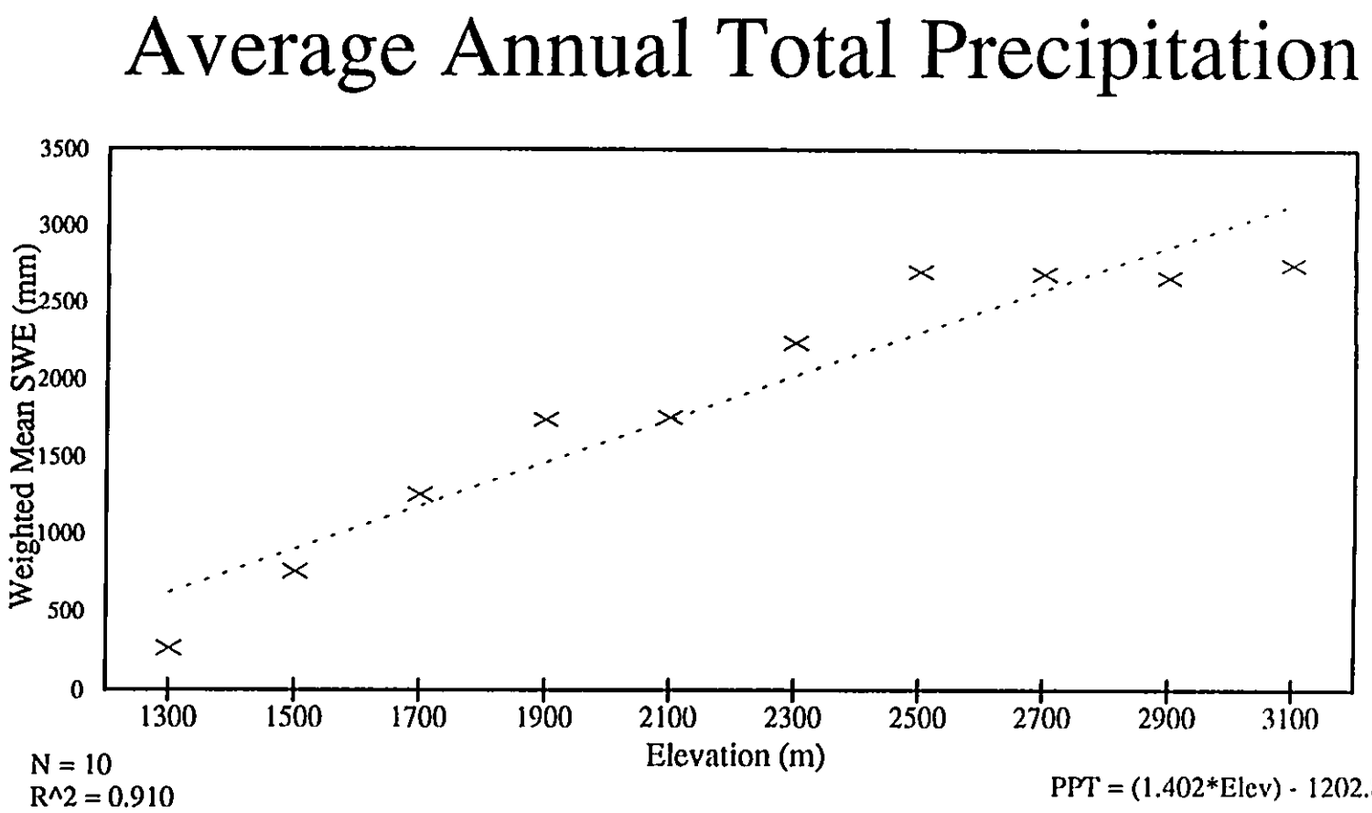

Figure 5.8 Area-weighted mean total annual precipitation as a function of elevation.

pressure. The same air parcel at different temperatures would report very different relative

Table 5.5 Areal extent of average annual total precipitation as a function of elevation in km^2.

Elevation Band	(mm) 0-500	501-1000	1001-1500	1501-2000	2001-2500	>2500	Total (km^2)	Weighted Mean (mm)
1200-1400	38.05	1.04	0.00	0.00	0.00	0.00	39.09	263.30
1401-1600	0.40	199.70	3.30	0.00	0.02	0.00	203.42	757.28
1601-1800	0.00	3.40	362.55	7.09	0.00	0.00	373.04	1254.95
1801-2000	0.00	0.00	6.74	405.86	0.00	0.01	412.61	1741.86
2001-2200	0.01	0.17	0.10	266.38	3.34	0.16	270.16	1755.90
2201-2400	0.06	0.11	0.16	3.30	90.70	1.59	95.92	2236.45
2401-2600	0.00	0.10	0.25	0.29	0.42	21.23	22.29	2701.77
2601-2800	0.00	0.01	0.06	0.13	0.01	3.90	4.11	2690.39
2801-3000	0.00	0.00	0.04	0.00	0.00	0.66	0.70	2664.29
3001-3200	0.00	0.00	0.00	0.00	0.00	0.05	0.05	2750.00
Total	38.52	204.53	373.20	683.05	94.49	27.60	1421.39	1486.83

humidities even though the actual quantity of water vapor or absolute humidity remains constant. Therefore, changes in temperature occurring as a result of increased or decreased elevation directly influence this ratio.

Figure 5.9 illustrates not only the distribution of relative humidity, but also exemplifies the flexibility with which model output may be analyzed. In this case, conditions are mapped using the most basic temporal unit, an individual day. It is apparent from the map that relative humidity is at least partially driven by elevation in that there is a general rise with increased altitude. As there is some deviation from the DEM, however, other factors obviously play a role. The east-west orientation of dark bands throughout the map indicate that aspect is also an important influence. The darkest areas, representing the lowest relative humidity, invariably occur along south-facing facets in the terrain. As with the change due to elevation,

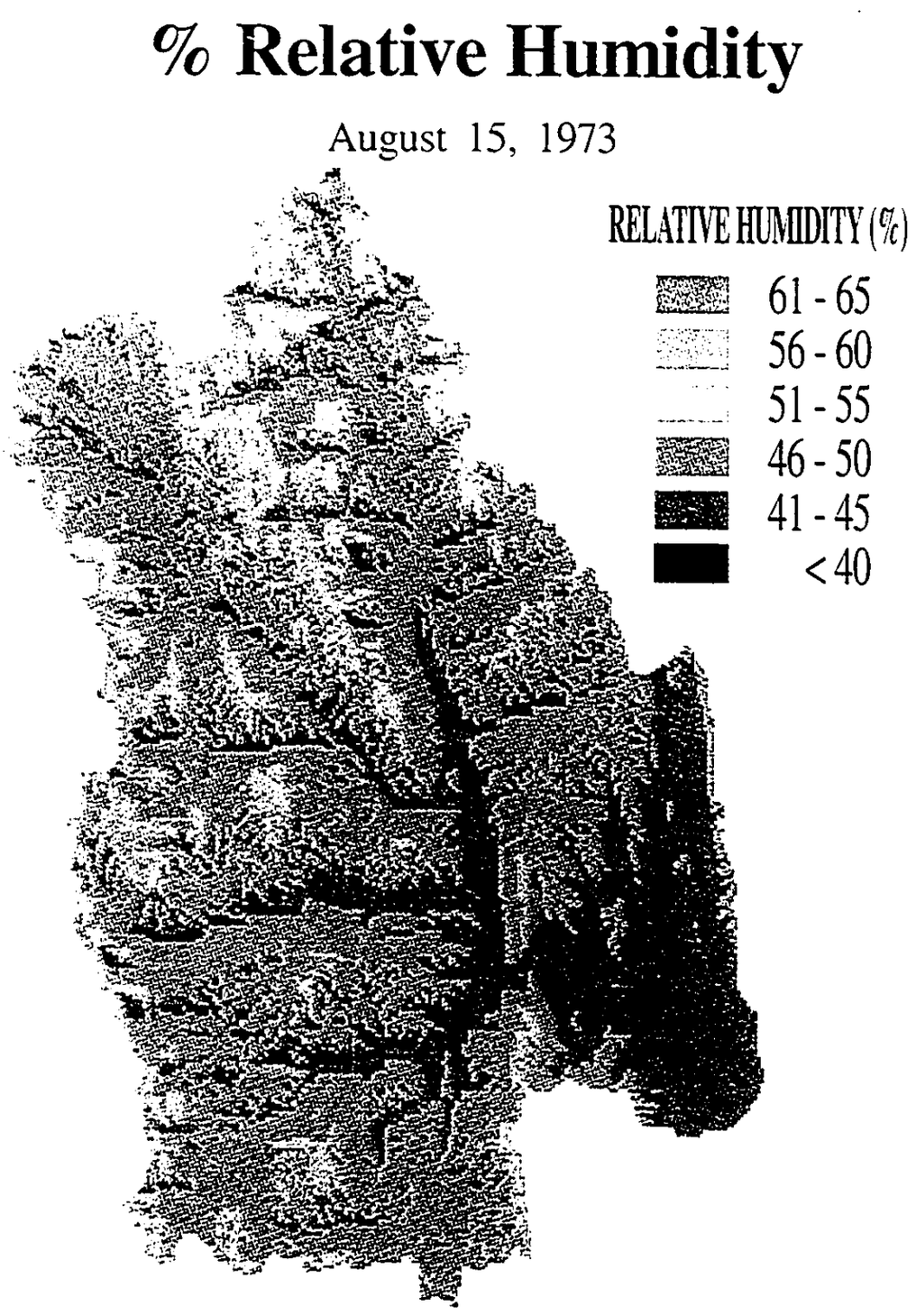

Figure 5.9 % Relative Humidity on August 15, 1973 as derived from microclimate simulations. South-facing slopes indicate a lower relative humidity than surrounding cells. Pixel size is 100m.

this effect is likely the direct result of changes in surface heating and therefore surrounding air temperature. It has been shown earlier that temperature decreases with altitude and that it is sensitive, at least in part, to terrain aspect. Therefore, higher temperatures on south-facing slopes and at lower elevations result in a decreased relative humidity. Conversely, lower temperatures on slopes other than south-facing and at higher elevations result in an increased relative humidity.

Table 5.6 shows a positive near linear relationship between relative humidity and elevation as evidenced by the data value distribution. Figure 5.10 too implies relative humidity is

Table 5.6 Areal extent of relative humidity as a function of elevation in km^2.

Elevation Band	%RH						Total (km²)	Weighted Mean(%RH)
	<40	41-45	46-50	51-55	56-60	61-65		
1200-1400	10.79	28.30	0.00	0.00	0.00	0.00	39.09	41.12
1401-1600	43.90	156.22	3.28	0.02	0.00	0.00	203.42	41.50
1601-1800	84.92	3.09	285.03	0.00	0.00	0.00	373.04	45.18
1801-2000	0.25	85.31	324.88	2.16	0.01	0.00	412.61	46.49
2001-2200	0.00	55.92	120.54	93.60	0.10	0.00	270.16	48.20
2201-2400	0.04	0.21	18.89	75.42	1.36	0.00	95.92	51.56
2401-2600	0.01	0.15	4.52	5.73	11.86	0.02	22.29	54.08
2601-2800	0.00	0.01	1.22	0.04	2.73	0.11	4.11	54.58
2801-3000	0.00	0.00	0.04	0.18	0.04	0.44	0.70	58.79
3001-3200	0.00	0.00	0.00	0.00	0.00	0.05	0.05	62.50
Total	139.91	329.21	758.40	177.15	16.10	0.62	1421.39	46.10

explained mostly by elevation. However, regression results found in table 5.7 suggest that aspect is slightly more important than it is for STEMP and that r^2 is notably improved by the inclusion of aspect and/or slope along with the vertical component. As with STEMP, the area-weighted mean relative humidity is calculated for the four aspect classes (table 5.8) and plotted as in figure 5.11. Interestingly, the south-facing slopes clearly produce significantly

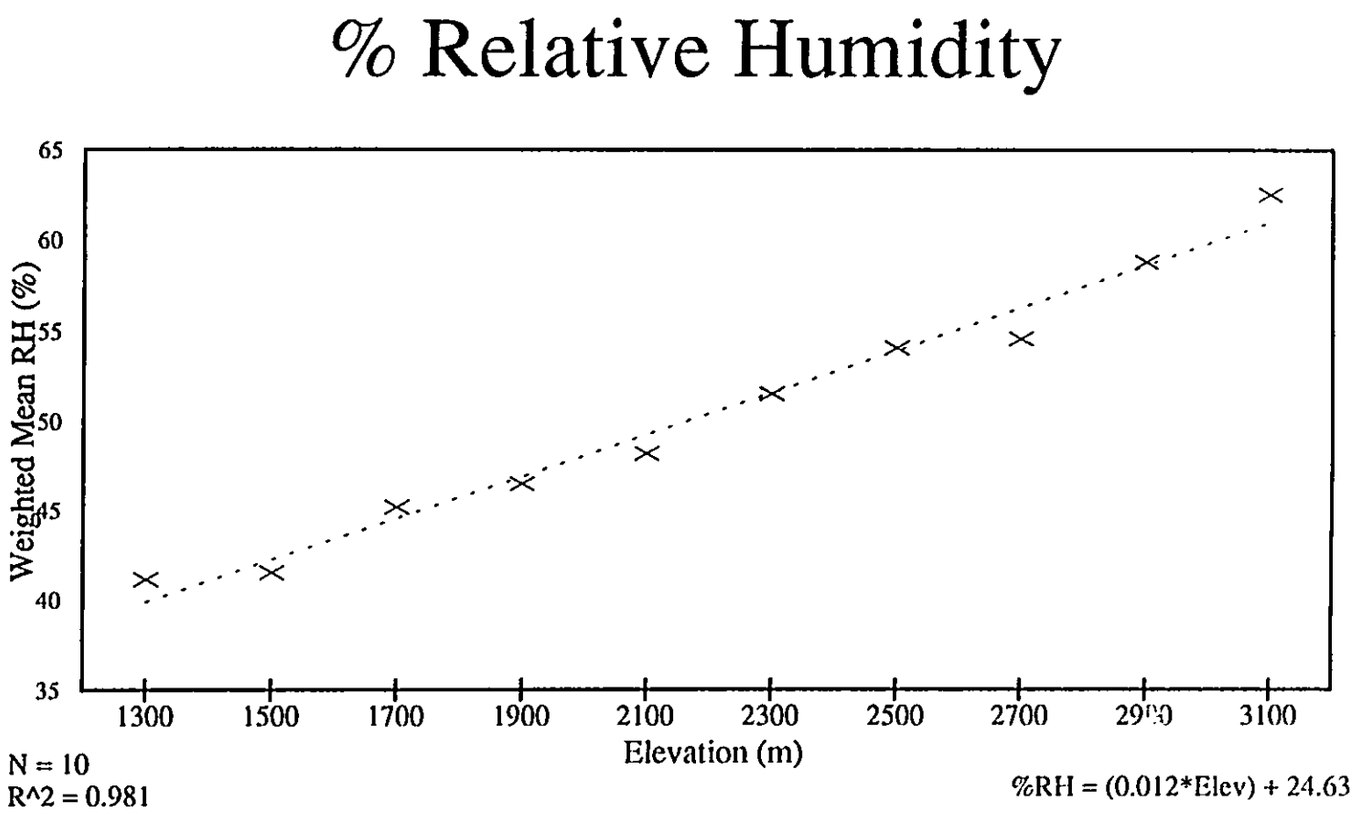

Figure 5.10 Area-weighted mean relative humidity (%) as a function of elevation.

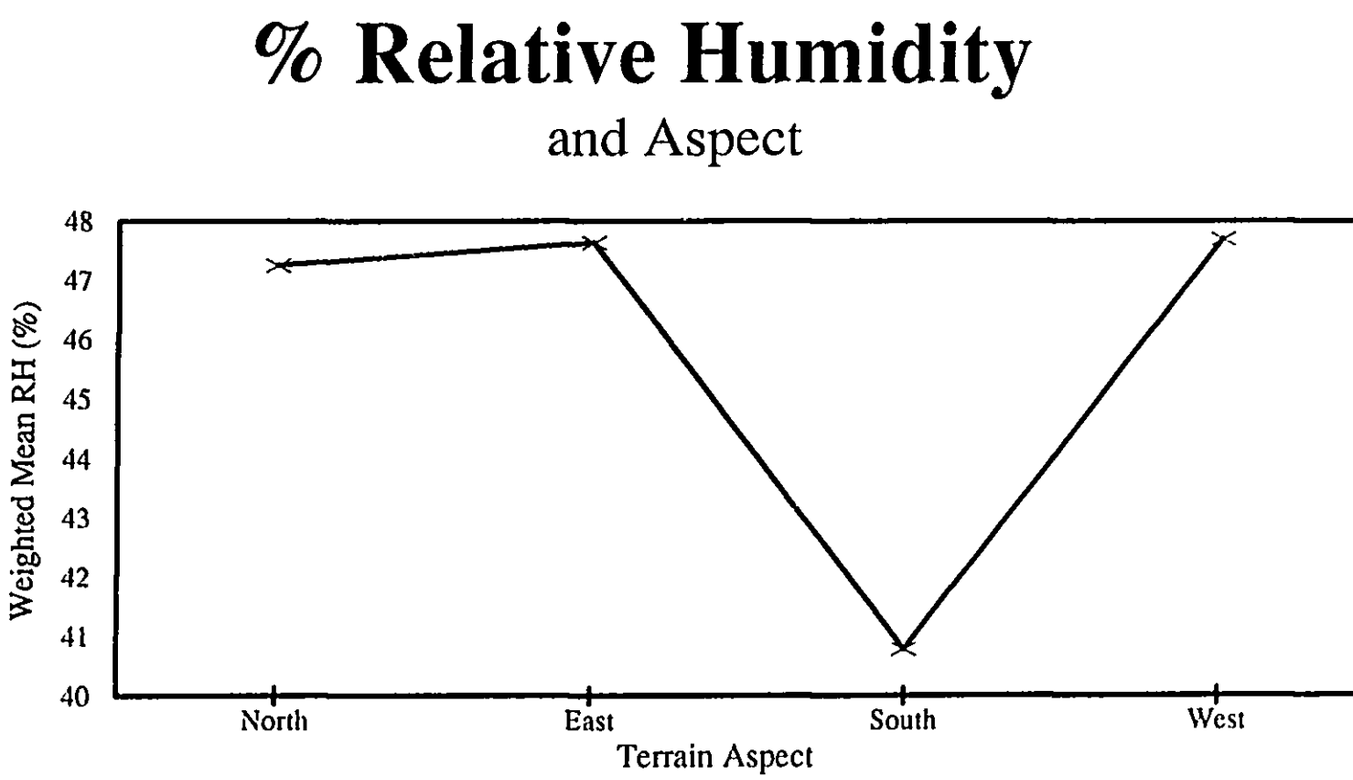

Figure 5.11 Area-weighted mean relative humidity (%) as a function of aspect.

lower relative humidities whereas the other aspects have relatively high humidities.

Table 5.7 Relative humidity regression analysis summary.

Independent Var(s)	Dependent Var	Constant	SEYE*	R^2	No. of Obs.	DOF*	X Coef(s)	SEC*
Elevation	RH	26.033	2.631	0.519	5782	5780	0.0107	0.000136
Aspect	RH	46.213	3.790	0.002	5782	5780	-0.0017	0.000504
Elevation	RH	26.340	2.625	0.521	5782	5779	0.0107	0.000135
Aspect							-0.0019	0.000349
Elevation	RH	26.908	2.613	0.526	5782	5778	0.0102	0.000156
Aspect							-0.0019	0.000347
Slope							0.0133	0.001856

SEYE* = Standard Error of the Y Estimate
DOF* = Degrees of Freedom
SEC* = Standard Error of Coefficient

Table 5.8 Areal extent of relative humidity as a function of aspect in km^2.

Aspect	% RH						Total	Weighted Mean %RH
	<40	41-45	46-50	51-55	56-60	61-65		
North	6.97	47.14	192.84	36.87	4.70	0.25	288.77	47.26
East	0.02	86.41	312.44	80.35	9.44	0.21	488.87	47.64
South	134.08	138.13	25.33	2.24	0.25	0.05	300.08	40.78
West	0.00	61.06	236.47	65.47	4.69	0.17	367.86	47.69
Total	141.07	332.74	767.08	184.93	19.08	0.68	1445.58	46.15

5.2 Snowpack Accumulation/Ablation

The modelled snowpack distribution is based on and therefore dependent upon simulated microclimate. As a result, shortcomings discussed in the previous section propagate through into this component of the model and thus affect overall accuracy. The best example of this is the overestimation of precipitation at higher altitudes which also results in an overestimation of snowpack in those areas. Fortunately, however, only 0.04 percent of the total basin area lies above 2600 metres which is the area of most concern (see table 3.1) for

simulation accuracy.

5.2.1 Snowpack Monitoring

As with the other variables, snowpack accumulation and ablation may be presented in a number of ways. Obviously, conditions can be depicted as daily, monthly, seasonally, and long-term averaged values or alternatively it may be possible to determine the appropriate time frame from the model output itself. Figures 5.12 and 5.13 represent the depiction of snowpack for a date which is chosen to be representative of spring snow conditions. Both show the same information, but the latter is displayed with the class at which a noticeable change occurs enhanced for ease of interpretation. Upon close inspection it is possible to detect a noticeable decrease in the snowpack depth of south-facing facets, especially in the western half of the basin. These areas have been enhanced in figure 5.13 so that they are more easily distinguished. Generally speaking, the effects of aspect are slight in the lower portions of the basin. However, there appears to be a critical elevation of approximately 2200 metres where slope orientation becomes a sufficient influence to cause increased or decreased accumulations. The variations that do occur are in the range of 100 to 150 millimetres of snow water equivalent.

Table 5.9 indicates an increase in snowpack accumulation with elevation which is logical given that generally precipitation is greater and temperature lower at higher altitudes. When the area-weighted snowpack depth is plotted against elevation as in figure 5.14, it is implied that elevation alone plays a major role in controlling April 1 snowpack depth. This is confirmed by the regression analysis results found in table 5.10 which implies no improvement

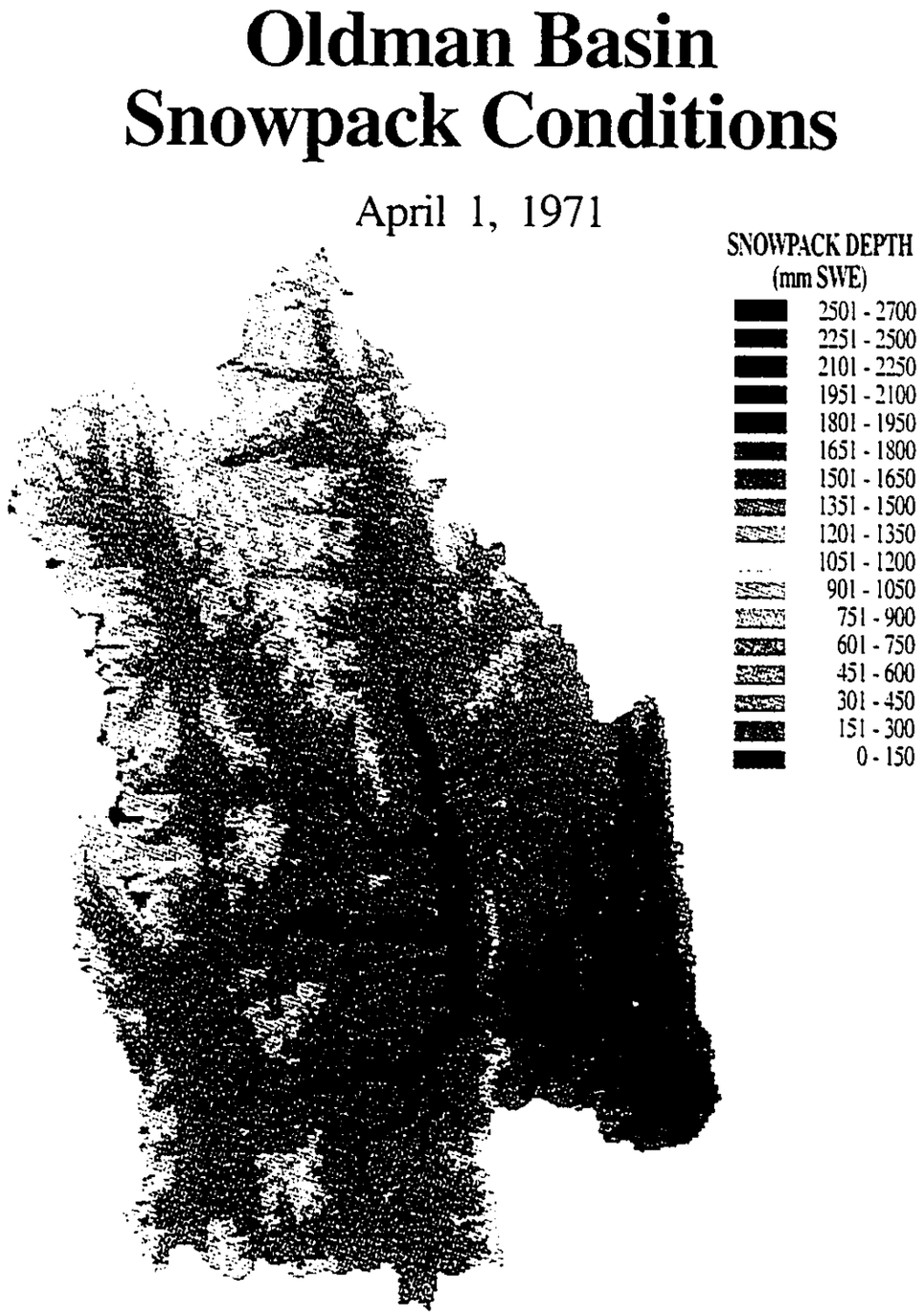

Figure 5.12 Snowpack conditions on April 1, 1971 as derived from the snowpack simulations. South-facing slopes indicate a lower snowpack depth than surrounding cells. Pixel size is 100m.

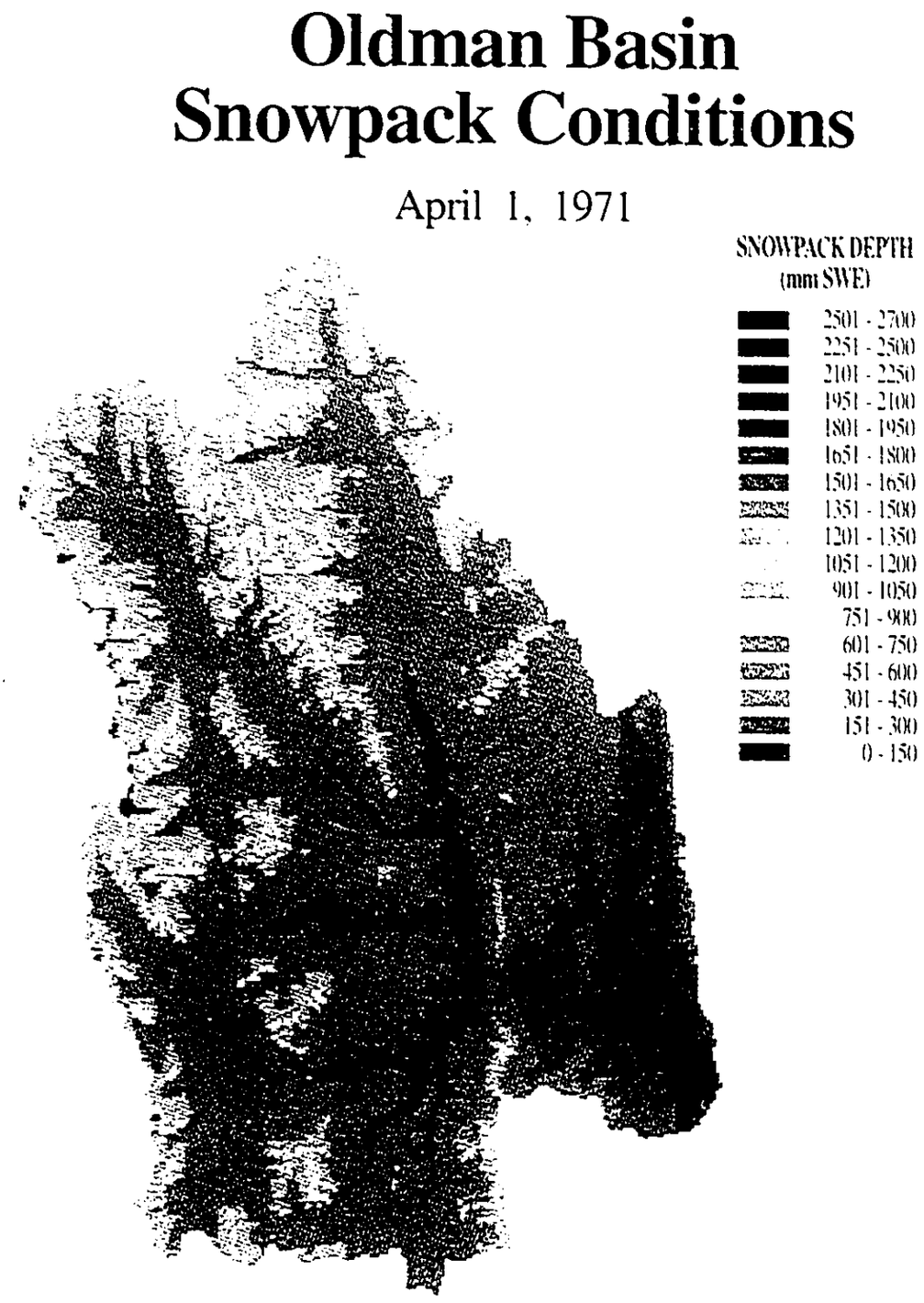

Figure 5.13 Snowpack conditions on April 1, 1971 as derived from the snowpack simulations. The 750-900 mm class has been highlighted to illustrate the class most noticeably affected by aspect. Pixel size is 100m.

Table 5.9 Areal extent of April 1, 1971 snowpack as a function of elevation in km^2.

Elevation Band	SWE (mm) 0-150	151-300	301-450	451-600	601-750	751-900	901-1050	1051-1200	1201-1350	1351-1500	1501-1650	1651-1800	1801-1950	1951-2100	2101-2250	2251-2500	2501-2700	Total (km^2)	Weight Mean (mm)
1200-1400	38.05	1.04	0.00	0.00	0.00	0.00	0.00	0.00	0.00	0.00	0.00	0.00	0.00	0.00	0.00	0.00	0.00	39.09	75.99
1401-1600	0.40	199.61	0.09	3.30	0.00	0.00	0.00	0.02	0.00	0.00	0.00	0.00	0.00	0.00	0.00	0.00	0.00	203.42	229.73
1601-1800	0.00	3.40	0.00	362.55	7.09	0.00	0.00	0.00	0.00	0.00	0.00	0.00	0.00	0.00	0.00	0.00	0.00	373.04	525.12
1801-2000	0.00	0.00	0.00	6.74	400.34	0.09	5.43	0.00	0.01	0.00	0.00	0.00	0.00	0.00	0.00	0.00	0.00	412.61	676.55
2001-2200	0.01	0.17	0.00	0.10	5.63	55.96	204.79	3.34	0.16	0.00	0.00	0.00	0.00	0.00	0.00	0.00	0.00	270.16	939.04
2201-2400	0.06	0.11	0.00	0.16	0.20	0.08	3.02	90.70	1.49	0.00	0.10	0.00	0.00	0.00	0.00	0.00	0.00	95.92	1119.20
2401-2600	0.00	0.10	0.00	0.25	0.18	0.05	0.06	0.42	20.77	0.00	0.44	0.00	0.02	0.00	0.00	0.00	0.00	22.29	1258.85
2601-2800	0.00	0.01	0.00	0.06	0.10	0.00	0.03	0.01	0.21	0.00	3.58	0.00	0.11	0.00	0.00	0.00	0.00	4.11	1521.72
2801-3000	0.00	0.00	0.00	0.04	0.00	0.00	0.00	0.00	0.00	0.00	0.04	0.18	0.44	0.00	0.00	0.00	0.00	0.70	1742.14
3001-3200	0.00	0.00	0.00	0.00	0.00	0.00	0.00	0.00	0.00	0.00	0.00	0.00	0.02	0.03	0.00	0.00	0.00	0.05	1965.00
Total	38.52	204.44	0.09	373.20	413.54	56.18	213.33	94.49	22.64	0.00	4.16	0.18	0.59	0.03	0.00	0.00	0.00	1421.39	648.33

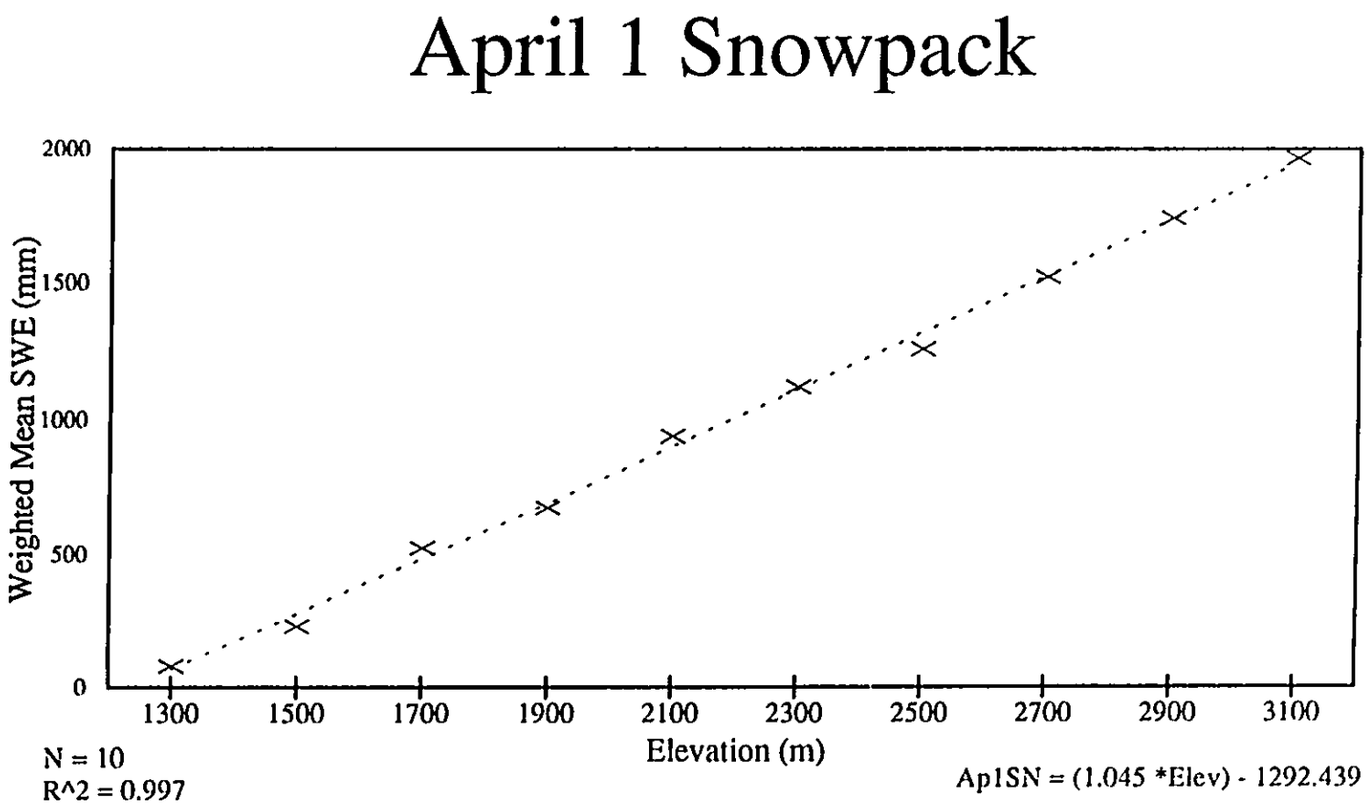

Figure 5.14 Area-weighted mean April 1, 1971 snowpack as a function of elevation.

in r^2 when aspect is used in combination with elevation, but the inclusion of slope and aspect together do result in a slight increase. Elevation alone produces an $r^2 = 0.922$.

5.2.2 Maximum Snowpack

Maximum snowpack accumulation is a fairly reliable indicator of the amount of melt water that will be available during the melt period. Total annual accumulations and the timing of snow dissappearance can be directly influenced by the depth of maximum accumlation. It is also indicative of the type of winter experienced in a region. Cold winters with lots of precipitation events will result in a substantially higher snowpack than will a warm winter having fewer events.

Figure 5.15 shows the 1970-1980 average maximum snowpack depth derived from the simulations. Again, it is apparent that elevation is a key control on the occurrence of

Table 5.10 April 1 snowpack regression analysis summary.

Independent Var(s)	Dependent Var	Constant	SEYE*	R^2	No. of Obs.	DOF*	X Coef(s)	SEC*
Elevation	Aprl Pack	-1216.904	75.129	0.922	5782	5780	1.0128	0.003875
Aspect	Aprl Pack	668.919	268.94	0.0002	5782	5780	-0.0367	0.035737
Elevation	Aprl Pack	-1208.498	74.960	0.922	5782	5779	1.0129	0.003867
Aspect							-0.0517	0.009961
Elevation	Aprl Pack	-1217.123	74.873	0.923	5782	5778	1.0214	0.004456
Aspect							-0.0519	0.009949
Slope							-0.2024	0.053177

SEYE* = Standard Error of the Y Estimate
DOF* = Degrees of Freedom
SEC* = Standard Error of Coefficient

maximum snow depth with aspect functioning as a secondary factor. The lower maximums

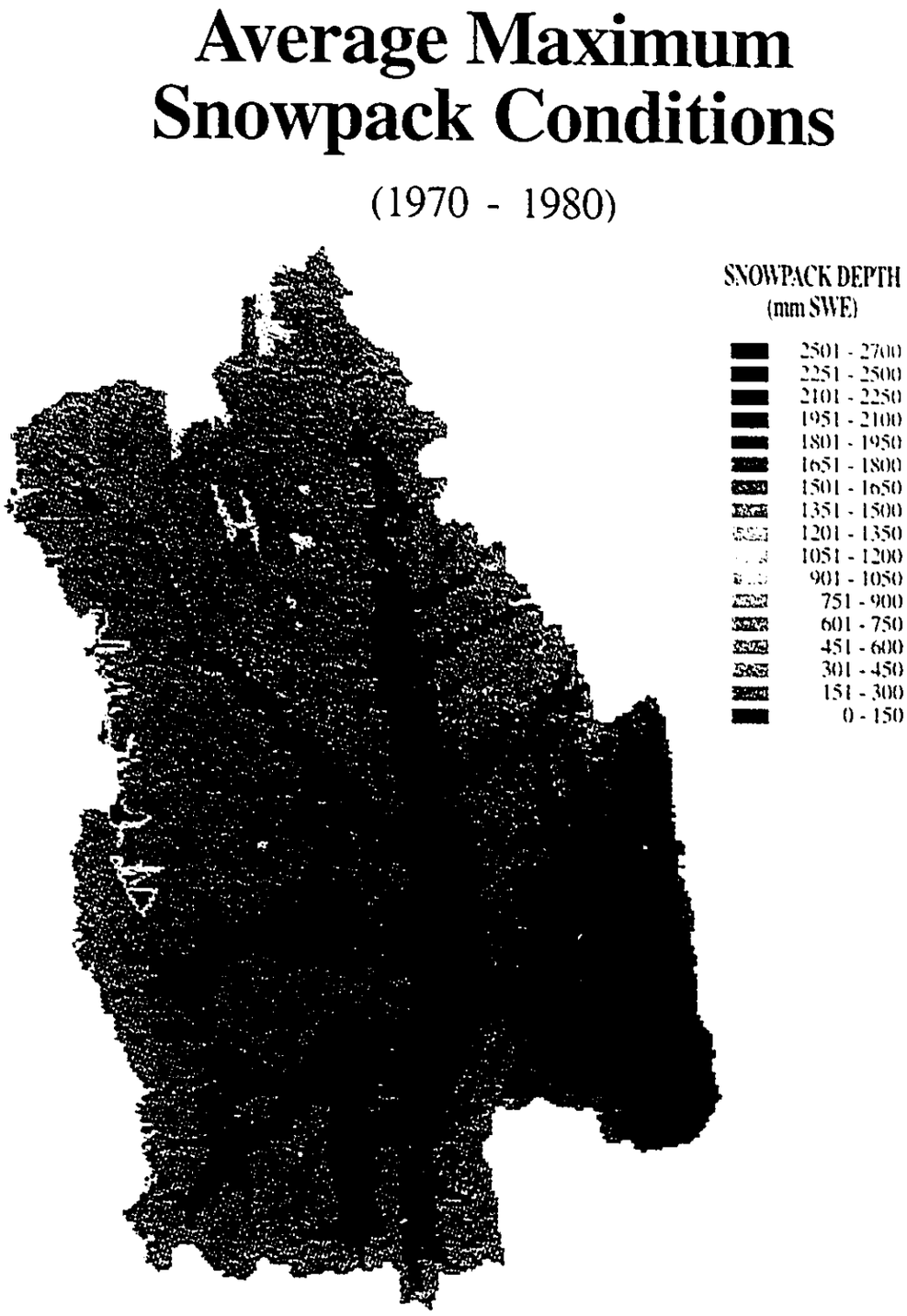

Figure 5.15 Average maximum snowpack conditions as derived from the snowpack simulations. Pixel size is 100m.

with respect to surrounding cells tend to form in areas of low elevation and along south-facing slopes. These areas have shallower snowpacks because they generally experience warmer temperatures as a result of solar heating. Obviously, temperature differences influence snow accumulation and subsequent melt. Although not accounted for in this model, wind speed and direction possibly contribute to snow redistribution after it has reached the ground.

The distribution of maximum snowpack classes versus elevation is presented in table 5.11 and plotted in figure 5.16. Both indicate a generally positive correlation between elevation and maximum accumulated snowpack. Figure 5.16 shows a truly non-linear relationship between elevation and the area-weighted mean maximum snowpack. The curved nature of the data points indicates a gradual increase in maximum snow depth at lower elevations while higher up, depth increases more rapidly with elevational changes. Apparently, elevation is not the only factor in determining snowpack depth and so one is inclined to believe that other parameters such as aspect and slope are involved. Since precipitation inputs are controlled exclusively by elevation in the model, snowfall amounts alone cannot explain this phenomenon. The logical source of this curved relationship would then be the effects aspect and slope have on other snowpack processes, melt being the most obvious. The regression analysis results in table 5.12 demonstrate, as with the April 1 snowpack, that elevation explains a great deal of the distributional variation ($r^2 = 0.816$) and that both aspect and slope may be included for improved estimation.

Table 5.11 Areal extent of 10-year average maximum snowpack as a function of elevation in km^2.

Elevation Band	SWE (mm) 0-150	151-300	301-450	451-600	601-750	751-900	901-1050	1051-1200	1201-1350	1351-1500	1501-1650	1651-1800	1801-1950	1951-2100	2101-2250	2251-2500	2501-2700	Total (km^2)	Weight Mean (mm)
1200-1400	39.09	0.00	0.00	0.00	0.00	0.00	0.00	0.00	0.00	0.00	0.00	0.00	0.00	0.00	0.00	0.00	0.00	39.09	75.00
1401-1600	200.12	3.28	0.00	0.00	0.02	0.00	0.00	0.00	0.00	0.00	0.00	0.00	0.00	0.00	0.00	0.00	0.00	203.42	77.48
1601-1800	87.83	278.30	6.91	0.00	0.00	0.00	0.00	0.00	0.00	0.00	0.00	0.00	0.00	0.00	0.00	0.00	0.00	373.04	192.46
1801-2000	0.25	91.75	315.17	5.43	0.00	0.00	0.00	0.01	0.00	0.00	0.00	0.00	0.00	0.00	0.00	0.00	0.00	412.61	343.46
2001-2200	0.18	0.21	61.48	204.79	3.34	0.00	0.00	0.16	0.00	0.00	0.00	0.00	0.00	0.00	0.00	0.00	0.00	270.16	492.54
2201-2400	0.18	0.15	0.28	10.88	82.84	0.00	0.00	1.49	0.00	0.00	0.02	0.08	0.00	0.00	0.00	0.00	0.00	95.92	663.33
2401-2600	0.10	0.26	0.22	0.06	0.42	0.00	4.06	16.71	0.00	0.00	0.23	0.21	0.00	0.00	0.02	0.00	0.00	22.29	1076.21
2601-2800	0.01	0.06	0.10	0.03	0.01	0.00	0.00	0.21	0.00	0.02	2.62	0.94	0.00	0.00	0.11	0.00	0.00	4.11	1539.23
2801-3000	0.00	0.04	0.00	0.00	0.00	0.00	0.00	0.00	0.00	0.00	0.02	0.02	0.00	0.18	0.44	0.00	0.00	0.70	1995.00
3001-3200	0.00	0.00	0.00	0.00	0.00	0.00	0.00	0.00	0.00	0.00	0.00	0.00	0.00	0.00	0.02	0.00	0.03	0.05	2430.00
Total	327.76	374.05	384.16	221.19	86.63	0.00	4.06	18.58	0.00	0.02	2.89	1.25	0.00	0.18	0.59	0.00	0.03	1421.39	324.14

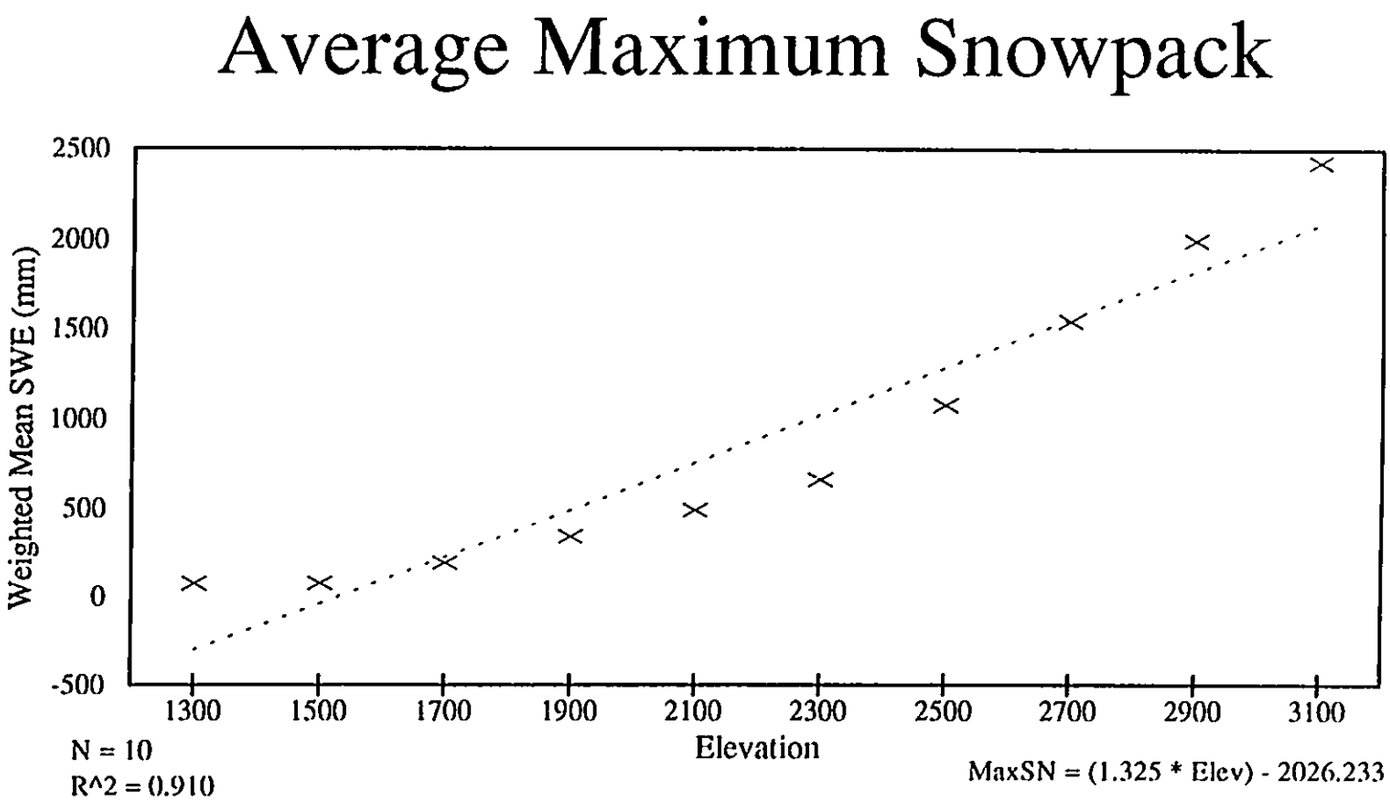

Figure 5.16 Area-weighted mean maximum snowpack as a function of elevation.

Table 5.12 Maximum snowpack regression analysis summary.

Independent Var(s)	Dependent Var	Constant	SEYE*	R^2	No. of Obs.	DOF*	X Coef(s)	SEC*
Elevation	MaxPack	-1122.422	92.988	0.816	5782	5780	0.7676	0.004797
Aspect	MaxPack	313.334	216.58	0.001	5782	5780	-0.0673	0.028780
Elevation	MaxPack	-1109.636	92.669	0.817	5782	5779	0.7677	0.004780
Aspect							-0.0787	0.012314
Elevation	MaxPack	-1083.710	91.989	0.820	5782	5778	0.7423	0.005474
Aspect							-0.0781	0.012240
Slope							0.6084	0.065334

SEYE* = Standard Error of the Y Estimate
DOF* = Degrees of Freedom
SEC* = Standard Error of Coefficient

Figure 5.17 delineates the mean Julian date at which maximum snowpack occurs as derived from the simulation model. There is a range between day 74 near the gauging station to day 144 at Tornado Mountain. This means that the maximum snowpack occurs in early to mid March in the lower regions in the basin, while snowpack at much higher elevations reach their peak as late as the end of May. Table 5.13 provides total area information relating the fourteen day time periods to the elevation bands as well as the area-weighted mean Julian date for each elevation band. The general trend shown in the dispersion of data values indicates an increase in Julian date with increased elevation. This makes sense that snow is still accumulating higher up even long after maximum snow depths have been reached at lower elevations. Figure 5.18 illustrates that the positive relationship between elevation and the weighted mean Julian date is curved rather than linear with a levelling off around Julian day 150 (late May) as annual accumulation ends and melt begins.

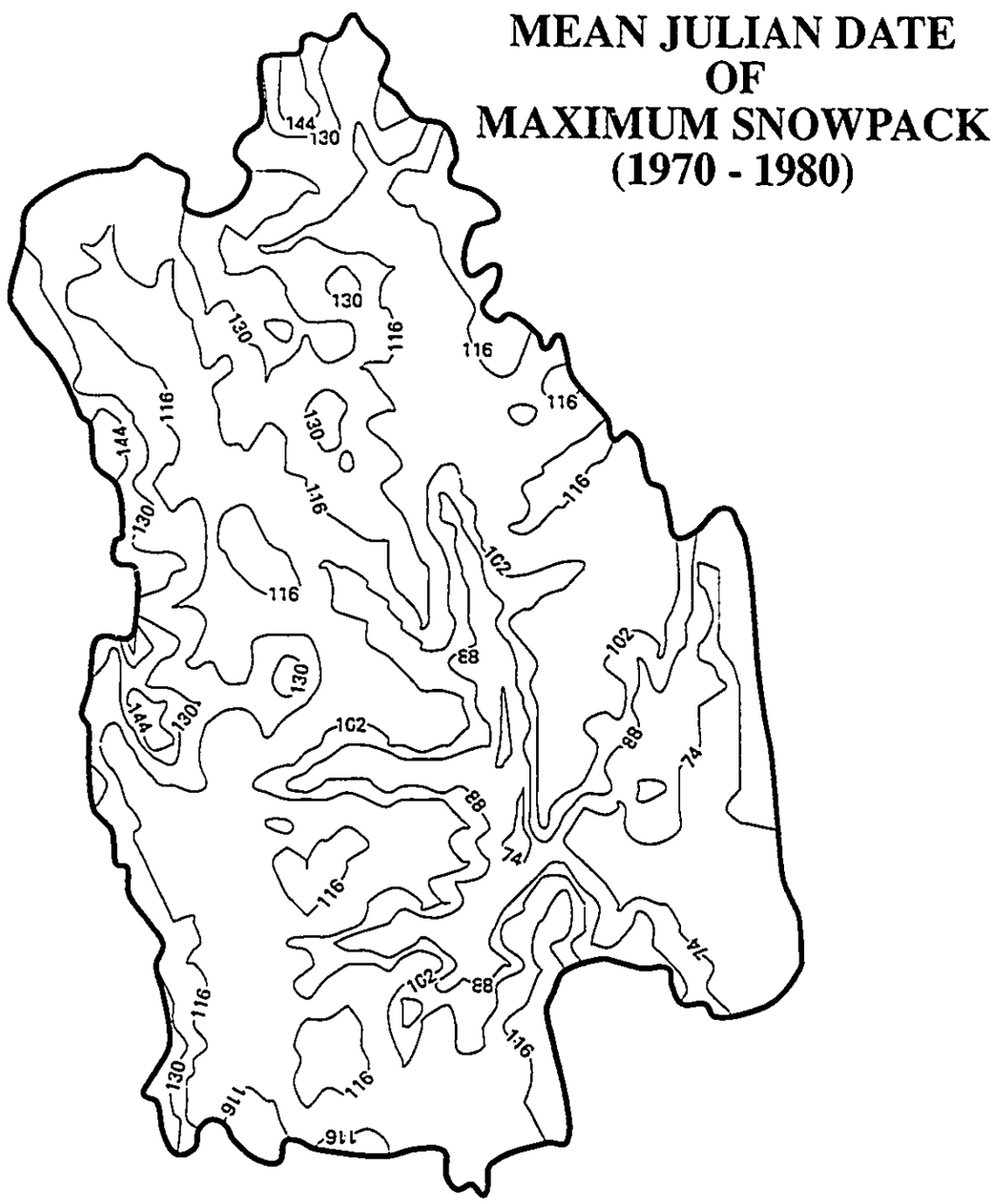

Figure 5.17 1970-1980 mean Julian date at which maximum snowpack occurs. Contour Interval = 14 days.

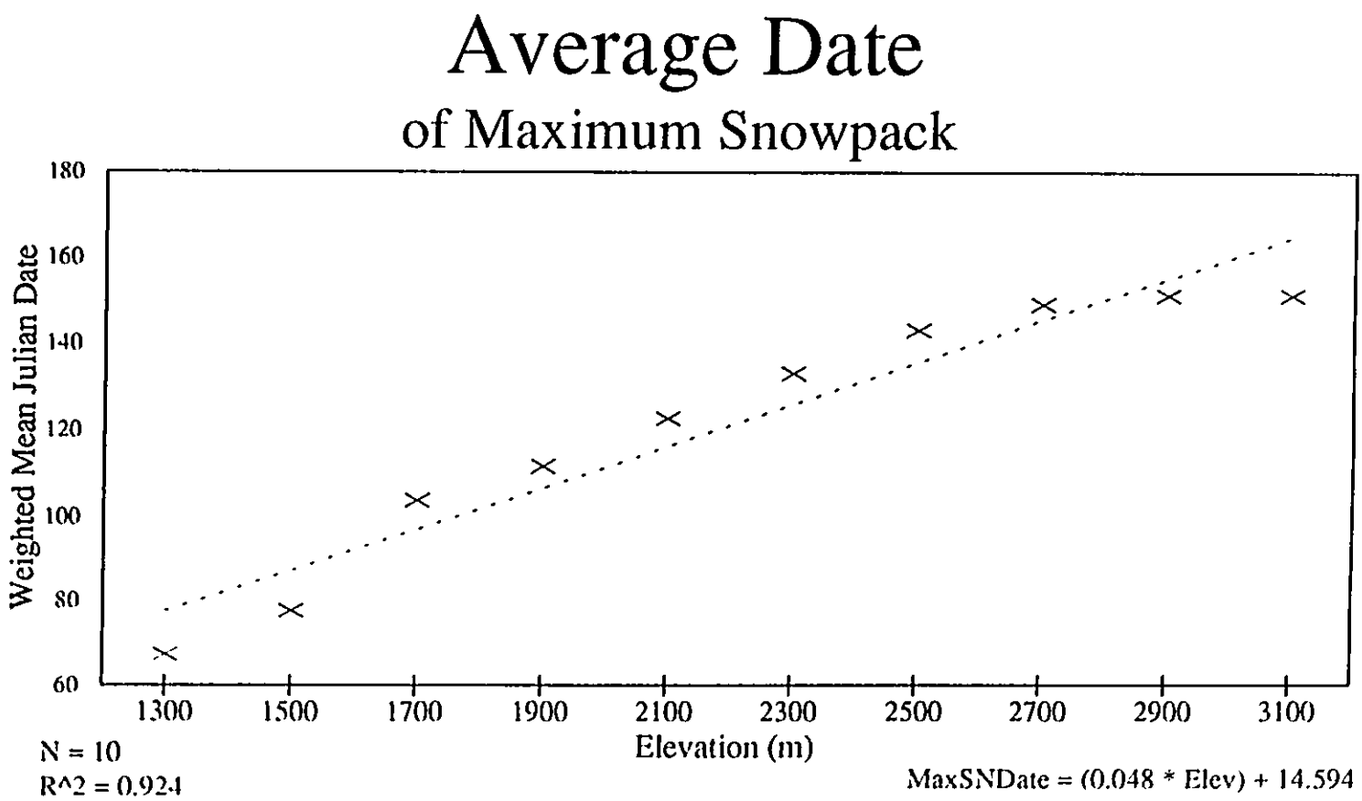

Figure 5.18 Area-weighted mean Julian date at which maximum snowpack occurs.

Table 5.13 Areal extent of date at which maximum snowpack occurs as a function of elevation in km^2.

Elevation Band	Julian Date 0-74	75-88	89-102	103-116	117-130	131-144	>144	Total (km^2)	Weighted Mean Date
1200-1400	38.30	0.78	0.01	0.00	0.00	0.00	0.00	39.09	67.29
1401-1600	80.65	91.91	29.53	1.13	0.00	0.00	0.00	203.22	77.63
1601-1800	0.26	28.76	79.81	263.95	0.26	0.00	0.00	373.04	103.83
1801-2000	0.00	0.11	3.15	324.49	84.30	0.56	0.00	412.61	111.78
2001-2200	0.00	0.00	0.02	30.76	214.54	23.47	1.37	270.16	122.76
2201-2400	0.00	0.00	0.00	0.30	34.97	51.54	9.11	95.92	133.14
2401-2600	0.00	0.00	0.00	0.00	0.92	10.76	10.61	22.29	143.09
2601-2800	0.00	0.00	0.00	0.00	0.00	0.61	3.50	4.11	148.92
2801-3000	0.00	0.00	0.00	0.00	0.00	0.00	0.70	0.70	151.00
3001-3200	0.00	0.00	0.00	0.00	0.00	0.00	0.05	0.05	151.00
Total	119.21	121.56	112.52	620.63	334.99	86.94	25.34	1421.19	107.74

5.2.3 Snow Melt

Of relative significance to the general timing at which maximum snowpack occurs is the period of snow melt. Again using the simulated data, a map of mean Julian date at which the snowpack disappears is developed (figure 5.19). For this map, snow disappearance is defined as the earliest date at which snowpack equals zero for several consecutive days. The results, not surprisingly, indicate that snow tends to melt earlier in the lower altitudes and tends to linger higher up. The actual range of values is between day 148 and day 218, mid to late May and late July to early August, respectively. The areal extent data presented in table 5.14 and figure 5.20 indicate a positive relationship between elevation and snowpack disappearance. As with the maximum snowpack date, the relationship between elevation and area-weighted Julian date is represented by a curve. The curve again levels off this time around Julian day 222 by which time all snow has disappeared from the basin.

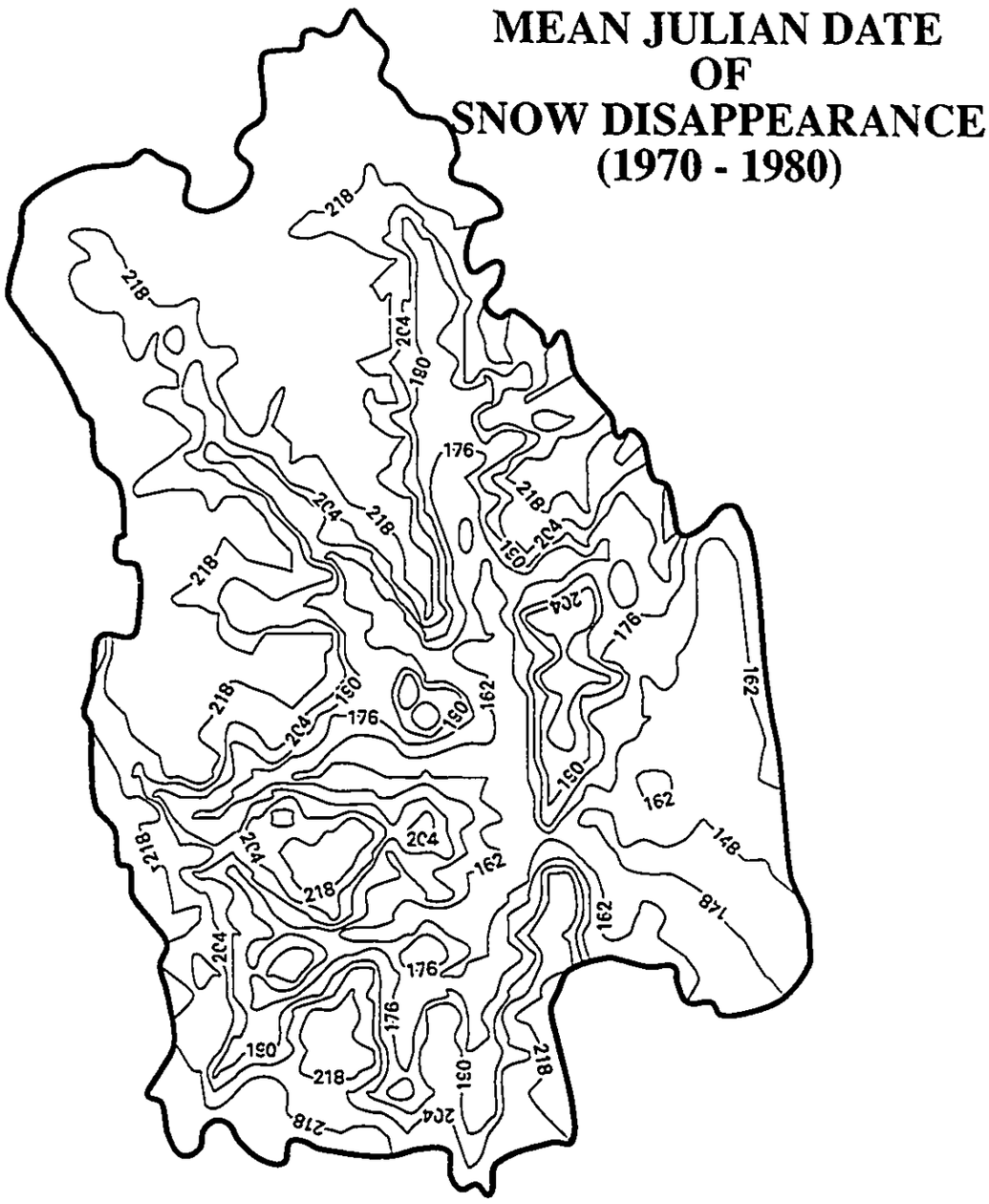

Figure 5.19 1970-1980 mean Julian date at which maximum snowpack occurs. Contour Interval = 14 days.

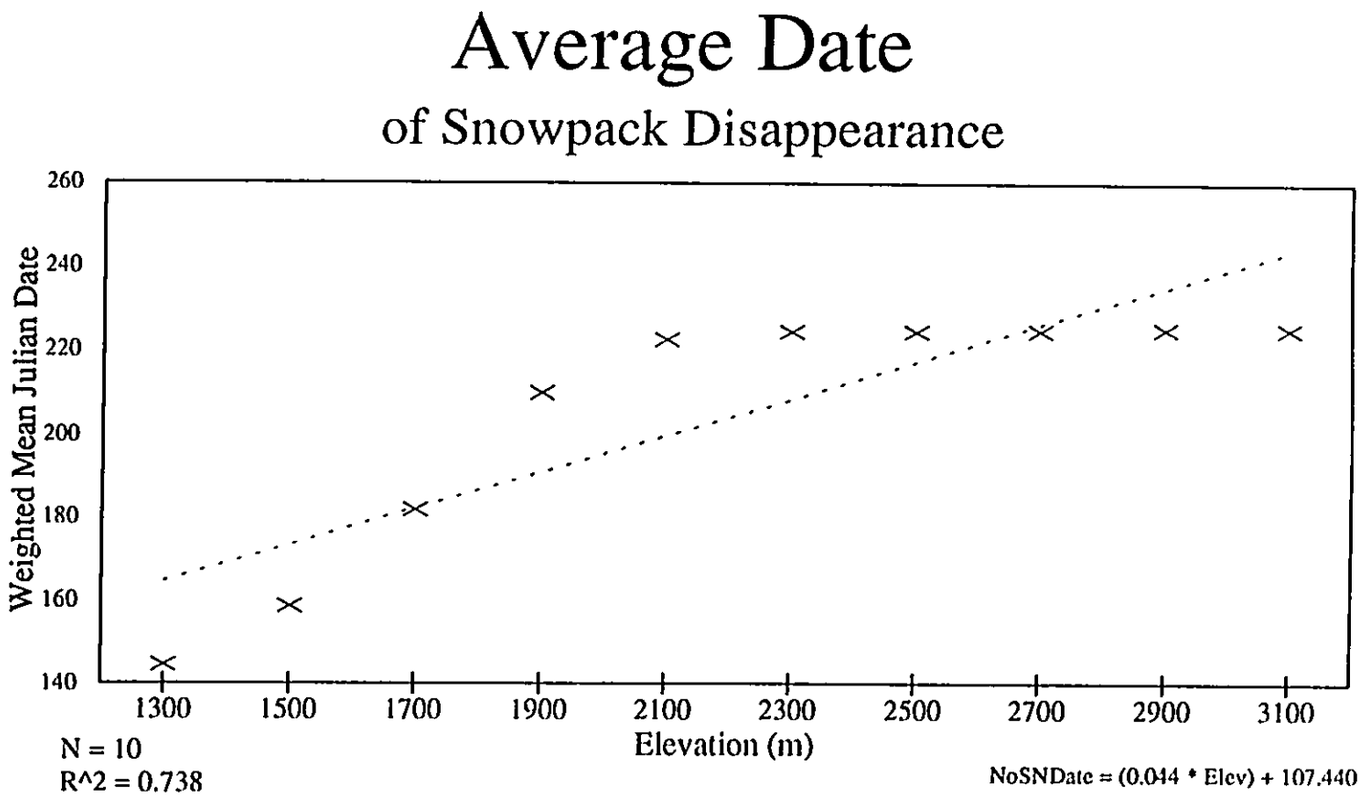

Figure 5.20 Area-weighted mean Julian date at which the snowpack disappears.

Table 5.14 Areal extent of date at which snowpack disappears as a function of elevation in km^2.

Elevation Band	Julian Date <148	149-162	163-176	177-190	191-204	205-218	219-233	Total (km^2)	Weighted Mean Date
1200-1400	29.63	9.28	0.18	0.00	0.00	0.00	0.00	39.09	144.45
1401-1600	2.17	149.88	50.01	1.36	0.00	0.00	0.00	203.42	158.48
1601-1800	0.00	10.21	109.72	167.67	72.29	11.94	1.21	373.04	181.86
1801-2000	0.00	0.00	0.51	19.29	85.43	211.21	96.17	412.61	210.00
2001-2200	0.00	0.00	0.00	0.08	1.87	45.74	222.47	270.16	222.42
2201-2400	0.00	0.00	0.00	0.00	0.00	4.26	91.66	95.92	224.38
2401-2600	0.00	0.00	0.00	0.00	0.00	1.04	21.25	22.29	224.35
2601-2800	0.00	0.00	0.00	0.00	0.00	0.12	3.99	4.11	224.59
2801-3000	0.00	0.00	0.00	0.00	0.00	0.00	0.70	0.70	225.00
3001-3200	0.00	0.00	0.00	0.00	0.00	0.00	0.05	0.05	225.00
Total	31.80	169.37	160.42	188.40	159.59	274.31	437.50	1421.39	197.05

5.2.4 Volumetric Forecasting

A potentially useful tool resulting from this research is the development of a technique whereby the total volume of snow water equivalent available for runoff may be approximated for any date throughout the melt season. To do this maps of the average snowpack conditions for each Julian day are overlaid with a map delineating the mean date at which the snowpack disappears. Total volume of water equivalent held in the snowpack is determined for areas above the snowline for a particular Julian date. This procedure is repeated for each of the "snow disappearance" isochrones and a graph is created with Julian date along the x-axis and total volume of SWE remaining along the y-axis (figure 5.21). The actual data values used are presented in table 5.15. It should be noted that the quantities represented in the graph include water which will contribute to both ground and surface water flow. This could be a very useful tool for forecasting the available water resources and for evaluating/monitoring such things as flood risk.

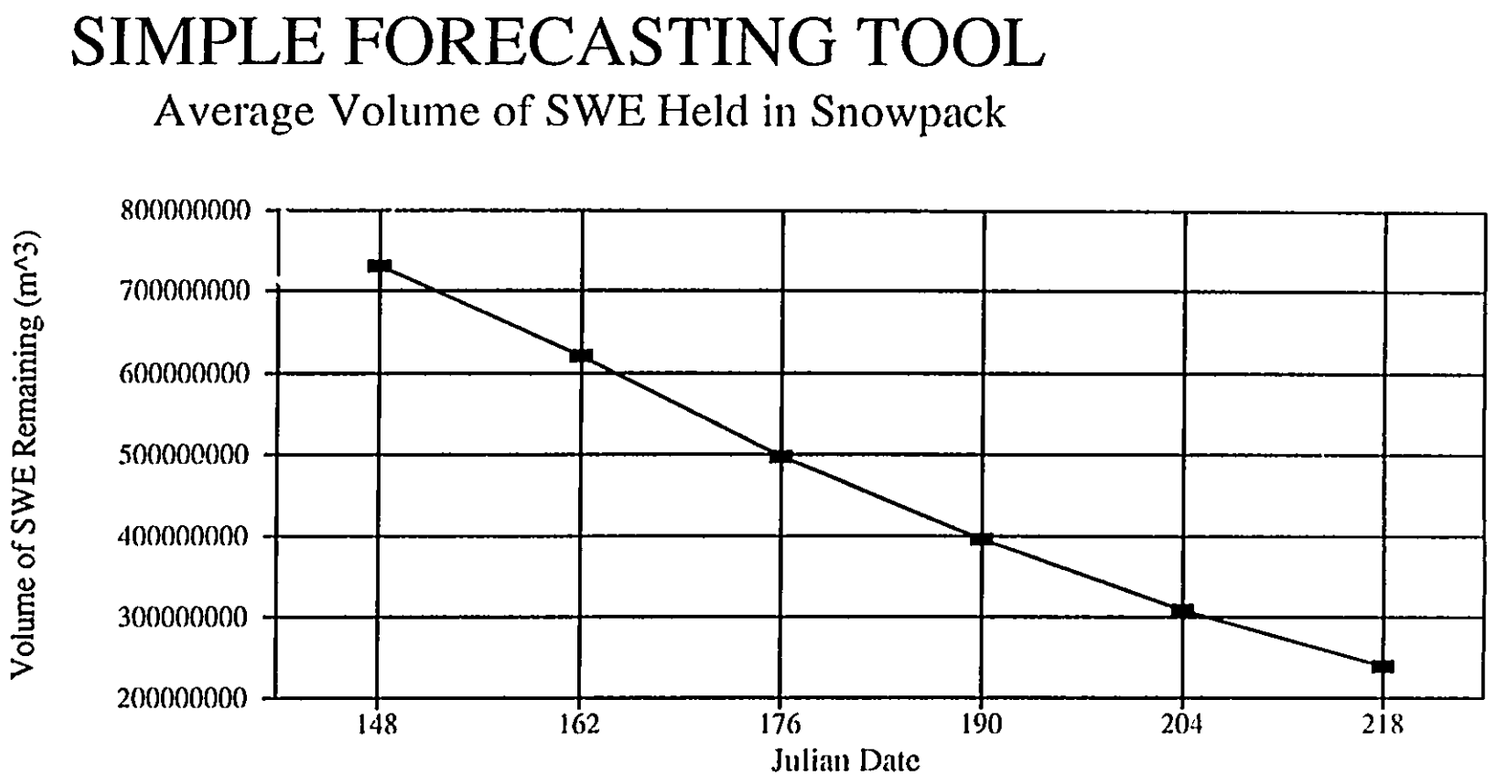

Figure 5.21 Simple forecasting tool for approximating the average volume of snow water equivalent (SWE) held in the remaining snowpack per Julian date.

Table 5.15 Simple volumetric forecasting tool illustrating the average volume of snow water equivalent held in the remainining snowpack at 14-day intervals.

Julian Date	Snow Covered Area (m^2)	Mean Depth of Snow (m)	Volume of SWE Remaining (m^3)	14-Day Melt Volume (m^3)
148	1413170000	0.51635	729690329.50	
162	1242080000	0.49970	620667376.00	109022953.50
176	1078460000	0.46067	496814168.20	123853207.80
190	890060000	0.44493	396014395.80	100799772.40
204	729950000	0.42214	308141093.00	87873302.80
218	452100000	0.52739	238433019.00	69708074.00

Chapter 6

SUMMARY AND FURTHER RESEARCH

6.1 Summary

A number of different data sources have been combined for this research. This non-trivial task is accomplished by means of Fortran programming, database management, and using a geographic information system (GIS). The integrated data approach to problem solving is crucial to projects such as this with highly variable data formats covering a large geographic area. Data sources used include observed meteorologic information, hardcopy maps, and digital elevation datasets.

PAMAP GIS is the tool by which all spatially referenced data is assembled. PAMAP is capable of storing up to 64 levels of information in a single map. Each of the 64 levels can contain graphic elements, one database, and one surface. The graphic elements may be one of points, lines, or text. Databases may be stored for either points, polygons, or vectors. Surfaces are generally used for such single attribute data as a digital elevation model (elevation, slope, and aspect), but can quite easily accommodate any XYZ information.

A digital geographic database is created for the upper Oldman River basin in southwestern Alberta by way of manual digitizing from 1:50,000 national topographic series (NTS) mapsheets. Map layers obtained in this manner include drainage basin boundary, hydrographic features, and natural land cover. The basin boundary is identified on the NTS maps as the topological divide and then digitized into a digital map layer. Hydrographic features include single (small) and double-sided (large) rivers as well as lakes. Natural land cover is distinguished simply as the differentiation between forested and non-forested areas displayed on the NTS maps.

A digital elevation model (DEM) is created from the commercially available gridded height data (50 metre) by importing the elevations and their corresponding UTM coordinates into PAMAP. Once there, the software offers a choice of three interpolation techniques to be used in generating a continuous surface coverage for the entire map area. For this study, the weighted average algorithm is used. It interpolates a pixel's value as a weighted average of the data points closest to the pixel. From the DEM surface, slope and aspect surfaces are derived.

Daily observed meteorologic data is available from Atmospheric Environment Service (AES) for many recording stations along the foothills of the Canadian Rocky Mountains. Several record local conditions year-round but most higher elevation sites report only for the summer season due to inaccessibility. As a result, very few weather stations are suitable for use and so snow pillows and snow courses are used. To do this, it was decided to select a period

during the winter when it could be assumed that "most" precipitation would be in the form of snow. This allows the combination of regular precipitation records with snow water equivalent readings from snow pillows and snow courses.

After compilation of the digital database is complete, gridded microclimate is simulated with a modification of MTCLIM (Hungerford, *et al.*, 1989). The modified program, SIMGRID, is capable of simulating the daily microclimate conditions for a user-defined number of grid points over any period of time. SIMGRID requirements include a number of parameters describing both the base station and each individual grid point site. For the base station, daily maximum/minimum air temperature, daily total precipitation, and average isohyet are basic requirements. The isohyet value is obtained from the long-term daily records using simple summation functions. When available, daily dewpoint temperatures are used but if they are not, minimum night temperature has been shown to be approximately equal (Hungerford, *et al.*, 1989). The capability of including a second precipitation base is also built in to improve the simulations. The only terrain variable needed for the base station is its elevation. For each individual grid site the basic requirements include elevation, slope, aspect, east-west horizon angles, leaf area index (LAI), and average isohyet. The horizon angles are set to a constant throughout the study area as is the leaf area index. The terrain-related variables are derived from the GIS and the site isohyet is approximated using a crude linear regression between elevation and precipitation.

The surface layers created in the GIS are produced at a one hundred metre pixel size. This

is sufficient to capture such mesoscale phenomena as snow distribution to wind, avalanches, terrain variables, and vegetation cover (Gray and Prowse, 1993). As a result of this, the 1445 km^2 study area is represented by 144,558 pixels/grid points for each layer of information. Surface information layers such as the DEM, slope, aspect, and land cover are easily exported to ascii files. These ascii files are related to one another using dBASE IV and FoxPro for Windows such that a single file containing easting, northing, elevation, slope, aspect, and land cover is created. First attempts at using this file as input into SIMGRID resulted in the program running extremely slowly. Therefore, it was decided to devise a method of grouping the site terrain variables to reduce the number of calculations. The range of elevations is grouped into ten 200m bands; aspect is grouped into four classes of 90° each; and slope is grouped into three classes of approximately 23° each. The combinations of the three variables are next simplified to produce a maximum number of distinct categories equalling one hundred and twenty (10*4*3 = 120). The result is a reduction in the number of points at which microclimate is simulated from 144,558 to 120, a drastic improvement in computational efficiency. Each of the 144,558 points has an associated category identifier which is used later for bringing simulation results back into the GIS.

Using the simplified terrain variable categories, daily microclimatic conditions are simulated for the ten year period between 1970 and 1980. This time frame is chosen primarily on the basis of the availability of AES climate records for these times. It is also a common period of continuous data coverage found at each of the chosen recording stations.

The microclimate results appear to be very good for temperature, but less than perfect for precipitation. Regression analysis between simulated and observed temperatures produce an $r^2 = 0.94$ over a one year period of daily simulations. The slope of the regression line is 0.92 and the y-intercept is 0.33 which together indicate an insignificant overestimation of lower temperatures and a likewise underestimation at higher temperatures. Precipitation is less successfully modelled producing $r^2 = 0.21$ for the same 365 day period. In other words, the model does not estimate daily total precipitation very well in this study area. It is worth noting, however, that precipitation in the mountains is by nature highly variable and difficult to model. When similar regression analysis is carried out using monthly total precipitation, r^2 increases to 0.66. This is still somewhat weak, but it does at least imply that total volume of water over longer time scales is more successfully modelled. After all, the amount of available water resources is driven more by monthly and seasonal trends than by individual daily precipitation events. Exceptions to this rule include such catastrophic events as triggered the flooding of southern Alberta rivers in June 1995 when several hundred millimetres of rain fell on an already above average snowpack. It is also theorized that the crudeness of the precipitation/elevation relationship compounds the problem in weak simulations. Methods of improving this component are discussed in a later section.

The grid-based microclimate is next employed in the estimation of daily snowpack conditions accumulation through to ablation. This is done within another program, SNOPAC, which operates on an adaptation of the UBC Watershed model snow melt routines (Pipes and Quick, 1977) in conjunction with an empirically-based accumulation model (Wyman, 1995). Unlike

many attempts at modelling snowpack, this program carries out calculations at a 100m pixel resolution from the same scaled microclimate. It is, therefore, sensitive to small scale variations in such things as aspect and slope where slight changes in solar radiation receipt at the surface are detectable. Generally, previous modelling attempts provide only snapshots or generalized pictures of snow cover conditions. An important improvement in this model is the generation of a continuous temporal record from which the daily conditions may be extracted for any stage thoughout the simulation period.

Regression analysis between simulated and observed snow water equivalent at several snow pillow sites is promising. Racehorse Creek which is at an elevation of 1920 metres produces an r^2 of 0.80, a y-intercept of 39.0, and a slope of 0.82 for the 1983-84 winter season (218 days). The same site for 1988-89 results in a slight increase in the correlation statistics (r^2=0.95, slope=0.80, y-intercept = -29.38), well within acceptable limits. The 1988-89 simulations for Lost Creek which sits at an elevation of 2130 metres are about par with either of the Racehorse Creek years. R^2 is 0.89, slope increases to 1.11, and y-intercept is 5.58. Generally speaking, the minute changes in total snow water equivalent are well reflected in the simulations for both locations during the accumulation period. Problems arise around about the time of snow accumulation peak. In both years, Racehorse peaks are underestimated while the Lost Creek simulations are over. A number of causes may be at the root of this problem, not the least of which is the problem with estimation of precipitation at higher elevations. This certainly contributes more to the Lost Creek site than to Racehorse Creek. Alternatively, more refinement needs to be done on the melt routines used. Perhaps

field data will assist in the calibration of certain parameters.

Several interesting products have resulted from this thesis work. The obvious ones include maps depicting average conditions for both microclimate and snowpack. There now exists a fine resolution average annual precipitation database covering the basin although it will be improved through the addition of several important factors that were previously unavailable. Another map has been generated for the average maximum snow water equivalent. This could be potentially useful for comparison type analysis in nearby watersheds. A significant outcome is the creation of two maps, one describing the mean date at which maximum snowpack occurs and the other the mean date at which the snow cover disappears. From the latter it was possible to derive a general relationship between Julian date and an the approximate total volume of water remaining for future runoff.

6.2 Suggestions for Further Research

Several aspects of the research methodology presented in this thesis lend themself to further work in hopes of refining the simulation results. Some of the suggestions to follow came about as a result of the findings and were not anticipated at the onset of the research design.

Important to the practical application of this model is a refinement of the microclimate simulator. At present the original program, MTCLIM, has been modified to accommodate simulations for a user-defined number of grid points for any time period. The limiting factor

in the latter is, of course, the capability of the computer on which the program is run. Looping structures within SIMGRID are easily modified to accommodate the correct number of grid points and days.

The inherent weakness of the microclimate simulator is found in precipitation estimations. This thesis presents a crude method of deriving site isohyet using elevation exclusively. Although this is not an entirely valid hypothesis, it did provide acceptable estimates so that model development could continue. As discussed earlier, the limited data used in creating this elevationally driven precipitation estimator indicated that other obvious controls on precipitation are statistically insignificant. This is definitely an area for further field work. Theoretically, the inclusion of slope, aspect, prevailing wind direction, and distance from the continental divide along with elevation will result in better simulations. Currently, such data are being collected by the Water Resources Institute at The University of Lethbridge for the Crowsnest basin which lies immediately south of the Upper Oldman basin. From this it is hoped to create an extensive climate/snow cover record representing spatially and temporally diverse areas. In terms of the spatial distribution of data collection, attempts are being made to include both vertical as well as horizontal variation. If these field data have sufficient coverage, other improvements such as seasonally adjusted temperature lapse rates may be derived.

Although snowpack accumulation is simulated reasonably well, there exist some shortcomings in snow melt routines. This certainly warrants more investigation if more accurate volume

estimates are expected. The current model is fairly simplistic in terms of snow melt in that it is heavily reliant upon air temperature. Not taken into consideration are the affects of such things as the absorption of rain and surface melt into the snowpack, snow densification, the occurrence of rain on snow, and the refreezing of melt (Wyman, 1995). Further investigation is needed to identify relationships between the point melt factor and terrain variable that may influence it. Another possible avenue to pursue is the role winds, particularly chinooks, play in snow melt. Certainly, such winds modify the typical vertical temperature profile as described by accepted lapse rates which are assumed to be consistent throughout the study area.

In the absence of widely dispersed observed snow cover information, a logical extension of this work is to incorporate remotely sensed imagery for qualifying and quantifying the simulated output at more than just individual points. At the very least, areal extent of the snow cover can be determined and compared with simulations. Rango (1990), for example, describes how snow cover derived from satellite imagery is used in a snow melt-runoff model. Leavesley and Stannard (1990) apply remotely sensed data to a distributed-parameter watershed model. Wankiewicz (1990) describes an example of correlations between spring runoff and satellite data collected in the microwave portion of the spectrum. Forsythe (1995) completed a master of science thesis using an integrated data source approach for snow modelling within a geographic information system. One of his primary datasets includes LandSat Thematic Mapper (TM) imagery. Clearly, the appropriateness of satellite imagery in the modelling of hydrologic processes has been established. Perhaps it could used to

further calibrate the model presented in this thesis.

It would be interesting to generate microclimate and snow cover maps from the regression equations provided in chapter 5. Using surface modelling techniques available within the GIS it is possible to derive these maps entirely from terrain surfaces such as elevation, aspect, and slope. These could be compared to the earlier simulation results as well as to data collected in current field projects to evaluate the potential for generating "quick looks" of the basin. If these proved to be acceptable, it is possible they be applied to nearby basins.

Finally, it is hoped that the model can be used as a tool to assist in the management of water resources. Using the simple forecasting tool presented in the previous chapter in conjunction with recorded spring runoff, it may be possible to estimate runoff volumes at a given point in time. These could aid in the prediction of water surpluses or deficits. An interesting task may be to simulate the snowpack for a series of winter seasons preceding major flood events. Attempts could then be made to identify warning signals, if any, of catastrophic melt events such as that which occurred in June of 1995.

REFERENCES

Ahrens, C.D., 1985. Meteorology Today, An Introduction to Weather, Climate, and the Environment (2nd edition). West Publishing Co., St. Paul.

Alberta Environment, 1983. Climate of Alberta: Report for 1983. Alberta Environment, Edmonton.

Alberta Environmental Protection, 1988. DEM Format Information. Unpublished information package provided with the digital data.

Assaf, H. and M.C. Quick, 1990. Updating Hydrological Model Forecasts. IN: Kite, G.W. and A. Wankiewicz (editors). Proceedings of the Workshop on Applications of Remote Sensing in Hydrology. Saskatoon, Saskatchewan. 13 and 14 February 1990. Environment Canada, Ottawa.

BC Environment, 1985. Snow Survey Measurements: Summary 1935-1985. British Columbia Ministry of Environment, Water Management Branch.

Barry, R.G., 1973. A Climatological Transect on the East Slope of the Front Range, Colorado. *Arctic and Alpine Research*, **5,2**: 89-110.

Barry, R.G., 1992. Mountain Weather and Climate (2nd edition). Routledge, New York.

Byrne, J.M., 1989. Three Phase Runoff Model for Small Prairie Rivers. *Canadian Water Resources Journal*, **14,2**: 17-28.

Byrne, J.M., 1990. Three Phase Runoff Model for Small Prairie Rivers. Unpublished Ph.D. Dissertation. Department of Civil Engineering, University of Alberta. Edmonton, Alberta.

Byrne, J.M., R. Barendregt, and D. Schaffer, 1989. Assessing Potential Climate Change Impacts on Water Supply and Demand in Southern Alberta. *Canadian Water Resources Journal*, **14,4**: 5-15.

Byrne, J.M., and R. McNaughton, 1991. Predicting Temporal and Volumetric Changes in Runoff Regimes Under Climate Warming Scenarios. *Canadian Water Resources Journal*, **16,2**: 129-141.

Byrne, J.M., 1991. Water Balance Assessments for Southern Alberta Under Forecast Climate Warming. IN: Byrne, J.M. and C. Fleming (editors). Proceedings of the IRDC-90, Irrigation Research and Development in the 1990s. The University of Lethbridge,

Lethbridge.

Christopherson, R.W., 1992. Geosystems: An Introduction to Physical Geography. MacMillan College Publishing, Inc., New York.

Environment Canada, 1985. Historical Streamflow Summary Alberta to 1984. Inland Waters Directorate, Water Resources Branch, Water Survey of Canada. Environment Canada, Ottawa.

Environment Canada, 1986. Climate Atlas-Canada, Map Series 2-Precipitation. Atmospheric Environment Service. Environment Canada, Ottawa.

Environment Canada, 1993. A Matter of Degrees: a primer on Global Warming. Office of Environmental Citizenship, Atmospheric Environment Service. Environment Canada, Ottawa.

Environment Canada, 1994. Modelling the Global Climate System.Climate Change Digest, **CCD 94-01**. Climate Products and Publications Division, Canadian Climate Centre. Downsview, Ontario.

Forsythe, K.W., 1995. Alpine Snow Modelling Using Geographic Information Systems. Unpublished M.Sc. Thesis. Department of Geography, University of Calgary. Calgary, Alberta.

Garen, D.C., 1995. Estimation of Spatially Distributed Values of Daily Precipitation in Mountainous Areas. IN: Guy, B.T. and J. Barnard (editors). Mountain Hydrology Peaks and Valleys in Research and Applications Conference Proceedings, May 16-19, 1995. Canadian Water Resources Association, Cambridge.

Golding, D.L., 1974. The Correlation of Snowpack with Topography and Snowmelt Runoff on the Marmot Creek Basin, Alberta. *Atmosphere*, **12,1:** 31-38.

Goodison, B.E., H.L. Ferguson, and G.A. McKay, 1981. Measurement and Data Analysis. IN: Handbook of Snow. Pergamon Press Canada Ltd., Willowdale.

Gray, D.M. and D.H. Male, 1981. Handbook of Snow. Pergamon Press Canada Ltd., Willowdale.

Gray, D.M. and T.D. Prowse, 1993. Snow and Floating Ice. IN: Handbook of Hydrology. McGraw-Hill, Inc., New York.

Hungerford, R.D., R.R. Nemani, S.W. Running, and J.C. Coughlan, 1989. MTCLIM: Mountain Microclimate Simulation Model. Research Paper INT-414. Ogden, UT:

U.S. Department of Agriculture, Forest Service, Intermountain Research Station.

Lauscher, F., 1976. Weltweite Typen der Höhenabhängigkeit des Niederschlags. *Wetter u. Leben*, **28:** 80-90.

Leavesley, G.H. and L.G. Stannard, 1990. Application of Remotely Sensed Data in a Distributed-Parameter Watershed Model. IN: Kite, G.W. and A. Wankiewicz (editors). Proceedings of the Workshop on Applications of Remote Sensing in Hydrology. Saskatoon, Saskatchewan. 13 and 14 February 1990. Environment Canada, Ottawa.

Lettenmaier, D.P. and E.F. Wood, 1993. Hydrologic Forecasting. IN: Handbook of Hydrology. McGraw-Hill, Inc., New York.

Loijens, H.S., 1972. Snow Distribution in an Alpine Watershed of the Rocky Mountains, Canada. IN: Distribution of Precipitation in Mountainous Areas, Volume 1. WMO, Geneva.

Maidment, D.R., 1993. Hydrology. IN: Handbook of Hydrology. McGraw-Hill, Inc., New York.

McBean, G.A., O. Slaymaker, T. Nothcote, P. LeBlond, and T.S. Parsons, 1992. Review of Models for Climate Change and Impacts on Hydrology, Coastal Currents and Fisheries in B.C. Climate Change Digest, **CCD 92-02.** Climate Services Division, Canadian Climate Centre. Downsview, Ontario.

Pipes, A. and M.C. Quick, 1977. UBC Watershed Model Users Guide. Department of Civil Engineering, University of British Columbia.

Price, L.W., 1981. Mountains & Man: A Study of Process and Environment. University of California Press, Berkley.

Rango, A., 1990. Effective Use of Satellite-Observed Snow Cover Data in the Snowmelt-Runoff Model. IN: Kite, G.W. and A. Wankiewicz (editors). Proceedings of the Workshop on Applications of Remote Sensing in Hydrology. Saskatoon, Saskatchewan. 13 and 14 February 1990. Environment Canada, Ottawa.

Saunders, I.R. and W.G. Bailey, 1994. Radiation and energy budgets of alpine tundra environments of North America. *Progress in Physical Geography*, **18,4:** 517-538.

Saunders, I.R. and J.M. Byrne, 1996. Generating regional precipitation from observed and GCM synoptic-scale pressure fields, southern Alberta, Canada. *Climate Research*, **6:** 237-249.

Smith, W., 1993. Water 2000: Institutional and Research Needs. *Canadian Water Resources Journal*, **18,3**: 247-252.

Spence, C., A. Dalton, and G. Kite, 1995. GIS Supports Hydrological Modelling. *GIS World*, **8,1**: 62-65.

Storr, D. and H.L. Ferguson, 1972. The Distribution of Precipitation in Some Mountainous Canadian Watersheds. IN: Distribution of Precipitation in Mountainous Areas, Volume 2. WMO, Geneva.

Strahler, A. and A. Strahler, 1979. Elements of Physical Geography. John Wiley & Sons, Inc., New York.

Tecle, A. and D.E. Rupp, 1995. Stochastic, Event-based, and Spatial Modeling of Cold-Season Precipitation. IN: Guy, B.T. and J. Barnard (editors). Mountain Hydrology Peaks and Valleys in Research and Applications Conference Proceedings, May 16-19, 1995. Canadian Water Resources Association, Cambridge.

Von Storch, H., E. Zorita, and U. Cubasch, 1993. Downscaling of Global Climate Change Estimates to Regional Scales: An Application to Iberian Rainfall in Wintertime. *Journal of Climate*, **6,6**: 1161-1171.

Walker, D.A., T.W. Hennigar, and D. Thirumurthi, 1992. Application of a Geographic Information System to a Local Groundwater Study. *Canadian Water Resources Journal*, **17,3**: 246-260.

Wankiewicz, A., 1990. Microwave Satellite Spring Runoff Correlations. IN: Kite, G.W. and A. Wankiewicz (editors). Proceedings of the Workshop on Applications of Remote Sensing in Hydrology. Saskatoon, Saskatchewan. 13 and 14 February 1990. Environment Canada, Ottawa.

Whiting, J., 1990. Determination of Characteristics for Hydrologic Modelling Using Remote Sensing. IN: Kite, G.W. and A. Wankiewicz (editors). Proceedings of the Workshop on Applications of Remote Sensing in Hydrology. Saskatoon, Saskatchewan. 13 and 14 February 1990. Environment Canada, Ottawa.

Wilson, E.M., 1990. Engineering Hydrology (4th ed.). The MacMillan Press Ltd., London.

Wyman,R.R., 1995. Modeling Snowpack Accumulation and Depletion. IN: Guy, B.T. and J. Barnard (editors). Mountain Hydrology Peaks and Valleys in Research and Applications Conference Proceedings, May 16-19, 1995. Canadian Water Resources Association, Cambridge.

Yarnal, B., 1984. A procedure for the classification of synoptic weather maps from gridded atmospheric pressure surface data. *Comp. Geosci.*, **10:** 397-410.

Zaltsberg, E., 1990. Potential Changes in Mean Annual Runoff From a Small Watershed in Manitoba Due to Possible Climatic Changes. *Canadian Water Resources Journal*, **15,4:** 333-344.

Zorita, E., V. Kharin, and H. von Storch, 1992. The Atmospheric Circulation and Sea Surface Temperature in the North Atlantic Area in Winter: Their Interaction and Relevance for Iberian Precipitation. *Journal of Climate*, **5:** 1097-1108.

Appendix A
MTCLIM

A.1 Sample Input and Output files

INIT.INI (INPUT)

```
*************** MTCLIM DATA FILE FOR INITALIZATION DATA ***************
* Simulate Pekisko climate from Coleman & Beaver Mines to validate code                *
VALIDATE.TP   INPUT DATA FILE      {Coleman(ppt1) & Beaver Mines(ppt2)}
VALIDATE.OUT  OUTPUT DATA FILE     {Pekisko} - 1989
N       DEW POINT TEMPERATURE SUPPLIED [Y OR N]
2       NO. OF PPT STATIONS [1 OR 2] IF 2 THEN USE 2 ISOHYETS BELOW
N       USE THRESHOLD RADIATATION [Y OR N]
T       TOTAL OR AVERAGE RADIATION [T OR A]
Y       USE YEARDAY (Julian) IN PLACE OF MONTH & DAY [Y OR N]
365     NDAYS - INTEGER VARIABLE; ALL THE REST ARE REAL
49.6    LATITUDE OF BASE STATION          {Coleman}
1439.0  SITE ELEVATION (metres)           {Pekisko}
1341.0  BASE ELEVATION (metres)           {Coleman}
330.0   SITE ASPECT  0 to 360 degrees (0=North; 180=South)
19.8    SITE SLOPE (Percent)
1.0     SITE LAI (all sided)
651.8   SITE ISOHYET (total annual precipitation..mm)
546.4   BASE ISOHYET STATION 1 (total annual precipitation..mm){Cmn}
605.1   BASE ISOHYET STATION 2 (optional) See No. of PPT Stations.{BM}
0.0     SITE EAST HORIZION (degrees)
0.0     SITE WEST HORIZION (degrees)
0.2     SITE ALBEDO  (0.2 = 20%)
0.65    TRANCF (Sea Level Atmospheric Transmissivity)
0.45    TEMPCF (Temperature Correction for Sine Approx)
6.4     TEMP LAPSE RATE (Deg C/1000 m)
8.2     LASPE RATE FOR MAXIMUM TEMPERATURE (Deg C/1000 m)
3.8     LAPSE RATE FOR MINIMUM TEMPERATURE (Deg C/1000 m)
2.7     DEW LAPSE RATE (Deg C/1000 m)
```

VALIDATE.TP (INPUT)

JULIAN	MAX_T	MIN_T	PPT_1	PPT_2
1	-1.50	-25.50	0.00	0.00
2	4.00	-9.00	0.00	0.00
3	7.00	-4.50	11.80	2.10
4	4.00	-2.00	19.00	22.00
5	-3.00	-6.00	6.00	20.00
.	.	.	.	.
.	.	.	.	.
.	.	.	.	.
355	-7.00	-29.00	0.00	0.00
356	3.50	-27.50	0.00	0.00
357	4.00	-13.50	0.00	0.00
358	3.50	0.00	0.00	0.00
359	6.00	1.00	0.00	0.00
360	6.00	2.50	0.00	0.00
361	4.00	2.50	0.00	4.00
362	0.00	-3.50	0.00	4.00
363	-0.50	-7.00	0.00	0.00
364	1.00	-3.50	0.00	0.00
365	6.00	-1.50	5.30	0.00

VALIDATE.OUT (OUTPUT)

```
*************** MTCLIM DATA FILE FOR INITALIZATION DATA ***************
* Simulate Pekisko climate from Coleman & Beaver Mines to validate code *
VALIDATE.TP   INPUT DATA FILE      {Coleman(ppt1) & Beaver Mines(ppt2)}
VALIDATE.OUT  OUTPUT DATA FILE     {Pekisko} - 1989
N       DEW POINT TEMPERATURE SUPPLIED [Y OR N]
2       NO. OF PPT STATIONS [1 OR 2] IF 2 THEN USE 2 ISOHYETS BELOW
N       USE THRESHOLD RADIATATION [Y OR N]
T       TOTAL OR AVERAGE RADIATION [T OR A]
Y       USE YEARDAY (Julian) IN PLACE OF MONTH & DAY [Y OR N]
365     NDAYS - INTEGER VARIABLE; ALL THE REST ARE REAL
49.6    LATITUDE OF BASE STATION          {Coleman}
1439.0  SITE ELEVATION (metres)           {Pekisko}
1341.0  BASE ELEVATION (metres)           {Coleman}
330.0   SITE ASPECT  0 to 360 degrees (0=North; 180=South)
19.8    SITE SLOPE (Percent)
1.0     SITE LAI (all sided)
651.8   SITE ISOHYET (total annual precipitation..mm)
546.4   BASE ISOHYET STATION 1 (total annual precipitation..mm){Cmn}
605.1   BASE ISOHYET STATION 2 (optional) See No. of PPT Stations.{BM}
0.0     SITE EAST HORIZION (degrees)
0.0     SITE WEST HORIZION (degrees)
0.2     SITE ALBEDO  (0.2 = 20%)
0.65    TRANCF (Sea Level Atmospheric Transmissivity)
0.45    TEMPCF (Temperature Correction for Sine Approx)
6.4     TEMP LAPSE RATE (Deg C/1000 m)
8.2     LASPE RATE FOR MAXIMUM TEMPERATURE (Deg C/1000 m)
3.8     LAPSE RATE FOR MINIMUM TEMPERATURE (Deg C/1000 m)
2.7     DEW LAPSE RATE (Deg C/1000 m)
```

JDAY	RADIATION KJ/M**2	STEMP C	MAXT C	MINT C	RH %	PPT mm
1	2591.13	-10.	-4.	-26.	27.	.00
2	625.87	-1.	2.	-9.	55.	.00
3	534.57	2.	5.	-5.	61.	8.17
4	220.98	1.	2.	-2.	81.	23.18
5	220.98	-6.	-5.	-6.	95.	14.35
.	.	.	.	.	.	.
.	.	.	.	.	.	.
.	.	.	.	.	.	.
355	2711.63	-15.	-10.	-29.	29.	.00
356	2733.09	-7.	1.	-28.	18.	.00
357	1294.63	-3.	2.	-14.	42.	.00
358	88.87	1.	2.	-0.	93.	.00
359	88.87	3.	4.	1.	86.	.00
360	88.87	3.	4.	2.	93.	.00
361	88.87	2.	2.	2.	99.	2.15
362	88.87	-3.	-2.	-4.	92.	2.15
363	88.87	-4.	-2.	-7.	78.	.00
364	88.87	-2.	-1.	-4.	88.	.00
365	146.47	2.	4.	-2.	75.	3.16

A.2 SIMGRID FORTRAN Code Listing

```
      PROGRAM SIMGRID
CM                    LAST MODIFIED [MM-DD-YY]: 01-02-96
CM  SIMGRID
CM  VERSION 1.0 6-13-95
CD  THIS PROGRAM PREDICTS MICROCLIMATE CONDITIONS FOR A GRID OF POINTS
CD  IN MOUNTAINOUS TERRAIN GIVEN BASE STATION METEOROLOGICAL DATA, PLUS
CD  SITE AND BASE STATION CHARACTERISTICS.
CD
CD
CVF SIMGRID FILES/VARIABLES
CVF  'IFILE':FILE CONTAINING BASE AND SITE DESCRIPTIONS - SEE 'README.DOC'
CVF        CODE BELOW DESCRIBES SOME OF THE FILES FORMAT.
CVF  BFILE: INPUT- BASE STATION CLIMATE DATA
CVF        FILE STRUCTURE: 1 LINE PER RECORD IN FREE FORMAT
CVF        THE ORDER OF VARIABLES IS FOUND IN SUBROUTINE BREAD.
CVF  GFILE: INPUT GRID POINT DATA FILE.
CVF  SFILE: OUTPUT- SIMULATED SITE CLIMATE FILE
CVF        WRITTEN IN FORMATTED OUTPUT AT END OF PROGRAM SIMGRID
CVF  INFILE: INTEGER FILE UNIT NUMBER CONNECTED TO BFILE
CVF
CVI SITE VARIABLES:
CVI  SLAT :  SITE LATITUDE
CVI  SELEV : SITE ELEVATION IN METERS
CVI  SASPCT: SITE ASPECT DEGREES
CVI  SSLOPE: SITE SLOPE  %
CVI  SLAI:  SITE LEAF AREA INDEX (ALL SIDES)
CVI  SISOH:  SITE ISOHYET
CVI  SALBDO: SITE ALBEDO %
CVI  SEHORZ: EAST-HORIZON
CVI  SWHORZ: WEST HORIZON
CVI  SFILE:  FILE NAME FOR OUTPUT OF MICROCLIMATE OF THE SITE
CVI
CVI BASE VARIABLES:
CVI  BELEV: BASE ELEVATION IN METERS
CVI  BISOH: BASE ISOHYET
CVI  BMAX:  BASE MAX TEMPERATURE, CELSIUS
CVI  BMIN:  BASE MIN TEMPERATURE, CELSIUS
CVI  BPPT:  BASE PRECIPITATION OF STATION(S), 1 OR 2 ARE SUPPORTED
CVI  BFILE: NAME OF THE FILE CONTAINING BASE STATION MET DATA
CVI
CVI PARAMETERS:
CVI  TLAPSE: LAPSE RATE FOR AIR TEMPERATURE
CVI  DLAPSE: LAPSE RATE FOR DEW POINT TEMPERATURE
CVI  MAXLAP: LAPSE RATE FOR MAX TEMPERATURE
CVI  MINLAP: LAPSE RATE FOR MIN TEMPERATURE
CVI  NDAYS:  # OF DAYS TO BE SIMULATED
CVI  MLAI:  MAXIMUM LEAF AREA INDEX, ASSUMED TO BE 10
CVI
CVO OUTPUT VARIABLES:
```

```
CVO  SRAD : SITE INCIDENT RADIATION
CVO  STEMP: DAYLIGHT AVERAGE AIR TEMPERATURE FOR THE SITE
CVO  SMIN:  NIGHT MINIMUM TEMPERATURE FOR THE SITE
CVO  SMAX:  MAXIMUM TEMPERATURE FOR THE SITE
CVO  SHUMD: DAYLIGHT AVERAGE RELATIVE HUMIDITY FOR THE SITE
CVO  SPPT:  PRECIPITATION AT THE SITE, CM
C
     REAL BMAX,BMIN,BDEW,SELEV,SLAT,SASPCT,SSLOPE
     REAL BISOH(2),BPPT(2),TRAN(365)
     REAL SISOH,SEHORZ,SWHORZ,SLAI,MLAI,SALBDO
     REAL SARAD,FARAD,TLAPSE,DLAPSE,SRAD,FRAD,MAXLAP,MINLAP
     REAL BELEV, TRANCF,TEMPCF,SMIN,SMAX,SHUMD,SPPT,STEMP
     CHARACTER*1 ANS0,ANS1,ANS2,ANS3,ANS4
     CHARACTER *12 SFILE,BFILE,IFILE,GFILE
     INTEGER INFILE
     INTEGER NDAYS,NPPT,J,JDAY,FLAG,NPIX,P,CAT,SYEAR,YR
     LOGICAL USEJD, USEENG, USEDEW, USETOT, USETHR
C MAX LAI IS SET TO 10.0
     DATA MLAI/10.0/
C BEGIN
     WRITE(*,'(//////////////////)')
     WRITE(*,*) '                    SIMGRID V1.0'
     WRITE(*,*) '               //////////A\\\\\\\\\\'
     WRITE(*,*) ' '
     WRITE(*,*) '       Mountainous Terrain Microclimate Simulator'
     WRITE(*,*) '                 Copyright 1995.'
     WRITE(*,*) ' '
     WRITE(*,*) ' '
     WRITE(*,*) '  * SIMGRID needs an Initialization file describing'
     WRITE(*,*) '    the Sites and Base Station.'
     WRITE(*,*) ' '
     WRITE(*,*) ' '
     WRITE(*,*) ' '
     WRITE(*,*) ' '
     WRITE(*,*) ' '
     WRITE(*,*) 'Enter the Initialization file name (ie. SIMGRID.INI):'
     WRITE(*,*) ' '
     READ(*,90)IFILE
 90   FORMAT(1A12)

C FORMAT FOR SIMGRID.INI IS 1 VALUE FOLLOWED BY COMMENTS, PER LINE
C REAL VALUES IN COLUMNS 1 TO 12, COMMENTS FROM 13 ONWARD.
C READ 1 VARIABLE PER LINE BY REUSING F12.0 FORMAT STATEMENT

     OPEN(7,FILE=IFILE,STATUS='OLD')
     READ(7,100) BFILE,GFILE,SFILE
 100  FORMAT(/,/,A12,/,A12,/,A12)

C QUESTIONS NOW ANSWERED IN THE SIMGRID.INI FILE.
C 'DO YOU HAVE DEW POINT TEMPERATURE (Y OR N) ?')
     READ(7,1) ANS0
C 'HOW MANY PRECIP STATIONS (1 OR 2) ?')
```

```
      READ(7,*) NPPT
C 'DO YOU WANT THRESHOLD FOR RADIATION (Y OR N) ?')
      READ(7,1) ANS1
C 'DO YOU WANT TOTAL RAD OR AVERAGE RAD (T OR A) ?')
      READ(7,1) ANS2
C 'USE YEARDAY(JULIAN DAY) INPLACE OF MONTH, DAY (Y OR N) ?'
      READ(7,1) ANS4
1     FORMAT(1A1)

CTEMP     USEENG=(ANS3 .EQ. 'E' .OR. ANS3 .EQ. 'E')
      USEDEW=(ANS0 .EQ. 'Y' .OR. ANS0 .EQ. 'Y' )
      USETHR=(ANS1 .EQ. 'Y' .OR. ANS1 .EQ. 'Y')
      USETOT=(ANS2 .EQ. 'T' .OR. ANS2 .EQ. 'T')
      USEJD=(ANS4 .EQ. 'Y' .OR. ANS4 .EQ. 'Y')

      READ(7,*) NDAYS
 101  FORMAT(F12.0)
      READ(7,101) SLAT,BELEV,SLAI
      READ(7,101) BISOH(1),BISOH(2),SEHORZ,SWHORZ,SALBDO
      READ(7,101) TRANCF,TEMPCF,TLAPSE,MAXLAP,MINLAP,DLAPSE
      READ(7,*) NPIX
      READ(7,*) SYEAR
      CLOSE(7)

C COMPUTE ATMOSPHERIC TRANSMISSIVITY
      INFILE = 8
      CALL TRANSM(INFILE,SELEV,TRAN,BFILE,NDAYS,TRANCF,
     1 USEDEW,USEENG,NPPT,USEJD)
C INITIALIZE OUTPUT FILE
      OPEN(INFILE,FILE=BFILE,STATUS='OLD')
      OPEN(10,FILE=GFILE,STATUS='OLD')
      OPEN(9,FILE=SFILE,STATUS='UNKNOWN')
C LOOP FOR NPIX
      DO 22 P=1,NPIX
 201    FORMAT(I8,4F9.3)
        YR=SYEAR-1
        READ(10,201) CAT,SELEV,SSLOPE,SASPCT,SISOH
        PRINT*,CAT,SELEV,SSLOPE,SASPCT,SISOH
C       LOOP FOR NDAYS - COMPUTE AND PRINT MICROCLIMATE
        DO 11 J=1,NDAYS
C         ECHO NDAYS TO SCREEN.
          PRINT*,J
          CALL BREAD(INFILE,JDAY,BMAX,BMIN,BDEW,BPPT,NPPT,
     1           USEDEW,USEENG,USEJD)
C         THE VARIABLE FLAG IS SET TO 1 FOR SLOPED TERRAIN; FLAT TO 0
          FLAG=1.0
          CALL RAD (SLAT,SASPCT,SSLOPE,JDAY,SEHORZ,SWHORZ,TRAN,
     1         SALBDO,SRAD,SARAD,FLAG,USETHR,USETOT)
          FLAG=0
          CALL RAD (SLAT,SASPCT,SSLOPE,JDAY,SEHORZ,SWHORZ,TRAN,
     1         SALBDO,FRAD,FARAD,FLAG,USETHR,USETOT)
          CALL TEMP (BMAX,BMIN,SELEV,BELEV,SLAI,MLAI,SARAD,FARAD,
```

```
     1         TLAPSE,TEMPCF,MAXLAP,MINLAP,STEMP,SMIN,SMAX)
          CALL HUMD (BDEW,DLAPSE,STEMP,SELEV,BELEV,SHUMD)
          IF(SHUMD .GE. 100.0) SHUMD=99.0
          CALL RAIN (NPPT,BPPT,BISOH,SISOH,SPPT)
CTEMP     YR=SYEAR
          IF(JDAY .EQ. 1) YR=YR+1
          CALL WRITE9(CAT,YR,JDAY,SRAD,STEMP,SMAX,SMIN,SHUMD,SPPT)
 11       CONTINUE
          WRITE(*,*)'Pixel ',P,' of ',NPIX,' complete.....'
          REWIND(8)
 22       CONTINUE
          STOP
          END
C ***** END MAIN PROGRAM *****


CC  SUBROUTINE: TRANSM - COMPUTES TRANSMISSIVITY FOR EACH DAY BASED ON
CC                BRISTOW, K.L. AND G.S. CAMPBELL 1984 ON THE
CC                RELATIONSHIP BETWEEN INCOMING SOLAR RADIATION
CC                AND DAILY MAXIMUM AND MINIMUM TEMPERATURE,
CC                AGRIC. FOR. METEOROL. 31, 159-66
CD
CD  ORIGINAL CODE WRITTEN BY R. K. NEMANI
CD  REWRITTEN BY J. C. COUGHLAN ON 4-1-89 (MTCLIM)
CD  MICROSOFT FORTRAN VERSION 4.1 IN STANDARD, TRANSPORTABLE FORTRAN
CD
CV  PARAMETERS
CVF  FILES:
CVF    INFILE :UNIT NUMBER FOR BASE STATION CLIMATIC INPUT FILE
CVI  INPUT:
CVI    SELEV  :SITE ELEVATION IN METERS
CVI    BFILE  :INPUT FILE NAME OF BASE STATION MET. DATA
CVI    NDAYS  :TOTAL NUMBER OF DAYS TO SIMULATE
CVI    USEDEW :FLAG TO DEW POINT PRESENT IN BFILE
CVI    NPPT   :NUMBER OF PREC STATIONS IN BFILE
CVO  OUTPUT:
CVO    TRANCF :CLEAR SKY TRANSMISSIVITY AT SEA LEVEL
CVO    TRAN   :ATMOSPHERIC TRANSMISSIVITY ARRAY
CVI
CVL  LOCAL VARIABLES
CVL    TAMP  :TEMPERATURE AMPLITUDE
CVL    DRAIN :RAINY DAYS
CVL    CLTRAN:CLEAR SKY TRANSMISSIVITY
CVL    XTRANS:ACTUAL TRANSMISSIVITY
CVL    TRANCF:SEA LEVEL CLEAR SKY TRANS (D.M.GATES 1980 BIOPHYSICAL ECOLOGY)
CVL    PCTRAN:% TRANSMITTANCE OF CLEAR SKY POTENTIAL. TEMP AMP OF 20 = 100%
CVL    PPTMIN:MIN PPT FOR REDUCING ATMOSPHERIC TRANS (CM)
CVL    TRANMN:(CONSTANT) MINIMUM TRANSMITTANCE IN %
CVL    JDAY  :YEARDAY FROM INPUT FILE
CVL    JDAY1 :FIRST DAY IN THE INPUT FILE
CVL    JDAYL :LAST DAY IN THE FILE
CVL    KDAY  :POINTER TO ARRAYS REFERENCED BY YEARDAY
```

```
CD
      SUBROUTINE TRANSM (INFILE,SELEV,TRAN,BFILE,NDAYS,TRANCF,
     1                   USEDEW,USEENG,NPPT,USEJD)
      REAL AMP(366),DRAIN(366),TRAN(366)
      REAL SELEV,TRANCF
      LOGICAL USEDEW,USEENG
      CHARACTER *12 BFILE
      INTEGER NPPT, INFILE, NDAYS
      LOGICAL USEJD

      REAL BPPTA(2), BPPT,BMAX,BMIN,BDEW,BMAX1,BMIN1,BPPT1,TAMP
      REAL DIFF,CLTRAN, PCTRAN,XTRANS
      REAL PPTMIN, TRANMN
      INTEGER K,KDAY,JDAY,JDAY1,JDAYL,I,M,J

C CONSTANTS
      DATA PPTMIN/0.254/
      DATA TRANMN/0.1/
C BEGIN
      K=0
      KDAY=0
      OPEN(INFILE,FILE=BFILE,STATUS='OLD')
      REWIND(INFILE)

C READ FOR THE 1ST DAY TO INITIALIZE THE LOOP
      CALL BREAD(INFILE,JDAY,BMAX,BMIN,BDEW,BPPTA,NPPT,
     1        USEDEW,USEENG,USEJD)
      IF (NPPT .EQ. 2) THEN
        BPPT = (BPPTA(1) + BPPTA(2)) / 2
      ELSE
        BPPT = BPPTA(1)
      ENDIF

C MAKE NOTE OF THE FIRST DAY
      JDAY1 = JDAY

C READ TO OBTAIN TEMP AMPLITUDE
      DO 12 J=1, NDAYS-1

        CALL BREAD(INFILE,KDAY,BMAX1,BMIN1,BDEW,BPPTA,NPPT,
     1          USEDEW,USEENG,USEJD)
        IF (NPPT .EQ. 2) THEN
          BPPT1 = (BPPTA(1) + BPPTA(2)) / 2
        ELSE
          BPPT1 = BPPTA(1)
        ENDIF

C COMPUTE AMPLITUDE
        TAMP = BMAX - ((BMIN + BMIN1)/2.)

C   RAINY DAY CORRECTIONS
        IF (BPPT .GT. PPTMIN) THEN
```

```
      K=K+1
      DRAIN(K) = JDAY
      TAMP =  TAMP* 0.75
     ENDIF

C   SWITCH THE VALUES FROM J+1 DAY TO J
      AMP(JDAY) = TAMP
      JDAY = KDAY
      BMAX = BMAX1
      BMIN = BMIN1
      BPPT=BPPT1
 12  CONTINUE

    JDAYL = JDAY

C EXCEPTION FOR THE LAST DAY
 121  TAMP = BMAX - BMIN
    IF (BPPT .GT. PPTMIN ) TAMP = TAMP*0.75
    AMP(JDAY) =TAMP

C CORRECT AMPL VALUES FOR PRE-RAINY DAYS
    DO 30 I=1,K
      KDAY = DRAIN(I)
C   CANNOT CORRECT THE 1ST AND 2ND DAY SO SKIP
      IF ((KDAY-2) .GE. JDAY1) THEN
        DIFF = AMP(KDAY-2) - AMP(KDAY-1)
        IF (DIFF.GE.2.0) AMP(KDAY-1) = AMP(KDAY-1) * 0.75
      ENDIF
 30   CONTINUE

C COMPUTE CLEAR SKY TRANSMITTANCE AT SITE (GATES 1980)
    CLTRAN = TRANCF + SELEV * 8.0E-5
    CLTRAN = AMIN1(CLTRAN,1.0)

C COMPUTE TRANSMISSIVITY FOR EACH DAY (BRISTOW AND CAMPBELL 1984)
    DO 40 M = JDAY1, JDAYL
    PCTRAN = (1 - EXP(-0.003*(AMP(M)**2.4)))
    XTRANS = CLTRAN * PCTRAN
    TRAN(M) = AMAX1(XTRANS,TRANMN)
 40  CONTINUE

C REWIND FILE 8 TO USE AGAIN
    REWIND(8)
    CLOSE (8)
    RETURN
    END

 CC  SUBROUTINE: RAD - COMPUTES INCIDENT SHORTWAVE RADIATION AND
 CC              NET SHORTWAVE RADIATION FOR ANY GIVEN DAY
 CC              BASED ON SURFACE CHARACTERISTICS, SUN-EARTH
 CC              GEOMETRY, AND TRANSMISSIVITY.
 CD
```

```
CD  DO LOOP MODIFIED BY DENNIS SHEPPARD 6-02-95 TO INCREASE THE
CD  COMPUTATIONAL EFFICIENCY.
CD
CD    VALIDATED TO BUFFO BY JCC ON 4-19-89
CD  ORIGINAL CODE WRITTEN BY R. K. NEMANI
CD  REWRITTEN BY J. C. COUGHLAN ON 4-1-89 (MTCLIM)
CD  MICROSOFT FORTRAN VERSION 4.1 IN STANDARD, TRANSPORTABLE FORTRAN
CD
CV  VARIABLES
CVI  INPUT
CVI    SLAT: SITE LATITUDE   DEGREES
CVI    SASPECT:SITE ASPECT  %
CVI    SSLOPE:SITE SLOPE  %
CVI    JDAY: CURRENT YEARDAY
CVI    SEHORZ:SITE EAST HORIZON IN DEGREES FROM 0
CVI    SWHORZ:SITE WEST HORI IN DEGREES FROM 0
CVI    TRAN:TRANSMISSIVITY ARRAY  %
CVI    ALBDO:SITE ALBEDO  %
CVI    FLAG:1 MEANS SLOPING TERRAIN, 0 MEANS FLAT SURFACE.
CVI    USETHR:THRESHOLD RADIATION OF 70 W/M^2
CVI    USETOT:TOTAL RADIATION IF = TO T  KJ/M^/DAY
CVI       ELSE DAYLIGHT AVERAGE  W/M^2
CVO  OUTPUT:
CVO    ARAD:ABSORBED RADIATION, W/M2
CVO    RADN:INCIDENT RADIATION  W/M2
CV
CVL  LOCAL VARIABLE LIST:
CVL    SOL  =SOLAR CONSTANT DERIVED FROM SOLCON ARRAY
CVL    AM   =OPTICAL AIR MASS FOR ANGLES > 21 DEGREES
CVL    A    =OPTICAL AIR MASS ARRAY FOR ANGLES BETWEEN
CVL         0 AND 21 DEGREES ABOVE HORIZON
CVL    DECL =DECLINATION
CVL    JDAY =DAY OF YEAR
CVL    ASP  =ASPECT IN DEGREES
CVL    DSLOP =SLOPE IN DEGREES
CVL    H    =ANGLE OF SUN FROM SOLAR NOON
CVL    TRAN =TRANSMISSIVITY CONSTANT
CVL    TRAM =TRANSMISSIVITY CORRECTED FOR AIR MASS
CVL    NNH  =CALCULATION INTERVAL IN SECONDS. 600 = 10 MINUTES
CVL    NC   =SECONDS IN ONE DAY (24 HOURS)
CVL    N    =NUMBER OF INTERVALS OF LENGTH NNH IN ONE DAY
CVL    DT   =DIRECT SOLAR PERPENDICULAR TO SUN ON THE
CVL         OUTSIDE OF ATMOSPHERE FOR INTERVAL (KJ/M**2)
CVL    ETF  =DIRECT SOLAR ON OUTSIDE OF ATMOSPHERE
CVL         PARALLEL TO EARTHS SURFACE FOR INTERVAL
CVL    GRAD =TOTAL DAILY RADIATION AT GIVEN LOCATION (KJ/M**2)
CVL    HRAD =DIRECT SOLAR ON EARTHS SURFACE (FLAT)     "
CVL    TDIF =TOTAL DAILY DIFFUSE RADIATION             "
CVL    DIFRAD=DIFFUSE ON SLOPE FOR INTERVAL            "
CLL    DRAD =DIRECT ON SLOPE FOR INTERVAL              "
CVL    CZA  =COSINE ZENITH ANGLE
CVL    CBSA =COSINE BEAM SLOPE ANGLE
```

```
CVL    GLOBF =GLOBAL RADIATION, DETERMINING DIFFUSE
CVL    DIFFL =DIFFUSE ON FLAT FOR INTERVAL
CVL    DAYL  =DAYLENGTH (HOURS)
CVL    ALBDO =ALBEDO
CVL
      SUBROUTINE RAD(SLAT,SASPCT,SSLOPE,JDAY,SEHORZ,SWHORZ,TRAN,
     1 ALBDO,RADN,ARAD,FLAG,USETHR,USETOT)
      INTEGER FLAG
      REAL SLAT,SASPCT,SSLOPE,SEHORZ,SWHORZ
      REAL ALBDO,ARAD,RADN
      REAL DEC(46),SOLCON(12),A(21),TRAN(365)
      LOGICAL USETHR,USETOT
C  LOCAL VARIABLES
      INTEGER NNH,NC,N,MO,IDEC,NH,K,ML
      REAL CONV,X,ASP,DLAT,SLOPE,DSLOP,XTRAN,DECL,GRAD,TDIF
      REAL COSDECL,COSDSLOP,COSDLAT,SINDECL,SINDSLOP,SINDLAT
      REAL DAYL2,DH,CZA,H,AM,TRAM,DT,ETF,HRAD,GLOBF,DIFFL,CBSA
      REAL DRAD,SE,DIFRAD,RADT,AVERAD,DAYL,SOL,TDRAD
C  CONSTANTS
      DATA A/2.90,3.05,3.21,3.39,3.69,3.82,4.07,4.37,4.72,5.12
     1,5.60,6.18,6.88,7.77,8.90,10.39,12.44,15.36,19.79,26.96
     2,30.00/
      DATA DEC/-23.,-22.,-21.,-19.,-17.,-15.,-12.,-9.,-6.,-3.,
     10.,3.,6.,9.,12.,14.,17.,19.,21.,22.,23.,23.5,23.5,23.,
     221.5,20.,18.,16.,14.,12.,9.,6.,3.,0.,-3.,-6.,-9.,-12.,
     3-15.,-17.,-19.,-21.,-22.,-23.,-23.5,-23.5/
      DATA SOLCON/1.445,1.431,1.410,1.389,1.368,1.354,1.354
     1,1.375,1.403,1.424,1.438,1.445/
C  FUNCTIONS
C CONVERSION STATEMENT FUNCTION FOR DEGREES TO RADIANS
      CONV(X)=X/57.296
C  BEGIN
C SET THE SLOPE & ASPECT VALUES DEPENDING ON THE FLAG VALUE
      IF (FLAG .GT. 0) THEN
        ASP=CONV(SASPCT)
        SLOPE=SSLOPE
      ELSE
        ASP=0
        SLOPE=0
      ENDIF
C
C CONVERT PERCENT SLOPE TO DEGREES AND TO RADIANS
      DLAT=CONV(SLAT)
      DSLOP=ATAN(SLOPE/100.)*57.29
      DSLOP=CONV(DSLOP)
      XTRAN=TRAN(JDAY)
      NNH=600
      NC=86400
      N=IFIX(NC/NNH+1.)
      DAYL=0.
      MO=IFIX(JDAY/30.+1.)
      IF (MO.GT.12)MO=12
```

```
C
C SOLCON ARRAY IS IN UNITS OF KW/M**2
      SOL=SOLCON(MO)
      IDEC=IFIX(1.+JDAY/8.)
      DECL=CONV(DEC(IDEC))
      GRAD=0.
      TDIF=0.
      TDRAD=0.
      NH=0
      DAYL2=0.
C
C PERFORM TRIGONOMETRIC FUNCTIONS OUTSIDE OF "DO LOOP" TO
C SAVE TIME  - DENNIS SHEPPARD.
C
      COSDECL=COS(DECL)
      COSDSLOP=COS(DSLOP)
      COSDLAT=COS(DLAT)
      SINDECL=SIN(DECL)
      SINDSLOP=SIN(DSLOP)
      SINDLAT=SIN(DLAT)
C
C DO LOOP INCREMENTS 10 MINUTES, STOPS AFTER 24 HOURS
      DO 11 K=1,N
        NH=NH+NNH
C   DETERMINE ANGLE FROM SOLAR NOON
      DH=(NH-43200)*.0041667
      H=CONV(DH)
      CZA=COSDECL*COS((DLAT))*COS((H))+SIN((DECL))
     1  *SIN((DLAT))
        IF(CZA.GT. 0.) THEN
C     DAYLENGTH BASED ON SOLAR ELEVATION ABOVE A FLAT HORIZON
          DAYL2=DAYL2+(NNH/3600.)
C     NEXT 6 LINES, DETERMINE OPTICAL AIR MASS
          AM=1./(CZA+.0000001)
          IF(AM.GT.2.9) THEN
            ML=IFIX(ACOS(CZA)/.0174533)-69
            IF(ML.LT.1)ML=1
            IF(ML.GT.21)ML=21
            AM=A(ML)
          ENDIF
          TRAM=XTRAN**AM
          DT=SOL*NNH
          ETF=CZA*DT
          HRAD=ETF*TRAM
          DT=DT*TRAM
          GLOBF=SQRT(HRAD*ETF)
          DIFFL=GLOBF*(1.-GLOBF/ETF)
          CBSA=-SINDSLOP*SIN(ASP)*SIN(H)
     1     *COSDECL+(-COS(ASP)*SINDSLOP
     2     *SINDLAT+COSDSLOP*COSDLAT)
     3     *COSDECL*COS(H)+(COS(ASP)*SINDSLOP
     4     *COSDLAT+COSDSLOP*SINDLAT)
```

```
     5    *SINDECL
          IF(CBSA.GE.0.) THEN
            DRAD=CBSA*DT
C  THE FOLLOWING THREE LINES COMPUTES A TOPOGRAPHIC REDUCTION OF
C  DIRECT RADIATION
C    EHE = EAST HORIZON ELEVATION (DEGREES)
C    WHE = WEST HORIZON ELEVATION (DEGREES)
            SE=1.57-ACOS(CZA)
            IF(DH.LT.0.AND.SE.LT.CONV(SEHORZ))DRAD=0.
            IF(DH.GT.0.AND.SE.LT.CONV(SWHORZ))DRAD=0.
          ELSE
            DRAD=0
          ENDIF
C
          DIFRAD=DIFFL*(COS((DSLOP*.5))**2.)
          RADT=(DRAD+DIFRAD)/FLOAT(NNH)
C  THE FOLLOWING PROVIDES A MINIMUM RADIATION THRESHOLD OF
C  70 W/M**2 (0.1 LY/MIN) FOR DAYLENGTH AND RADIATION SUMMATION.
          IF(USETHR) THEN
            IF(RADT.GT.0.07) THEN
              DAYL = DAYL + (NNH/3600.)
              GRAD = GRAD + DRAD + DIFRAD
              TDIF = TDIF + DIFRAD
              TDRAD = TDRAD + DRAD
            ENDIF
          ELSE
            DAYL = DAYL + (NNH/3600.)
            GRAD = GRAD + DRAD + DIFRAD
            TDIF = TDIF + DIFRAD
            TDRAD = TDRAD + DRAD
          ENDIF
        ENDIF
    11  CONTINUE
       IF(USETOT) THEN
         RADN = GRAD
         ARAD = RADN * (1- ALBDO)
       ELSE
         AVERAD=(GRAD/(DAYL*3600.))
C      CONVERT KW/M**2 TO W/M**2
         RADN = AVERAD * 1000.0
         ARAD = RADN * (1-ALBDO)
       ENDIF
       RETURN
       END

CC  SUBROUTINE: TEMP - COMPUTES SITE DAYLIGHT AVERAGE TEMPERATURE,
CC                AND SITE MAX & MIN TEMPS BASED ON BASE STATION
CC                DATA AND THEN CORRECTS IT FOR ELEVATION, SLOPE,
CC                AND ASPECT.
CD
CVI PARAMETER LIST
CVI
```

```
CVI INPUT:
CVI  BMAX  :BASE STATION MAX TEMP
CVI  BMIN  :BASE STATION MIN TEMP
CVI  SELEV :SITE ELEVATION IN METERS
CVI  BELEV :BASE ELEVATION IN METERS
CVI  SLAI  :SITE LAI (ALL SIDES)
CVI  MLAI  :MAXIMUM LAI (ALL SIDES) FOR SIMGRID ALGORITHMS
CVI  SARAD :SITE RADIATION KJ/M^2/DAY
CVI  FARAD :FLAT SURFACE RADIATION AT SITE KJ/M^2/DAY
CVI  TLAPSE :LAPSE RATE FOR DAYLIGHT AVE TEMP  C/1000M
CVI  TEMPCF :CONSTANT FOR DAYLIGHT AVE. TEMP (RUNNING ET.AL. EQ. 1)
CVI  MAXLAP :LAPSE RATE FOR MAX TEMPS C/1000M
CVI  MINLAP :LAPSE RATE FOR MIN TEMPS C/1000M
CVO OUTPUT:
CVO  STEMP  :SITE DAYLIGHT AVE TEMP C
CVO  SMIN  :SITE MIN TEMP C
CVO  SMAX  :SITE MAX TEMP C
CVL
CVL LOCAL VARIABLE LIST
CVL  MLAPSE: LAPSE RATE FOR NIGHT MIN TEMPERATURES
CVL  DAYLT: DAYLIGHT AVERAGE TEMPERATURE
CVL  TSYNOP: SYNOPTIC TEMPERATURE AT THE SITE
CVL  RADRAT: RATIO OF FLAT AND SLOPE RADIATION
CVL  TADD : TEMPERATURE INCREMENT FOR SOUTH SLOPES
CVL  TSUB : TEMPERATURE DECREMENT FOR NORTH SLOPES
CVL  MLAI : MAXIMUM LAI (ALL SIDES)
C
      SUBROUTINE TEMP (BMAX,BMIN,SELEV,BELEV,SLAI,MLAI,SARAD,
     1    FARAD,TLAPSE,TEMPCF,MAXLAP,MINLAP,STEMP,SMIN,SMAX)

      REAL BMAX, BMIN, SELEV, BELEV, SLAI, MLAI, SARAD, TEMPCF
      REAL FARAD, TLAPSE, MAXLAP, MINLAP,STEMP, SMIN, SMAX
C  LOCAL VARIABLES
      REAL LAI,TMEAN
      REAL DAYLT,DELEV,TSYNOP,RADRAT,TSUB,TADD
C IF SITE LAI > MAX LAI THEN USE MAX LAI IN EQUATIONS BELOW
      IF (SLAI .GT. MLAI) THEN
       LAI = MLAI
      ELSE
       LAI = SLAI
      ENDIF
C COMPUTE DAYLIGHT AVERAGE TEMP
      TMEAN= (BMAX+BMIN)/2.0
      DAYLT= ((BMAX-TMEAN)*TEMPCF) + TMEAN
C CORRECT FOR LAPSE RATE
      DELEV = SELEV-BELEV
      TSYNOP = DAYLT - TLAPSE * (DELEV / 1000.0)
      SMIN = BMIN - (DELEV/1000.0 * MINLAP)
      SMAX = BMAX - (DELEV/1000.0 * MAXLAP)
C COMPUTE THE RATIO OF SLOPE AND FLAT RADIATION
      RADRAT = SARAD/FARAD
```

```
C          ADJUST SYNOPTIC TEMP TO OBTAIN SLOPE TEMP
C  ADDITIONS MADE ON 10/88 TO ADJUST MAX TEMPS TO RADIATION.
C  NOT VALIDATED BY LITERATURE.
C  NOT ADJUSTING MINIMUM TEMPERATURE BECAUSE LONGWAVE NIGHT ADJUSTMENT.
C
    IF (RADRAT.LT.1.0) THEN
      TSUB=((1/RADRAT)*(1+(LAI/MLAI)))
      STEMP = TSYNOP -  TSUB
      SMAX = SMAX - TSUB
    ELSE
      TADD=(RADRAT* (1-(LAI/MLAI)))
      STEMP = TSYNOP + TADD
      SMAX = SMAX + TADD
    ENDIF
    RETURN
    END


CC  SUBROUTINE: HUMD - COMPUTES RELATIVE HUMIDITY BASED ON BASED
CC                ON BASE STATION DEW POINT.
CD
CVI  PARAMETERS
CVI INPUT:
CVI    BDEW   :BASE STATION BEW POINT C
CVI    DLAPSE :DEW POINT LAPSE RATE
CVI    STEMP  :DAYLIGHT AVE. TEMP. LAPSE RATE
CVI    SELEV  :SITE ELEVATION IN METERS
CVI    BELEV  :BASE ELEVATION IN METERS
CVO OUTPUT:
CVO    SHUMD  :SITE HUMIDITY %
CVL
CVL  LOCAL VARIABLES
CVL    SDEW   :SITE DEW POINT  C
CVL    ES     :AMBIENT VAPOR DENSITY
CVL    ESD    :SATURATED VAPOR DENSITY
    SUBROUTINE HUMD (BDEW,DLAPSE,STEMP,SELEV,BELEV,SHUMD)
    REAL BDEW, DLAPSE,STEMP,SELEV,BELEV,SHUMD
    REAL SDEW,ES,ESD
C CORRECT DEW POINT FOR LAPSE
    SDEW = BDEW - (DLAPSE * ((SELEV-BELEV)/1000.))
C COMPUTE RELATIVE HUMIDITY
    ES = 6.1078 * EXP((17.269*SDEW)/(237.3 + SDEW))
    ESD = 6.1078 * EXP((17.269 * STEMP)/(237.3 + STEMP))
    SHUMD=(ES/ESD) * 100.0
    RETURN
    END


CC  SUBROUTINE: RAIN - COMPUTES SITE PRECIPITATION BY MULTIPLYING
CC                THE BASE STATION PRECIPITATION WITH THE RATIO
CC                OF BASE AND SITE ISOHYETS.
CC
```

```
C NPPT: NUMBER OF BASE PPT STATIONS
      SUBROUTINE RAIN (NPPT,BPPT,BISOH,SISOH,SPPT)
      INTEGER NPPT
      REAL BISOH(2),SISOH,SPPT,BPPT(2)
      REAL RAT1,RAT2
C COMPUTE RATIO OF THE ISOHYET(S)
C     RAT1 = SISOH/BISOH(1)
      RAT1 = SISOH/146.9
      IF (NPPT .EQ. 2) THEN
C       RAT2 = SISOH/BISOH(2)
        RAT2 = SISOH/176.1
        SPPT = ( BPPT(1)*RAT1 + BPPT(2)*RAT2 ) / 2.0
      ELSE
        SPPT = RAT1*BPPT(1)
      ENDIF
      RETURN
      END


CC  SUBROUTINE: WRITE9 - WRITE TO OUTPUT FILE.
CC
      SUBROUTINE WRITE9(CAT,YR,JDAY,SRAD,STEMP,SMAX,SMIN,SHUMD,SPPT)
       INTEGER JDAY,CAT,YR
       REAL SRAD,STEMP,SMAX,SMIN,SHUMD,SPPT
       PRINT 110,CAT,YR,JDAY,SRAD,STEMP,SMAX,SMIN,SHUMD,SPPT
       WRITE(9,110) CAT,YR,JDAY,SRAD,STEMP,SMAX,SMIN,SHUMD,SPPT
 110   FORMAT(1X,I4,1X,I3,1X,I3,2X,F8.2,4(F6.1),1X,F8.1)
       RETURN
       END


CC  SUBROUTINE: BREAD - READ BASE STATION DATA.
CC
CVI VARIABLES
CVI  INPUT:
CVF      INFILE: INTEGER UNIT NUMBER OF BASE STATION CLIMATIC INPUT FILE
CVI      USEDEW: IS DEW POINT SUPPLIED IN FILE
CVI         IF NOT THEN SET IT TO NIGHT MINIMUM TEMPERATURE.
CVI      USEENG: IS INPUT IN ENGLISH OR SI UNITS
CVO  OUTPUT:
CVO      JDAY: YEARDAY
CVO      BMAX: MAXIMUM TEMPERATURE
CVO      BMIN: MINIMUM TEMPERATURE
CVO      BDEW: DEW POINT TEMPERATURE
CVO      NPPT: NUMBER OF BASE STATIONS 1 OR 2
CF    FUNCTION F2C: DEGREE F TO DEGREE C
      SUBROUTINE BREAD(INFILE,JDAY,BMAX,BMIN,BDEW,BPPT,NPPT,
     1            USEDEW,USEENG,USEJD)
      INTEGER INFILE, JDAY, NPPT
      REAL BMAX,BMIN
      REAL BPPT(2)
      LOGICAL USEDEW, USEENG
```

```
      LOGICAL USEJD
C
      REAL F2C,X,YEARDAY
      INTEGER DAY, MON
      F2C(X) = (X-32)*0.5556

C BEGIN
      IF (USEJD) THEN
       IF(USEDEW) THEN
        IF(NPPT .EQ. 1) THEN
          READ(INFILE,*) JDAY, BMAX, BMIN, BDEW, BPPT(1)
          BPPT(2) = 0.0
        ELSE
          READ(8,*) JDAY, BMAX, BMIN, BDEW, BPPT(1), BPPT(2)
        ENDIF
       ELSE
        IF(NPPT .EQ. 1) THEN
          READ(INFILE,*) JDAY, BMAX, BMIN, BPPT(1)
          BPPT(2) = 0.0
          BDEW=BMIN
        ELSE
          READ(INFILE,*) JDAY, BMAX, BMIN, BPPT(1), BPPT(2)
          BDEW = BMIN
        ENDIF
       ENDIF
      ENDIF

      IF (USEENG) THEN
C CONVERT ENGLISH UNITS TO SI
        BPPT(1) = BPPT(1) * 2.54
        BPPT(2) = BPPT(2) * 2.54
        BMAX = F2C(BMAX)
        BMIN = F2C(BMIN)
        BDEW = F2C(BDEW)
      ENDIF

      RETURN
      END
C
C ---------- END LISTING ----------

CD COMMENT GUIDE:
CD
CD 'C'  ANY OLD COMMENT NOT TO BE EXTRACTED TO A DOCUMENTATION FILE
CD 'CV' VARIABLE
CD 'CVF' FILE PARAMETER/VARIABLE
CD 'CVI' INPUT PARAMETER/VARIABLE
CD 'CVO' OUTPUT PARAMETER/VARAIBLE
CD 'CVL' LOCAL VARIABLE
CD 'CM' MODULE NAME AND CALLINF CONVENTION
CD 'CD' DESCRIPTION OF MODULE
CD 'CF' STATEMENT FUNCTIONS
```

Appendix B
SITES.DBF Database Structure

B.1 SITES database structure

FIELD	FIELD NAME	TYPE	WIDTH	DECIMALS	INDEX
1	EASTING	Numeric	11	3	N
2	NORTHING	Numeric	12	3	N
3	ELEVATION	Numeric	9	3	N
4	SLOPE	Numeric	8	3	N
5	ASPECT	Numeric	8	3	N
6	PRCNT_FOR	Numeric	12	3	N
TOTAL:			61		

SITES.DBF is an important input into the microclimate simulator. It provides topographic information which is used primarily in the adjustment of solar radiation receipt at a location. The data structure described above is used in the creation of SITES.DBF as well as by the "READ" statements within the model. The fields themselves are self explanatory with the possible exception being PRCNT_FOR. This field contains a value representing the percentage of forest cover per unit area which is reflected in the model by the Leaf Area Index (LAI).

Appendix C
SNOPAC

C.1 SNOPAC Code Listing

```
      PROGRAM SNOPAC
CH                          LAST MODIFIED: 01-02-96
CH
CH    THIS PROGRAM READS THE GRIDDED MICROCLIMATE AS SIMULATED BY
CH    SIMGRID, CALCULATES SNOW MELT FOR EACH DAY, AND THEN WRITES
CH    THE RESULT TO AN OUTPUT FILE.
CH
CH    VERSION 1.0   COPYRIGHT 1995
CH    ORIGINAL CODE WRITTEN BY DENNIS SHEPPARD ON 6-26-95
CH    MICROSOFT FORTRAN 5.0

CC
      REAL SRAD,STEMP,SMAX,SMIN,SHUMD,SPPT,LASTTREQ,LASTMELT
      REAL PACK,TREQ,TCEADJ,MELT,SNOW,TMEAN
      INTEGER CAT,YR,JDAY,NUMDAY
      CHARACTER*12 INFILE,OUTFILE
      WRITE(*,'(/////////////)')
      WRITE(*,*) '                    SnoPac Ver. 1.0'
      WRITE(*,*) '                   ////////...\\\\\\\'
      WRITE(*,*) ''
      WRITE(*,*) '                   Snowmelt Simulator'
      WRITE(*,*) '                    Copyright 1995'
      WRITE(*,*) ''
      WRITE(*,*) ''
      WRITE(*,*) ''
      WRITE(*,*) ''
      WRITE(*,*) ''
      WRITE(*,*) ''
      WRITE(*,*) '    Enter the input file name :'
      READ(*,100) INFILE
      WRITE(*,*) '    How many DAYS are in ',INFILE,'?'
      READ(*,*) NUMDAY
      WRITE(*,*) '    Enter the output file name :'
      READ(*,100) OUTFILE
  100 FORMAT(1A12)
      OPEN(7,FILE=INFILE,STATUS='OLD')
      OPEN(9,FILE=OUTFILE,STATUS='UNKNOWN')
CC
CC    LOOP FOR 120 CATEGORIES OF ELEVATION, SLOPE, AND ASPECT.
```

```
CC
      DO 20 J=1,120
       LASTTREQ = 0.0
       LASTMELT = 0.0
       PACK = 0.0
       SNOW = 0.0
CC
CC    LOOP FOR NUMBER OF DAYS (IE. 731 FOR 1971 AND 1972)
CC
       DO 10 I=1,NUMDAY
        READ(7,150) CAT,YR,JDAY,SRAD,STEMP,SMAX,SMIN,SHUMD,SPPT
 150     FORMAT(1X,I4,1X,I3,1X,I3,1X,I3,2X,F8.2,4(F6.1),1X,F8.1)
CTEMP        PRINT 150, CAT,YR,JDAY,SRAD,STEMP,SMAX,SMIN,SHUMD,SPPT
        CALL SNOWMELT(SMAX,SMIN,LASTTREQ,TREQ,TCEADJ,MELT)
        CALL SNOWACC(SMAX,SMIN,SPPT,SNOW)
        PACK = PACK + SNOW - LASTMELT
        IF(PACK .LT. 0.0) PACK = 0.0
        POTMELT = MELT
        IF(PACK .LE. 0.0) MELT = 0.0
CTEMP        IF(SMIN .LE. 0.0) MELT = 0.0
        TMEAN = (SMAX + SMIN)/2
        IF(TMEAN .LT. 2.0) MELT = 0.0
        ACTMELT = MELT
        IF(PACK .LT. MELT) ACTMELT = PACK
        IF(JDAY .EQ. 91) THEN
         CALL WRITER(CAT,YR,JDAY,SMAX,SMIN,SPPT,PACK,TREQ,
     1    TCEADJ,POTMELT,ACTMELT)
        ENDIF
        LASTTREQ = TREQ
        LASTMELT = ACTMELT
        PRINT *, I
 10    CONTINUE
 20   CONTINUE
      STOP
      END

CC*---------- END OF MAIN PROGRAM ----------*CC


      SUBROUTINE WRITER(CAT,YR,JDAY,SMAX,SMIN,SPPT,PACK,TREQ,TCEADJ,
     1 POTMELT,ACTMELT)
CH    THIS SUBROUTINE WRITES CALCULATED OUTPUT TO SCREEN AND/OR FILE.

      REAL SMAX,SMIN,SPPT,PACK,TREQ,TCEADJ,POTMELT,ACTMELT
      INTEGER CAT,YR,JDAY
 150  FORMAT(I3,1X,I3,1X,I3,1X,3(F7.1),F10.1,4(F7.1))
CTEMP     PRINT 150, CAT,YR,JDAY,SMAX,SMIN,SPPT,PACK,TREQ,TCEADJ,
CTEMP     1 POTMELT,ACTMELT
      WRITE(9,150) CAT,YR,JDAY,SMAX,SMIN,SPPT,PACK,TREQ,TCEADJ,
     1 POTMELT,ACTMELT
      RETURN
      END
```

```
      SUBROUTINE SNOWMELT(SMAX,SMIN,LASTTREQ,TREQ,TCEADJ,MELT)
CH    THIS SUBROUTINE ESTIMATES DAILY SNOW MELT AS DEPTH OF WATER.  THE
CH    METHOD WAS DEVELOPED FOR USE IN THE UBC WATERSHED MODEL.
CH
CR    PIPES, ANTHONY AND MICHAEL QUICK, 1977.  UBC WATERSHED MODEL USERS
CR      GUIDE.  DEPARTMENT OF CIVIL ENGINEERING, UNIVERSITY OF BRITISH
CR      COLUMBIA.
CC
      REAL ANMLTF,SMAX,SMIN,LASTTREQ,TREQ,TCEADJ,MELT,TMEAN
      REAL PTM
      INTEGER XTDEWP
CC
CC    PTM = POINT MELT FACTOR SET TO 1.8 (WYMAN, R.R., 1995).
CC    XTDEWP = REFERENCE DEWPOINT CONTROLLING ENERGY PARTITIONING BETWEEN
CC          MELT AND SUBLIMATION SET TO 18 DEGREES CELCIUS.
CC    ANMLTF = DECAY CONSTANT SET TO 0.85.
CC
      PTM = 1.8
      XTDEWP = 18
      ANMLTF = 0.85
      TMEAN = (SMAX + SMIN)/2
      TRANGE = SMAX - SMIN
      TREQ = ANMLTF * LASTTREQ + TMEAN
      TCEADJ = (SMIN + (TRANGE/2))/(XTDEWP + (TRANGE/2))
      MELT = PTM * (SMAX + TCEADJ * SMIN)
      RETURN
      END


      SUBROUTINE SNOWACC(SMAX,SMIN,SPPT,SNOW)
CH    THIS SUBROUTINE ESTIMATES DAILY SNOW WATER EQUIVALENT IN MM.
CH
CR    WYMAN,R.R., 1995. MODELING SNOWPACK ACCUMULATION AND
CR      DEPLETION.  IN: GUY, B.T. AND J. BARNARD, 1995.  MOUNTAIN HYDROLOGY,
CR      PEAKS AND VALLEYS IN RESEARCH AND APPLICATIONS CONFERENCE
CR      PROCEEDINGS.  MAY 16-19 IN VANCOUVER, B.C.
CC
      REAL SMAX,SMIN,SPPT,SNOW,RAIN,TMEAN
      TMEAN = (SMAX + SMIN)/2
      IF(TMEAN .LT. 0.6) RAIN = 0
      IF((0.6 .LE. TMEAN) .AND. (TMEAN .LE. 3.6)) RAIN=
     1 SPPT*((TMEAN/3)-0.2)
      IF(TMEAN .GT. 3.6) RAIN = SPPT
      SNOW = SPPT - RAIN
      RETURN
      END

CC
CC*--------- COMMENT LEGEND ----------*CC
CC
```

CH - PROGRAM OR SUBROUTINE HEADER
CR - BIBLIOGRAPHIC REFERENCE
CTEMP - TEMPORARILY COMMENTED OUT
CC - INTERNAL DOCUMENTATION